UNIVERSITÉ DU QUÉBEC À MONTRÉAL

THÈSE PRÉSENTÉE À L'UNIVERSITÉ DU QUÉBEC À CHICOUTIMI
COMME EXIGENCE PARTIELLE
DU DOCTORAT EN RESSOURCES MINÉRALES
OFFERT À
L'UNIVERSITÉ DU QUÉBEC À MONTRÉAL
EN VERTU D'UN PROTOCOLE D'ENTENTE AVEC
L'UNIVERSITÉ DU QUÉBEC À CHICOUTIMI

PAR

GUILLAUME ST-ONGE

PROPRIÉTÉS MAGNÉTIQUES ET SÉDIMENTOLOGIQUES DE SÉQUENCES HOLOCÈNES DE L'ESTUAIRE DU ST-LAURENT ET DU FJORD DU SAGUENAY, CANADA

JANVIER 2004

Bibliothèque
Paul-Émile-Boulet

UQAC
Université du Québec
à Chicoutimi

Mise en garde/Advice

Afin de rendre accessible au plus grand nombre le résultat des travaux de recherche menés par ses étudiants gradués et dans l'esprit des règles qui régissent le dépôt et la diffusion des mémoires et thèses produits dans cette Institution, **l'Université du Québec à Chicoutimi (UQAC)** est fière de rendre accessible une version complète et gratuite de cette œuvre.

Motivated by a desire to make the results of its graduate students' research accessible to all, and in accordance with the rules governing the acceptation and diffusion of dissertations and theses in this Institution, the **Université du Québec à Chicoutimi (UQAC)** is proud to make a complete version of this work available at no cost to the reader.

L'auteur conserve néanmoins la propriété du droit d'auteur qui protège ce mémoire ou cette thèse. Ni le mémoire ou la thèse ni des extraits substantiels de ceux-ci ne peuvent être imprimés ou autrement reproduits sans son autorisation.

The author retains ownership of the copyright of this dissertation or thesis. Neither the dissertation or thesis, nor substantial extracts from it, may be printed or otherwise reproduced without the author's permission.

UNIVERSITÉ DU QUÉBEC À MONTRÉAL

THESIS PRESENTED AT THE UNIVERSITÉ DU QUÉBEC À CHICOUTIMI
AS A PARTIAL FULFILMENT
FOR THE PHD IN MINERAL RESOURCES
OFFERED AT
THE UNIVERSITÉ DU QUÉBEC À MONTRÉAL
AS PART OF AN AGREEMENT WITH
THE UNIVERSITÉ DU QUÉBEC À CHICOUTIMI

BY

GUILLAUME ST-ONGE

MAGNETIC AND SEDIMENTOLOGICAL PROPERTIES OF HOLOCENE SEQUENCES FROM THE ST. LAWRENCE ESTUARY AND SAGUENAY FJORD, CANADA

JANUARY 2004

RÉSUMÉ

Trois longues séquences sédimentaires ont été prélevées dans l'estuaire du St-Laurent (MD99-2220 et MD99-2221) et le fjord du Saguenay (MD99-2222) dans le cadre du programme international IMAGES (*International Marine Past Global Change Study*), en 1999, afin 1) de reconstuire les variations holocènes d'orientation et d'intensité du champ magnétique terrestre, 2) d'établir une chronostratigraphie holocène pour les séquences sédimentaires de l'est du Canada, 3) de déterminer la fréquence des événements accidentels tels que les crues et le séismes survenus au cours de l'Holocène dans le fjord du Saguenay et 4) de développer des traceurs sédimentologiques et/ou magnétiques des variations climatiques holocènes décennales à millénaires dans l'estuaire du St-Laurent. Les propriétés magnétiques des carottes MD99-2220 et MD99-2221 ainsi que 13 datations au ^{14}C ont permis d'établir une chronostratigraphie pour les derniers 8 500 ans dans l'est du Canada. Les variations d'orientation du champ magnétique terrestre (inclinaison et déclinaison) enregistrées dans les sédiments de la carotte MD99-2220 peuvent être corrélées avec celles d'enregistrements lacustres nord-américains et indiquent que les décalages temporels observés entre les différents enregistrements sont problement liés aux différentes chronologies plutôt qu'à la dérive de la composante non-dipolaire du champ magnétique terrestre. De façon similaire, les fluctuations séculaires à millénaires de l'intensité du champ magnétique terrestre enregistrées dans les sédiments de la carotte MD99-2220 peuvent être corrélées avec celles d'enregistrements lacustres nord-américains et européens. De plus, la corrélation entre les fluctuations de l'intensité du champ magnétique terrestre et le taux de production d'isotopes cosmogéniques tels le ^{14}C et le ^{10}Be, au cours de l'Holocène, confirme que l'intensité du champ magnétique terrestre module le taux de production de ces isotopes à des échelles de temps séculaire à millénaire.

Les propriétés magnétiques, sédimentologiques et physiques de la carotte MD99-2222 ont permis de mettre en évidence la présence d'au moins 14 couches accidentelles mises en place au cours des derniers 7200 ans dans le fjord du Saguenay. Ces couches sont facilement identifiables par leur couleur gris pâle et par leurs bases sableuses qui diffèrent fortement des sédiments très foncés et « bioturbés » mis en place sous des conditions plus stables. Des analyses aux rayons-X et granulométriques, réalisées à maille serrée dans chacune des couches accidentelles, ont permis de déterminer leur mécanisme de dépôt. L'ensemble des données ainsi que la situation géologique et sédimentologique du fjord du Saguenay laissent croire que la grande majorité de ces couches auraient été déposées à la suite de séismes de magnitude élevée. Nos résultats illustrent ainsi que la fréquence des séismes majeurs dans le fjord du Saguenay aurait grandement diminué depuis ~4000 ans, ce qui est en accord avec une modélisation numérique qui montre que la réactivation des failles, en raison de l'allègement glacio-isostatique post-glaciaire, aurait eu lieu principalement entre ~7000 et 4000 ans.

Finalement, l'analyse à maille serrée de la granulométrie des sédiments de la carotte MD99-2220 et d'une carotte boîte, prélevée au même site dans l'estuaire du St-Laurent, a permis de développer un traceur du débit printannier du fleuve St-Laurent. Nos résultats indiquent qu'un débit printannier élevé accroît le transport et le dépôt de silts dans l'estuaire du St-Laurent. Ainsi, des fluctuations décennales du débit printannier et quelques événements exceptionnels ont-il été décelés à partir du pourcentage de silt au cours des derniers 800 ans. Des variations décennales des températures hivernales de l'eau de surface de l'estuaire du St-Laurent ont aussi été observées et indiquent une variabilité importante des conditions hivernales dans l'est du Canada au cours des derniers siècles. De plus, un changement concomitant des moyennes du pourcentage de silt et des températures de surface a été enregistré vers ~500 années cal. BP. La date de ce changement synchrone ainsi que la baisse subséquente des températures de surface marquent probablement le début du Petit Âge Glaciaire. Le pourcentage de silt est également corrélé à un indice de l'oscillation nord-atlantique de 1865 à 2000, ce qui laisse croire que les précipitations dans le bassin versant des Grands-Lacs/fleuve St-Laurent auraient pu être influencées par l'oscillation nord-atlantique au cours des derniers siècles. Par ailleurs, le pourcentage de silt met en évidence une augmentation importante de la fréquence des fortes crues printannières, depuis 1975.

ABSTRACT

Three long sedimentary sequences were recovered from the St. Lawrence Estuary (MD99-2220 and MD99-2221) and Saguenay Fjord (MD99-2222) as part of the International Marine Past Global Change Study (IMAGES) program in 1999 in order to 1) reconstruct changes of Earth's magnetic field intensity and direction during the Holocene, 2) set a Holocene chronostratigraphy for Eastern Canadian sedimentary sequences, 3) determine the frequency of catastrophic events such as floods and earthquakes in the Saguenay Fjord during the Holocene and 4) develop sedimentological and/or magnetic proxies of Holocene decadal to millennial climatic variations in the St. Lawrence Estuary. The magnetic properties of cores MD99-2220 and MD99-2221 along with 13 accelerator mass spectrometry (AMS) ^{14}C dates allowed the setting of a chronostratigraphy for the last 8 500 years in Eastearn Canada. Directional changes (inclination and declination) of Earth's magnetic field recorded in the sediments of core MD99-2220 can be correlated with changes observed in North American lacustrine sediments and indicate that the temporal offset between the records are due to the different chronologies rather than the drift of the non-dipole field. Similarly, the relative paleointensity (RPI) record reconstructed for core MD99-2220 compares favorably with North American and European Holocene RPI records at millennial and even some centennial timescales. Comparisons between core MD99-2220 RPI proxy with the ^{10}Be flux record from the Greenland Summit (GISP2) ice core and a ^{14}C production rate record confirm that geomagnetic modulation may control the millennial and even some centennial scale variability within cosmogenic isotope records.

The magnetic, sedimentological and physical properties of core MD99-2222 allowed the identification of at least 14 rapidly deposited layers (RDL) that were accumulated in the Saguenay Fjord during the last 7200 years. These layers are easily recognizable by their sandy bases and light grey color, contrasting sharply with the dark grey bioturbated background sediments. Digital X-radiography and high-resolution grain size analyses performed in each RDL were used to determine the mechanism responsible for their deposition. The presented data along with the geological and sedimentological setting of the Saguenay Fjord suggest that these RDL were triggered by strong earthquakes. This thesis also illustrates that earthquake frequency was dramatically reduced since ~4000 years. This observation is consistent with ice-load modeling during deglaciation in Eastern Canada, which suggests that the greatest fault instability would be expected between 4000 and 7000 years.

Finally, high-resolution grain size analyses from core MD99-2220 and a box core sampled at the same site in the St. Lawrence Estuary were used to derive a paleodischarge proxy for the St. Lawrence River. The results illustrate that an increase in the spring freshet discharge of the St. Lawrence River increases the transport and deposition of silts in the St. Lawrence Estuary. Therefore, high frequency decadal-scale fluctuations of the spring

freshet discharge along with a few exceptional events were reconstructed for the past 800 cal BP using the percent-silt record. Decadal-scale variations are also observed in the reconstructed February sea-surface temperatures (SST) of the St. Lawrence Estuary and indicate an important variability in winter conditions over Eastern Canada during the last centuries. In addition, a synchronous change in the average percent silt and average reconstructed February SST was recorded around ~500 cal BP. The timing of the concomitant change along with the subsequent colder reconstructed February SST hint at the inception of the Little Ice Age. A relationship between the percent silt and a NAO index from 1865 to 2000 AD is also observed, suggesting that multidecadal-scale precipitation variations in the Great Lakes/St. Lawrence River watershed may have been influenced by the NAO during the last centuries. Finally, the percent silt record indicates that the frequency of large spring freshets drastically increased since 1975 AD.

REMERCIEMENTS

Je tiens tout d'abord à remercier très sincèrement mon directeur de thèse, Claude Hillaire-Marcel, qui m'a soutenu, conseillé, dirigé, encouragé et permis d'oeuvrer à l'intérieur d'une équipe très dynamique et stimulante. Je le remercie également de toujours avoir eu à coeur ma formation scientifique et de toujours avoir pris le temps de répondre à mes questions. J'exprime également toute ma gratitude à Anne de Vernal pour son amitié, son aide et sa passion contagieuse de la science. Je remercie aussi sincèrement mon co-directeur de thèse, David Piper, pour ses judicieux conseils et son aide en sédimentologie.

Je tiens aussi à exprimer toute ma gratitude à Joseph Stoner qui m'a initié au paléomagnétisme et qui m'a constamment guidé et aidé tout au long de ce doctorat. Je le remercie également de ne jamais avoir cessé de m'encourager, en plus de me faire comprendre de ne jamais rien tenir pour acquis. Joe, you are a big part of my success !

Je remercie aussi sincèrement Thierry Mulder pour mon séjour très fructueux à Bordeaux ainsi que pour les analyses sur la carotte MD99-2222. Je remercie aussi Kenneth Verosub de m'avoir permis de réaliser les analyses paléomagnétiques dans son laboratoire à l'Université de Californie à Davis. Je remercie aussi Anne de Vernal, Jacques Locat et Jim Channel d'avoir accepté d'être sur mon jury.

Je suis également très reconnaisssant envers tous les membres d'équipage et scientifiques des missions océanographiques auxquelles j'ai participées et qui ont, en plus

d'enrichir ma formation, permis l'échantillonnage de sédiments d'une qualité remarquable. Un merci spécial à Guy Bilodeau et André Rochon pour leur travail très exigeant leur du deuxième leg de la mission IMAGES-V. Merci à Céline Hallé-Polèse, Louise Bernier et Isabelle Jacob pour leur grande disponibilité et leur oreille attentive. Un gros merci également à tous les membres et étudiants du GEOTOP.

Un gros merci à Jean-François Hélie et Julie Leduc pour leur encouragement coustant, mais surtout pour leur grande amitié et tous les bons moments que nous avons passés ensembles. Merci à Vincent et Mia, Dominic et Caroline, Annie, Brigitte et Marc ainsi que Christian et Patricia pour leur amitié inébranlable.

Merci à mes parents, Hugues et Franca St-Onge, pour leur soutien inconditionnel et de m'avoir toujours poussé à réaliser mes rêves. Merci à mon frère, Alexandre, qui est toujours là pour moi. Un merci du fond de mon coeur à ma femme, Hélène, pour tous les compromis, son soutien, son amour et sa façon de toujours voir le bon côté des choses et qui est en grande partie responsable de mon succès. Enfin, je remercie mes enfants Olivier, Sarah et Marianne qui me rappellent constamment à quel point la vie est précieuse et merveilleuse. Je dédie cette thèse à ma femme et mes enfants.

En terminant, je remercie le CRSNG, le FCAR, le GEOTOP, l'UQÀM, Ressources Naturelles du Canada, Pêches et Océans Canada ainsi que le projet Saguenay post-déluge, le programme IMAGES, le FACC et la FCSCA pour leur soutien financier.

TABLE DES MATIÈRES

CHAPITRE I

INTRODUCTION GÉNÉRALE

Les propriétés magnétiques de matériaux géologiques ou archéologiques permettent de reconstituer les variations d'intensité et d'orientation du champ magnétique terrestre au cours des temps géologiques. De telles observations sont par ailleurs essentielles à une modélisation réaliste de la géodynamo interne de la Terre (Dormy *et al.*, 2000) et à une meilleure estimation des taux de production d'isotopes cosmogéniques tels le ^{14}C et le ^{10}Be durant le Quaternaire (Bard, 1998).

En outre, l'analyse des propriétés magnétiques de sédiments s'avère un outil efficace de datation et de corrélation (*e.g.*, King *et al.*, 1983 ; Thompson et Oldfield, 1986 ; Saarinen, 1999). En effet, l'établissement de courbe de référence des variations d'orientation et d'intensité du champ magnétique terrestre de séquences sédimentaires bien datées a permis des corrélations locales, régionales voire globales, très précises (*e.g.*, Brachfeld et Banerjee, 2000 ; Saarinen, 1999 ; Stoner *et al.*, 2000 ; Stoner *et al.*, 2002). De plus, l'utilisation récente de *u-channels* pour le sous-échantillonnage des carottes sédimentaires, en vue de leur analyse en continu, et le développement d'une nouvelle génération de magnétomètres cryogéniques permettent de mesurer et d'induire différents types de magnétisation, rapidement et de façon précise (Weeks *et al.*, 1993). Ces mesures

magnétiques dépendent de la concentration, de la minéralogie et de la granulométrie magnétique et ont été employées avec succès comme traceurs de changements environnementaux et climatiques. (*e.g.*, Thompson et Oldfield, 1986 ; Reynolds et King, 1995 ; Maher et Thompson, 1999). L'analyse des propriétés magnétiques de sédiment est donc un outil polyvalent permettant à la fois des observations sur la variabilité du champ magnétique terrestre, des corrélations et des reconstitutions paléoclimatiques. C'est dans cette optique d'outil polyvalent que l'analyse des propriétés magnétiques de sédiments a été sélectionnée comme principale méthode d'analyse des séquences sédimentaires holocènes du fjord du Saguenay et de l'estuaire du St-Laurent.

Le fjord du Saguenay et l'estuaire du St-Laurent n'ont pas d'équivalent, dans l'est canadien, pour leurs très hautes vitesses de sédimentation (0,2 à 7 cm/an ; Smith et Walton, 1981 ; Smith et Schafer, 1999 ; Zhang, 2000). Celles-ci permettent le carottage de séquences sédimentaires avec une résolution chronologique exceptionnelle, de l'ordre de la décennie et même de l'année. Le carottage de plusieurs séquences sédimentaires holocènes, durant la campagne océanographique IMAGES-V (*International Marine Past Global Change Study*) à bord du Marion Dufresne II, en juillet 1999, offrait une chance unique de reconstruire les variations d'orientation et d'intensité du champ magnétique terrestre avec une résolution temporelle jusqu'ici inégalée, ainsi que l'opportunité de développer des traceurs sédimentologiques et magnétiques des variations climatiques ou environnementales décennales à millénaires dans l'est du Canada au cours de l'Holocène.

Trois thèmes ont servi de base à cette thèse et seront maintenant abordés dans cette introduction générale: 1) la reconstruction des variations d'intensité et d'orientation du champ magnétique terrestre durant l'Holocène, 2) l'établissement d'une chronostratigraphie holocène des séquences sédimentaires de l'est du Canada, et 3) le développement de traceurs sédimentologiques et magnétiques des variations climatiques décennales à millénaires dans le fjord du Saguenay et l'estuaire du St-Laurent au cours l'Holocène.

Variations d'intensité et d'orientation du champ magnétique terrestre durant l'Holocène

Il est généralement admis que le champ magnétique terrestre est principalement créé par le mouvement des fluides riches en fer du noyau externe (Glatzmaier et Roberts, 1995, 1996 ; Buffet, 2000). L'intensité et l'orientation de ce champ magnétique varient dans le temps selon des échelles allant de quelques secondes à des millions d'années (*e.g.*, Merril *et al.*, 1996 ; McElhinny et McFadden, 2000 ; Dormy *et al.*, 2000). Aujourd'hui, les variations d'intensité et d'orientation peuvent être mesurées grâce aux observatoires géomagnétiques, à certains satellites et à quelques archives historiques, mais ces enregistrements ne remontent jamais au-delà des derniers ~400 ans (McElhinny et McFadden, 2000). Par contre, les matériaux géologiques et archéologiques constituent des archives naturelles des variations d'intensité et d'orientation du champ magnétique terrestre à travers les temps géologiques.

Les laves volcaniques et certains artefacts telles les poteries enregistrent, en refroidissant sous le point de Curie, une magnétisation qui est absolue et dont les processus d'acquisition sont bien compris (Dunlop et Özdemir, 1997 ; Tauxe, 1998 ; McElhinny et McFadden, 2000). Toutefois, ces types de matériaux présentent une distribution spatiale et temporelle très hétérogène, car leur analyse dépend de la découverte de laves et d'artefacts. Ils ne fournissent ainsi qu'une image très fragmentaire et sporadique de la variabilité du champ magnétique terrestre. Par opposition, de nombreuses études ont démontré que les sédiments étaient susceptibles de constituer des archives continues des variations d'intensité et d'orientation du champ magnétique terrestre à travers les temps géologiques (*e.g.*, Stoner *et al.*, 1995; Guyodo et Valet, 1996, 1999 ; Roberts, 1997 ; Lund, 1996 ; Peck *et al.*, 1996 ; Saarinen, 1999 ; Ali *et al.* 1999 ; Brachfeld et Banerjee, 2000), même si une partie des processus responsables de l'acquisition de la magnétisation dans les sédiments demeure incomprise (Tauxe, 1993 ; Tauxe, 1998 ; Katari *et al.*, 2000 ; Katari et Bloxham, 2001).

Les sédiments holocènes sont, quant à eux, particulièrement propices à l'enregistrement des variations d'intensité et d'orientation du champ magnétique terrestre à cause de leur large distribution spatiale, leur enregistrement continu et leur possibilité de datation par la méthode du ^{14}C. La plupart des connaissances sur les variations de l'intensité et de l'orientation du champ magnétique durant l'Holocène a été obtenue à partir de sédiments lacustres. Des courbes des variations d'inclinaison et de déclinaison avec des oscillations bien définies ont été construites en Europe, Amérique du Nord, Australie, Argentine, Japon et Sibérie (*e.g.*, Barton et McElhinny, 1981 ; Creer and Tucholka, 1982 ;

Creer *et al.*, 1983 ; Constable et McElhinny, 1985 ; Verosub *et al.*, 1986; Lund, 1996 ; Peck *et al.*, 1996 ; Saarinen, 1999 ; Ali *et al.* 1999 ; Brachfeld et Banerjee, 2000). Des décalages temporels dans les différents enregistrements lacustres ont été observés et parfois interprétés comme la dérive de la composante non-dipolaire du champ magnétique terrestre (*e.g.*, Creer, 1981 ; Verosub *et al.*, 1986). Cette dérive se serait effectuée principalement vers l'ouest (*westward drift*) selon un taux de 0,062 à 0,25°/an (Creer, 1981 ; Verosub *et al.*, 1986). Mais, cette interprétation doit être regardée d'un oeil critique puisque ces chronologies lacustres, généralement basées sur des datations au ^{14}C de sédiment brut, ont souvent été affectées par une contamination de carbone ancien, "vieillissant" ainsi les âges ^{14}C (Hagstrum et Champion, 2002). Outre les incertitudes liées à la chronologie des enregistrements lacustres qui conduisent à mettre en doute une telle dérive, la compilation de plusieurs enregistrements nord-américains lacustres, couvrant les derniers 12 000 ans BP, par Lund (1996), n'indique aucune dérive vers l'ouest significative au cours de l'intervalle. Cet auteur démontre au contraire que si dérive il y a eu en Amérique du Nord, celle-ci se serait plutôt effectuée vers le nord et seulement au cours de l'intervalle 5500-1500 ans BP. Afin de trancher entre l'une ou l'autre de ces hypothèses, des séquences holocènes bien datées et bien corrélées doivent être examinées.

Des études de la variation de la paléointensité relative (PIR) du champ magnétique terrestre enregistrée dans des sédiments marins ont montré que certaines oscillations des courbes de PIR, avec des périodes de l'ordre de 10^4-10^5 ans, pouvaient être corrélées sur des distances de plusieurs milliers de kilomètres allant de l'Atlantique Nord, à la Méditerranée, à l'océan Indien , à l'océan Pacifique (*e.g.*, Tric *et al.*, 1992; Tauxe and

Shackleton, 1994 ; Yamazaki and Ioka, 1994 ; Stoner *et al.*, 1995; Guyodo et Valet, 1996, 1999 ; Roberts, 1997) et, même, d'un hémisphère à l'autre (Stoner *et al.*, 2002). Quelques enregistrements sédimentaires de la PIR, dont la résolution temporelle est suffisamment élevée, ont aussi révélé que les oscillations millénaires pouvaient être corrélées à une échelle globale, laissant croire que le champ magnétique terrestre global (composante dipolaire) varierait au moins selon une échelle de temps millénaire (Channell *et al.*, 2000 ; Stoner *et al.*, 2000; Snowball et Sandgren, 2002) et peut être même selon une échelle de temps séculaire.

Cette dernière hypothèse a des répercussions importantes au niveau de l'estimation des taux de production d'isotopes cosmogéniques tels que ^{10}Be et le ^{14}C puisque ceux-ci sont influencés par les fluctuations de l'intensité du champ magnétique terrestre (Elsaesser *et al.*, 1956 ; Bard, 1998). De plus, en se basant sur l'hypothèse que l'intensité du champ magnétique terrestre n'influence que le taux de production d'isotopes cosmogéniques à des échelles de temps > 10^3 ans, les variations du taux de production d'isotopes cosmogéniques ont souvent été utilisées comme traceur des variations solaires (Bard, 1997 ; van Geel *et al.*, 1999 ; Bond *et al.*, 2001) ou des variations de la circulation thermohaline (Muscheler *et al.*, 2000; Clark *et al.*, 2001). En réalité, la fréquence à laquelle le champ magnétique terrestre n'affecte plus le taux de production des isotopes cosmogéniques est inconnue, principalement à cause de l'absence d'enregistrements continus de l'intensité du champ magnétique terrestre présentant une résolution temporelle décennale à séculaire.

En dépit des nombreuses études consacrées aux variations d'inclinaison et de déclinaison, il existe très peu d'enregistrements de l'intensité du champ magnétique

terrestre pour l'Holocène. La majorité des enregistrements proviennent de matériaux volcaniques ou archéologiques. Toutefois, la résolution temporelle dans ces matériaux n'est pas suffisante pour déceler des variations décennales à séculaires (McElhinny et Senanayake, 1982 ; Yang *et al.*, 2000) et la majorité des enregistrements ne couvrent que les 2000 dernières années (Hongre *et al.*, 1998 ; Yongjae *et al.*, 2000). De plus, une très grande variance est observée dans les estimations d'intensité absolue couvrant les derniers 12 000 ans (Teanby et Gubbins, 2000). Les quelques enregistrements holocènes lacustres disponibles proviennent de Sibérie (Lac Baïkal ; Peck *et al.*, 1996), de Finlande (Lac Pohjajärvi ; Saarinen, 1998), de Suède (lacs Sarsjön et Frängsjön ; Snowball et Sandgren, 2002) et d'Amérique du Nord (Lac Leboeuf, Pennsylvanie, USA ; King *et al.*, 1983 et Lac Pepin, Minnesota, USA ; Brachfeld et Banerjee, 2000). D'une part, la résolution temporelle, de l'ordre de 1 échantillon à tous ~150 ans dans le cas du Lac Baikal, est donc insuffisante pour déceler les variations de très haute férquence. D'autre part, dans le cas des enregistrements des lacs Pohjajärvi et Leboeuf, la série chronologique ne dépasse pas 4000 ans BP. Or, afin de déterminer la variabilité (locale, régionale et globale) de l'intensité du champ magnétique terrestre durant l'Holocène, il est donc indispensable d'examiner plusieurs enregistrements sédimentaires continus avec la plus haute résolution temporelle possible. Pour ce premier thème, nous tenterons de répondre aux trois questions suivantes : 1) quel a été le comportement de la composante non-dipolaire du champ magnétique durant l'Holocène dans l'est du Canada ? 2) quelle fut l'échelle de temps des variations de la composante dipolaire du champ magnétique terrestre durant l'Holocène ? 3) quelle a été

l'influence des variations de l'intensité du champ magnétique terrestre sur le taux de production des isotopes cosmogéniques durant l'Holocène ?

Chronostratigraphie holocène des séquences sédimentaires de l'est du Canada

La datation et la corrélation de différentes séquences sédimentaires sont indispensables pour déterminer les variations d'intensité et d'orientation du champ magnétique terrestre, mais aussi pour la reconstruction des variations climatiques ou environnementales. Rappelons-le, l'avantage de l'utilisation de sédiments holocènes est la possibilité de leur datation par la méthode du ^{14}C. L'Holocène est aussi une période pour laquelle, grâce aux mesures de ^{14}C dans les cernes de croissance des arbres, il a été possible de convertir les âges ^{14}C conventionnels en âges calendaires et ainsi de tenir compte des variations du rapport $^{14}C/^{12}C$ dans le temps (Stuiver *et al.*, 1998).

Tel que mentionné ci-dessus, les variations d'intensité et d'orientation du champ magnétique terrestre permettent des corrélations locales, régionales ou globales. Par exemple, les études récentes de Saarinen (1999) et Kotilainen *et al.* (2000) indiquent qu'il est possible de corréler des séquences sédimentaires en utilisant les variations d'orientation du champ magnétique terrestre avec une précision supérieure à 50 ans. Par ailleurs, Stoner *et al.* (2000) démontrent qu'il est possible de corréler les fluctuations millénaires du taux de production d'isotopes cosmogéniques déterminées à partir de carottes de glace groenlandaises et les variations de la PIR d'une carotte sédimentaire de l'Atlantique Nord. Or, si les variations de plus haute fréquence ($\leq 10^3$ ans) de l'intensité du champ magnétique

terrestre se révélaient globales, des corrélations entre les variations de la PIR et le taux de production d'isotopes cosmogéniques tels le ^{14}C et le ^{10}Be seraient envisageables. Ceci permettrait la synchronisation des enregistrements sédimentaires avec la chronologie de la carotte de glace GISP2 (Meese *et al.*, 1994) et/ou avec la dendrochronologie de Stuiver *et al.* (1998), qui sont considérées comme les deux meilleures chronologies holocènes (Sarnthein *et al.*, 2002).

L'examen des propriétés magnétiques couplé avec des datations au ^{14}C sera ainsi utilisée pour l'établissement d'une chronostratigraphie holocène des séquences sédimentaires de l'estuaire du St-Laurent. À l'aide des courbes des variations de la PIR et du taux de production des isotopes cosmogéniques tels que le ^{10}Be et le ^{14}C, nous tenterons également de comparer cette chronostratigraphie avec la chronologie de la carotte de glace GISP2 (Meese *et al.*, 1994) et la dendrochronologie de Stuiver *et al.* (1998). De plus, les variations d'intensité et d'orientation du champ magnétique terrestre pourraient servir ici à établir, par corrélation avec des séquences bien datées, une chronostratigraphie pour les sédiments du fjord du Saguenay qui sont difficiles à dater par la méthode du ^{14}C à cause d'une importante dissolution des fossiles carbonatés (St-Onge *et al.*, 1999; Leduc, 2001).

Traceurs sédimentologiques et magnétiques des variations climatiques décennales à millénaires dans le fjord du Saguenay et l'estuaire du St-Laurent au cours l'Holocène

Les exemples d'événements climatiques ou hydrologiques extrêmes sont abondants durant la dernière décennie. Au Canada, ils incluent notamment les crues spectaculaires de la rivière Saguenay (Québec), en 1996, et de la rivière Rouge (Manitoba), en 1997. L'augmentation prévue des émissions de gaz à effet de serre au cours des prochaines décennies laisse supposer que la fréquence et l'amplitude de ces événements extrêmes augmenteront (IPCC, 2001). Mais, aucune démonstration univoque de cette hypothèse n'a encore été faite, principalement à cause du manque de données climatiques fiables sur la variation naturelle du climat à des échelles de temps excédant les données instrumentales. L'accès à des archives géologiques ayant une résolution temporelle annuelle à décennale permettrait d'identifier les événements extrêmes survenus au cours des derniers millénaires et ainsi de déterminer la fréquence "naturelle" des événements extrêmes durant l'Holocène : une donnée essentielle pour comprendre l'effet des activités anthropiques sur le climat. Pour pallier ce manque de connaissance de la variabilité "naturelle" du climat, dans l'est du Canada, un projet pluridisciplinaire dont l'objectif principal était d'établir un enregistrement holocène des variations climatiques décennales à millénaires dans l'estuaire du St-Laurent et le fjord du Saguenay a été mis sur pied grâce à un financement du Fonds d'action pour les changements climatiques (FACC), puis suivi dans le cadre d'un projet de la Fondation canadienne pour les sciences du climat et de l'atmosphère (FCSCA). Le développement de traceurs sédimentologiques et magnétiques des variations climatiques

que l'on présente ici s'insère dans le cadre de ce projet pluridisciplinaire. La problématique des deux sites sélectionnés, soit le Fjord du Saguenay et l'estuaire du St-Laurent, sera maintenant abordée.

Le fjord du Saguenay

Le fjord du Saguenay est caractérisé par de puissantes séquences sédimentaires (Syvitski et Praeg, 1989 ; Praeg et Syvitski, 1991) mises en place avec des vitesses de sédimentation de l'ordre 0,2 à 7 cm/an (Smith et Walton, 1980; Zhang, 2000). De telles vitesses de sédimentation résultent en une séquence holocène exédant 100 m d'épaisseur dans certaines parties du fjord (Syvitski et Praeg, 1989 ; Praeg et Syvitski, 1991). De plus, au cours des derniers siècles, le fjord du Saguenay a été affecté par de fréquents événements accidentels. Ils incluent notamment les tremblements de terre de 1663 et de 1988, les glissements de terrain de Kénogami, en 1924, et de Saint-Jean-Vianney, en 1971, ainsi que la crue exceptionnelle de 1996. Plusieurs études ont révélé la présence de dépôts de plusieurs centimètres, voire plusieurs mètres, dans le bassin supérieur du fjord et dans la baie des Ha!Ha! associés à ces événements accidentels (Locat et Leroueil, 1988; Perret *et al.*, 1995; Smith et Walton, 1980; Schafer et Smith, 1987, 1988; Syvitski et Schafer, 1996; Syvitski et Praeg, 1989; Praeg et Syvitski, 1991; St-Onge *et al.*, 1999; St-Onge et Hillaire-Marcel, 2001). Ces dépôts sont généralement constitués d'une argile silteuse facilement identifiable par sa couleur gris pâle et son homogénéité qui diffèrent fortement de celles des

sédiments beaucoup plus foncés et « bioturbés » mis en place sous des conditions plus stables. La base sableuse de tels dépôts accidentels peut être mise en évidence par des pics de susceptibilité magnétique et de densité (St-Onge et Hillaire-Marcel, 2000). L'analyse à maille serrée des propriétés magnétiques des sédiments d'une longue carotte sédimentaire prélevée dans le fjord du Saguenay, en parallèle avec des analyses sédimentologiques et physiques (granulométrie, réflectance et rayons-X) effectuées dans des intervalles ciblés, seront ainsi entrepris dans le but d'identifier des couches accidentelles, de déterminer les mécanismes de dépôt ainsi que les fréquences respectives des différents types d'événements accidentels survenus au cours de l'Holocène.

L'estuaire du St-Laurent

L'estuaire du St-Laurent se caractérise également par de puissantes séquences sédimentaires holocènes (Syvitski et Praeg, 1989; Praeg et Syvitski, 1991) mises en place avec des vitesses de sédimentation variant de 0,3 à 0,7 cm/an (Jennane, 1992 ; Smith et Schafer, 1999 ; Zhang, 2000). De telles vitesses de sédimentation ont ainsi permis la reconstruction, à partir des assemblages de kystes de dinoflagellés, des conditions estivales de la masse d'eau de surface de l'estuaire du St-Laurent (température, salinité et couvert de glace) au cours du dernier siècle avec une résolution temporelle d'environ 2 ans (Mekireche-Telmat, 1997). Ces reconstructions montrent des fluctuations importantes de la température et de la salinité, variant respectivement de 9 à 16°C et de 25 à 30. L'analyse

spectrale de ces oscillations révèle des cycles compatibles avec ceux de l'oscillation nord-atlantique (Cook, 2003 et références incluses).

L'oscillation nord-atlantique (*North Atlantic Oscillation*-NAO) est maintenant reconnue comme un phénomène atmosphérique récurrent très marquant aux moyennes et hautes latitudes de l'Hémisphère Nord. Des changements de température et de précipitation observés sur de vastes régions de l'Atlantique, l'Amérique du Nord, l'Arctique, l'Eurasie et la Méditerranée sont maintenant associés à la NAO (Hurrell *et al.*, 2003). La NAO est définie par un indice qui représente la différence de pression atmosphérique au niveau de la mer entre les Açores et l'Islande (Van Loon et Rogers, 1979). Un indice positif correspond à de forts vents d'ouest et des tempêtes hivernales plus importantes au-dessus de l'Atlantique Nord. Les hivers sont alors doux et pluvieux en Europe du Nord et plus froids dans le nord du Canada et au Groenland (Hurrel, 1995). Un indice négatif correspond à une diminution des vents d'ouest traversant, avec une trajectoire plus mériodionale, l'Atlantique Nord. La Méditerranée reçoit ainsi de l'air plus chaud et humide, alors que l'Europe du Nord connaît des conditions plus sèches et froides.

Les données instrumentales ainsi que des reconstitutions de l'indice de la NAO obtenues à partir de cernes de croissance d'arbres, de carottes de glace et de coraux ont permis de mettre en évidence la variabilité temporelle de la NAO. La NAO varie selon des cycles de 7 à 25 ans (Cook *et al.*, 2003 et références incluses), mais aussi à plus basse fréquence selon des cycles de 54 à 68 ans (Lutherbacher et al., 1999) et de 80 à 90 ans (Appenzeller, 1998). Toutefois, les reconstructions de la NAO remontent rarement au-delà

des derniers 400 ans, exceptionnellement des derniers 600 ans (Cook et al., 2003), ce qui est insuffisant pour déterminer la variabilité "naturelle" de ce phénomène.

Objectifs

Dans le cadre des trois thèmes exposés ci-dessus, les objectifs principaux de la présente thèse sont les suivants :

1. Reconstruire les variations d'intensité et d'orientation du champ magnétique terrestre au cours de l'Holocène dans l'est du Canada avec une résolution temporelle de l'orde de la décennie ;
2. Établir une chronostratigraphie holocène pour les séquences sédimentaires de l'est du Canada ;
3. Identifier et déterminer la fréquence des événements accidentels (crues, glissements de terrain et séismes) durant l'Holocène dans le fjord du Saguenay ;
4. Développer des traceurs sédimentologiques et/ou magnétiques des variations climatiques décennales à millénaires telle la NAO dans l'estuaire du St-Laurent.

Afin d'atteindre ces objectifs, les propriétés magnétiques, sédimentologiques et physiques de plusieurs carottes sédimentaires ont été analysées à maille serrée. Les résultats sont présentés et discutés dans les trois prochains chapitres. Ceux-ci ont été rédigés en Anglais sous forme d'articles scientifiques et prennent ainsi la forme exigée par

les revues à comité de lecture où ils sont parus ou sont appelés à paraître. Le premier chapitre intitulé : *Holocene paleomagnetic records from the St. Lawrence Estuary, eastern Canada: centennial- to-millennial-scale geomagnetic modulation of cosmogenic isotopes* a été publié dans la revue *Earth and Planetary Science Letters* (v. 209, p. 113-130). Dans cet article, nous avons d'abord établi une chronostratigraphie pour les derniers 8500 ans dans l'est du Canada. Nous avons ensuite reconstitué les variations d'orientation et d'intensité du champ magnétique terrestre en portant une attention particulière à l'influence des variations d'intensité sur le taux de production des isotopes cosmogéniques.

Le deuxième chapitre intitulé : *Earthquake and flood-induced turbidites in the Saguenay Fjord (Québec): a Holocene paleoseismicity record* est maintenant sous presse dans la revue *Quaternary Science Reviews*. Dans cet article, à partir des propriétés magnétiques, physiques et sédimentologiques des sédiments d'une longue séquence sédimentaire, nous avons identifié et déterminé le mécanisme de dépôt de plusieurs couches accidentelles mises en place en cours des derniers 7 200 ans dans le fjord du Saguenay.

Le dernier chapitre intitulé : *Decadal-scale precipitation variations in the Great Lakes/St. Lawrence River watershed as revealed by a 800-year paleodischarge proxy record* sera, quant à lui, soumis à la revue *Geology* ou *Marine Geology*. Dans cet article, nous avons développé un traceur sédimentologique du débit printannier du fleuve St-Laurent pour les derniers 800 ans.

Ma contribution aux trois articles est d'abord soulignée par le fait que je suis le premier auteur de chacun d'eux, ayant réalisé la majeure partie de leur rédaction.

Toutefois, j'ai bénéficié des infrastructures et de la supervision du Dr. Joseph Stoner (Université de Californie, Davis - maintenant à l'INSTAAR) pour les aspects paléomagnétiques ainsi que du Dr. David Piper (Commission géologique du Canada, Atlantique) et du Dr. Thierry Mulder (Université de Bordeaux 1) pour les aspects sédimentologiques. Par ailleurs, dans le dernier article, j'ai utilisé les températures de surface reconstituées par le Professeure Anne de Vernal (UQÀM). L'ensemble du programme analytique et d'échantillonnage ainsi que la rédaction des trois articles ont été supervisés par mon directeur de thèse, le Professeur Claude Hillaire-Marcel (UQÀM). En terminant, toutes les données brutes ont été compilées et gravées sur un disque compact qui est placé à la fin de la présente thèse.

Références

Ali, M., Oda, H., Hayashida, A., Takemura, K., et Torii, M. 1999. Holocene paleomagnetic secular variation at Lake Biwa, Central Japan. Geophysical Journal International, **136** : 218-228.

Appenzeller, C., Stocker, T.F., et Anklin, M. 1998. North Atlantic Oscillation dynamics recorded in Greenland ice cores. Science, **282** : 446-449.

Bard, E. 1998. Geochemical and geophysical implications of the radiocarbon calibration. Geochimica et Cosmochimica Acta, **62** : 2025-2038.

Bard, E., Raisbeck, G.M., Yiou, F., Jouzel, J. 1997. Solar modulation of cosmogenic nuclide production over the last millennium: comparison between C-14 and Be-10 records. Earth and Planetary Science Letters, **150** : 453-462.

Barton, C.E., et McElhinny, M.W. 1981. A 10000 yr geomagnetic secular variation record from three Australian maars. Geophysical Journal of the Royal Astronomical Society, **67** : 465-485.

Bond, G., Kromer, B., Beer, J., Muscheler, R., Evans, M.N., Showers, W., Hoffmann, S., Lotti-Bond, R., Hajdas, I., et Bonani, G. 2001. Persistent solar influence on North Atlantic climate during the Holocene. Science, **294** : 2130-2136.

Brachfeld, S., et Banerjee, S.K. 2000. A new high-resolution geomagnetic relative paleointensity record for the North American Holocene: A comparison of sedimentary and absolute intensity data. Journal of Geophysical Research, **105** : 821-834.

Buffett, B.A. 2000. Earth's Core and the Geodynamo. Science, **288** : 2007-2012.

Channell, J.E.T., Stoner, J.S., Hodell, D.A., et Charles, C. 2000. Geomagnetic paleointensity for the last 100 kyr from the subantarctic South Atlantic: a tool for inter-hemispheric correlation. Earth and Planetary Science Letters, **175** : 145-160.

Clark, P.U., Marshall, S.J., Clarke, G.K.C., Hostetler, S.V., Licciardi, J.M., Teller, J.T. 2001. Freshwater forcing of abrupt climate change during the last glaciation. Science, **293** : 283-287.

Constable, C.G., et McElhinny, M.W. 1985. Holocene geomagnetic secular variation records from north-eastern Australian lake sediments. Geophysical Journal of the Royal Astronomical Society, **81** : 103-120.

Cook., E.R. 2003. Multi-proxy reconstruction of the North Atlantic Oscillation (NAO) index: a critical review and a new well-verified winter NAO index reconstruction back to AD 1400. *in* The North Atlantic Oscillation Climatic Significance and Environmental Impact, J.W. Hurrel *et al.* (Éds.), American Geophysical Union, Geophysical Monograph, **134** : 63-79.

Creer, K.M. 1981. Long-period geomagnetic secular variations since 12,000 yr BP. Nature, **292** : 208-212.

Creer, K.M., et Tucholka, P. 1982. Secular variation as recorded in lake sediments: a discussion of North American and European results. Philosophical Transactions of the Royal Society of London, Series A, **306** : 87–102.

Creer, K.M., Valencio, D.A., Sinito, A.M., Tucholka, P., et Vilas, J.F.A. 1983. Geomagnetic secular variations 0-14,000 yr. B.P. as recorded by lake sediments from Argentina. Geophysical Journal of the Royal Astronomical Society, **74** : 199–221.

Dormy, E., Valet, J.P., et Courtillot, V. 2000. Numerical models of the geodynamo and observational constraints. Geochemistry Geophysics Geosystems, **1** : article numéro 200GC000062.

Dunlop, D.J., et Özdemir, Ö. 1997. Rock Magnetism Fundamentals and Frontiers. Cambridge University Press, Cambridge.

Elsaesser, W., Ney, E.P., et Winckler, J.R. 1956. Cosmic-ray intensity and geomagnetism. Nature, **178** : 1226-1227.

Glatzmeier, G.A., et Roberts, P.H. 1995. A three-dimensional self-consistent computer simulation of a geomagnetic field reversal. Nature, **377** : 203-209.

Glatzmeier, G.A., et Roberts, P.H. 1996. Rotation and Magnetism of Earth's Inner core. Science, **274** : 1887-1891.

Guyodo, Y., et Valet, J.P. 1996. Relative variations in geomagnetic intensity from sedimentary records-the past 200,000 years. Earth and Planetary Science Letters, **143**: 23-46.

Guyodo, Y., et Valet, J.P. 1999. Global changes in intensity of the Earth's magnetic field during the past 800 kyr. Nature, **399** : 249-252.

Hagstrum, J.T., et Champion, D.E. 2002. A Holocene paleosecular variation record from ^{14}C-dated volcanic rocks in western North America. Journal of Geophysical Research, **107** : *10.1029/2001JB000524*.

Hurrel, J.W., Kushnir, Y., Ottersen, G., and Visbeck, M., 2003, An overview of the North Atlantic Oscillation, *in* Hurrel, J.W., *et al.*, éds., The North Atlantic Oscillation Climatic Significance and Environemental Impact. American Geophysical Union, Geophysical Monograph, **134** : 1-35.

Hurrel, J.W. 1995. Decadal Trends in the North Atlantic Oscillation: Regional Temperatures and Precipitation. Science, **269** : 676-679.

Hongre, L., Hulot, G., et Khokhlov, A. 1998. An analysis of the geomagnetic field over the past 2000 years. Physics of the Earth and Planetary Interiors, **106** : 311-335.

IPCC. 2001. Summary for Policymakers. A report of working group I of the International Panel on Climate Change. Cambridge University Press, Cambridge.

Jennane, A. 1992. Application de la méthode du plomb-210 dans l'estuaire maritime et le golfe du St-Laurent. Taux de sédimentation, flux et modes d'ablation. Mémoire de maîtrise, UQÀM, Montréal.

Katari, K., Tauxe, L., et King, J. 2000. A reassessment of post-depositional remanent magnetism: preliminary experiments with natural sediments. Earth and Planetary Science Letters, **183** : 147-160.

Katari, K., et Bloxham, J. 2001. Effects of sediment aggregate size on DRM intensity: a new theory. Earth and Planetary Science Letters, **186** : 113-122.

King, J.W., Banerjee, S.K., Marvin, J.A., et Lund, S.P. 1983. Use of small amplitude paleomagnetic fluctuations for correlation and dating of continental climate changes. Palaeogeography, Palaeoclimatology, Palaeoecology, **42** : 167–183.

Kotilainen, A.T., Saarinen, T., et Winterhalter, B. 2000. High-resolution paleomagnetic dating of sediments deposited in the central Baltic Sea during the last 3000 years. Marine Geology, **166** : 51-64.

Leduc, J. 2001. Étude des populations de foraminifères benthiques dans les sédiments du Fjord du Saguenay. Mémoire de maîtrise, UQÀM, Montréal.

Locat, J., et Leroueil, S. 1988. Physical and geotechnical characteristics of recent Saguenay Fjord sediments. Canadian Geotechnical Journal, **25** : 382-388.

Lund, S.P. 1996. A comparison of paleomagnetic secular variation records from North America. Journal of Geophysical Research, **101** : 8007-8024.

Luterbacher, J., Schmutz, C., Gyalistras, D., Xoplaki, E., et Wanner, H. 1999. Reconstruction of monthly NAO and EU indices back to AD 1675. Geophysical Research Letters, **26** : 2745-2748.

Maher, B.A., et Thompson, R. (Éds.) 1999. Quaternary Climates, Environments and Magnetism. Cambridge University Press, Cambridge.

McElhinny, M.W., et Senanayake, W.E. 1982. Variations in the Geomagnetic Dipole 1: The past 50,000 years. Journal of Geomagnetism and Geoelectricity, **34** : 39-51.

McElhinny, M.W., et McFadden, P.L. 2000. Paleomagnetism. Academic Press, San Diego.

Meese, D.A., Alley, R.B., Fiacco, R.J., Germani, M.S., Gow, A.J., Grootes, P.M., Illing, M., Mayewski, P.A., Morrison, M.C., Ram, M., Taylor, K.C., Yang, Q., et Zielinski, G.A. 1994. Preliminary depth-age scale of the GISP2 ice core: Special CRREL Report **94-1**.

Mekireche-Telmat, R. 1997. Contenu palynologique et flux microfloristiques récents dans l'estuaire maritime du Saint-Laurent. Mémoire de maîtrise, UQÀM, Montréal.

Merrill, R.M., McElhinny, M., et McFadden, P. 1996. The magnetic field of the Earth: paleomagnetism, the core and the deep mantle. Academic Press, San Diego.

Muscheler, R., Beer, J., Wagner, G., Finkel, R.C. 2000. Changes in deep-water formation during the Younger Dryas event inferred from ^{10}Be and ^{14}C records. Nature, **408** : 567-570.

Peck, J.A., King, J.W., Colman, S.M., et Kravchinsky, V.A. 1996. A 84-kyr paleomagnetic record from the sediments of Lake Baikal. Journal of Geophysical Research, **101** : 11365-11385.

Perret, D., Locat, J., et Leroueil, S. 1995. Strength development with burial in fine-grained sediments from the Saguenay Fjord. Canadian Geotechnical Journal **32** : 247-262.

Praeg, D.B., et Syvitski, J.P.M. 1991. Marine geology of the Saguenay Fjord. Geological Survey of Canada, Open File, **2395**.

Reynolds, R.L., et King, J.W. 1995. Magnetic records of climate change. Reviews of Geophysics, **33**, supplément (rapport IUGG) : 101-110.

Roberts, A.P., Lehman, B., Weeks, R.J., Verosub, K.L., et Laj, C. 1997. Relative paleointensity of the geomagnetic field over the last 200,000 years from ODP Sites 883 and 884, North Pacific : A record of global paleointensity variations ? Earth and Planetary Science Letters, **152** : 11-23.

Saarinen, T. 1998. High-resolution paleosecular variation in northern Europe during the last 3200 years. Physics of the Earth and Planetary Interiors, **106** : 299-309.

Saarinen, T. 1999. Palaeomagnetic dating of Late Holocene sediments in Fennoscandia. Quaternary Science Review, **18** : 889-897.

Sarnthein, M., Kennett, J.P., Allen, J.R.M., Beer, J., Grootes, P., Laj, C., MacManus, J., et Ramesh, R. 2002. Decadal-to-millennial-scale climate variability-chronology and mechanisms: summary and recommendations. Quaternary Science Reviews, **21** : 1121-1128.

Schafer, C.T., et Smith, J.N. 1988. Evidence of the occurrence and magnitude of terrestrial landslides in recent Saguenay fjord sediments. *in* Natural and Man-Made Hazards, M.I. El-Sabh et T.S. Murty. (Éds.), D. Reidel, Dordrecht, p. 137-145.

Schafer, C.T., et Smith, J.N. 1987. Hypothesis for submarine landslide cohesionless sediment flows resulting from a 17th-century earthquake-triggered landslide in Quebec, Canada. Geo-Marine Letters **7** : 31-37.

Smith, J.N., et Walton, A. 1980. Sediment accumulation rates and geochronologies measured in the Saguenay Fjord using Pb-210 dating method. Geochimica et Cosmochimica Acta, **44** : 225-240.

Smith, J.N., et Schafer, C.T. 1999. Sedimentation, bioturbation and Hg uptake in the sediments of the Estuary and Gulf of St. Lawrence. Limnology and Oceanography, **44** : 207-219.

Snowball, I., et Sandgren, P. 2002. Geomagnetic field variations in the northern Sweden during the Holocene quantified from varved lake sediments and their implications for cosmogenic nuclide production rates. The Holocene, **12**: 517-530.

Stoner, J.S., Laj, C., Channell, J.E.T., et Kissel, C. 2002. South Atlantic and North Atlantic geomagnetic paleointensity stacks (0-80 ka): implications for inter-hemispheric correlation. Quaternary Science Reviews, **21** : 1141-1151.

Stoner, J.S., Channell, J.E.T., Hillaire-Marcel, C., et Kissel, C. 2000. Geomagnetic paleointensity and environmental record from Labrador Sea core MD99-2024: global marine sediment and ice core chronostratigraphy for the last 110 kyr. Earth and Planetary Science Letters, **183** : 161-177.

Stoner, J.S., Channell, J.E.T., et Hillaire-Marcel, C. 1995. Late Pleistocene relative geomagnetic paleointensity from the deep Labrador Sea: Regional and global correlations. Earth and Planetary Science Letters, **134** : 237-252.

St-Onge, G., Leduc, J., Bilodeau, G., de Vernal, A., Devillers, R., Hillaire-Marcel, C., Loucheur, V., Marmen, S., Mucci, A., et Zhang, D. 1999. Caractérisation des sédiments récents du fjord du Saguenay à partir de traceurs physiques, géochimiques, isotopiques et micropaléontologiques. Géographie physique et Quaternaire, **53** : 339-350.

St-Onge, G., et Hillaire-Marcel, C. 2000. Inventaire des couches accidentelles récentes dans le fjord du Saguenay à partir des propriétés physiques de carottes de forages. 53^{e} conférence canadienne de géotechnique, Montréal. Comptes-rendus de la conférence : 145-151.

St-Onge, G., et Hillaire-Marcel, C. 2001. Isotopic constraints on sedimentary inputs and organic carbon burial rates in the Saguenay Fjord, Quebec. Marine Geology, **186** : 1-22.

Stuiver, M., Reimer, P.J., Bard, E., Beck, J.W., Burr, G.S., Hughen, K.A., Kromer, B., McCormac, G., Van der Plicht, J., et Spurk, M. 1998. INTCAL98 radiocarbon age calibration, 24,000-0 cal BP. Radiocarbon, **40** : 1041-1083.

Syvitski, J.P.M., et Praeg, D.B. 1989. Quaternary sedimentation in the St. Lawrence Estuary and adjoining areas, Eastern Canada: An overview based on high-resolution seismo-stratigraphy. Géographie physique et Quaternaire, **43** : 291-310.

Syvitski, J.P.M., et Schafer, C.T. 1996. Evidence for earthquake-triggered basin collapse in Saguenay Fjord, Canada. Sedimentary Geology, **104** : 127-153.

Tauxe, L. 1993. Sedimentary records of relative paleointensity: theory and practice. Reviews of Geophysics, **31** : 319–354.

Tauxe, L., et Shackleton, N.J. 1994. Relative palaeointensity records from the Ontong-Java Plateau. Geophysical Journal International, **117** : 769–782.

Tauxe, L. 1998. Paleomagnetic Principles and Practice. Kluwer Academic Publishers, Dordrecht, Hollande.

Teanby, N., et Gubbins, D. 2000. The effects of aliasing and lock-in process on paleosecular variation records from sediments. Geophysical Journal International, **142** : 563-570.

Thompson, R., et Oldfield, F. 1986. Environmental Magnetism. Allen and Unwin, Londres.

Tric, E., Valet, J.-P., Tulcholka, P., Paterne, M., Labeyrie, L., Guichard, F., Tauxe, L., et Fontugne, M. 1992. Paleointensity of the geomagnetic field during the last 80,000 years. Journal of Geophysical Research B: Solid Earth, **97** : 9337–9351.

van Geel, B., Raspopov, O.M., Renssen, H., van der Plicht, J., Dergachev, V.A., Meijer, H.A.J. 1999. The role of solar forcing upon climate change. Quaternary Science Reviews, **18** : 331-338.

van Loon, H., et Rogers, J.C. 1978. The seasaw in winter temperatures between Greenland and Northern Europe : part I, General description. Monthly Weather Review, **106** : 296-310.

Verosub, K.L., Mehringer Jr., P.J., et Waterstraat, P. 1986. Holocene secular variation in western North America: paleomagnetic record from Fish Lake, Harney County, Oregon. Journal of Geophysical Research B: Solid Earth, **91** : 3609–3623.

Weeks, R., Laj, C., Endignoux, L., Fuller, M., Roberts, A., Manganne, R., Blanchard, E., et Goree, W. 1993. Improvements in long-core measurement techniques: applications in palaeomagnetism and palaeoceanography. Geophysical Journal International, **114** : 651–662.

Yamazaki, T., et Ioka, N. 1994. Long-term secular variation of the geomagnetic field during the last 200 kyr recorded in sediment cores from the western equatorial Pacific. Earth and Planetary Science Letters, **128** : 527–544.

Yang, S., Odah, H., et Shaw, J. 2000. Variations in the geomagnetic dipole moment over the last 12 000 years. Geophysical Journal International, **140** : 158-162.

Yongjae, Y., et Dunlup, J. 2000. Archemagnetism of Ontario potsherds from the last 2000 years. Journal of Geophysical Research, **105** : 19 419-19 433.

Zhang, D., 2000. Fluxes of short-lived radioisotopes in the marginal marine basins of Eastern Canada. Thèse de doctorat. UQÀM, Montréal, Québec.

CHAPITRE II

HOLOCENE PALEOMAGNETIC RECORDS FROM THE ST. LAWRENCE ESTUARY, EASTERN CANADA: CENTENNIAL- TO MILLENNIAL-SCALE GEOMAGNETIC MODULATION OF COSMOGENIC ISOTOPES

Guillaume St-Onge[1,*], Joseph S. Stoner[b,c] and Claude Hillaire-Marcel[a]

Publié dans *Earth and Planetary Science Letters* (2003), 209, 113-130

[1] Centre de recherche en géochimie et géodynamique (GEOTOP-UQÀM-McGILL), Université du Québec à Montréal, Case postale 8888, Succursale Centre-Ville, Montréal, Québec, H3C 3P8, Canada, Tel: 514-987-4630, Fax: 514-987-3635.
[b] Department of Geology, University of California, Davis, CA 95616, USA.
[c] Now at: Institute of Arctic and Alpine Research (INSTAAR), University of Colorado, Boulder, CO 80309-0450, USA.
* *E-mail address*: guillaume_st-onge@inrs-ete.uquebec.ca (G. St-Onge), now at INRS-ETE, C.P. 7500, Ste-Foy, Québec, G1V 4C7, Canada

Abstract

Two long Holocene piston cores (MD99-2220 and MD99-2221) were raised from the St. Lawrence Estuary, Eastern Canada because of the expanded Holocene sediment sequence this location provides. A u-channel based paleomagnetic study, supported by an accelerator mass spectrometry (AMS) ^{14}C chronology, rock-magnetic and sedimentological data, indicates that these sediments provide a paleomagnetic directional paleosecular variation (PSV) and relative paleointensity (RPI) proxy records for the last ~8500 cal BP. Sedimentation rates vary from ~1.2 to 4.2 m/kyr. Comparison of inclination and declination features with other North American Holocene PSV records are generally consistent and temporal offsets are within chronological uncertainties. The normalized natural remanent magnetization intensity record, a RPI proxy, from the postglacial sediments of core 2220 compares favorably with North American and European Holocene RPI records at millennial and even some centennial timescales. Comparisons between core 2220 RPI proxy with the ^{10}Be flux record from the Greenland Summit (GISP2) ice core [Finkel and Nishiizumi, J. Geophys. Res. 102 (1997) 26699-26706] and a ^{14}C production rate record [Bond et al., Science 294 (2001) 2130-2136] suggest that geomagnetic modulation may control the millennial- and even some centennial-scale variability within cosmogenic isotope records. This implies that core 2220 RPI record reflects changes in global scale geomagnetic field at these timescales.

Keywords: paleomagnetism, paleointensity, secular variations, Holocene, cosmogenic isotopes

1. Introduction

Its has long been known that the magnetic remanence preserved within geological and archeological materials provides the only archive from which observations on the past behavior of Earth's magnetic field can be made beyond historical times (e.g., [1] and references therein). Our knowledge and understanding of the temporal characteristics of the geodynamo, the source of most of the Earth's magnetic field, is based on these observations constrained by detailed knowledge of the historical field [e.g., 2]. Though dating has always been problematic, it is clear that patterns of Holocene directional variability determined from continuously deposited sediments show variability with periods between 1–2 kyr that display regionally consistent secular variation patterns, but with distinct departures between regions [3]. In contrast, our knowledge of geomagnetic intensity during the Holocene (paleointensity) is less well constrained, regional variability is not expressly known, and archeomagnetically derived estimates of the global dipole moment [e.g., 4, 5, 6] indicate variability with much longer periods than observed from the directional record. However, recent relative paleointensity studies from Pleistocene sediments suggest that global variations may occur at millennial timescales [7].

It is well established that the geomagnetic field shields the Earth from cosmic rays, and that variation in its strength is one of the control on the production rate of cosmogenic isotopes such as ^{10}Be, ^{14}C and ^{36}Cl [8-11]. Cosmogenic isotope records have been used to infer solar [12-14] and thermohaline circulation variability [15], based on the assumption that the geomagnetic field only affects the low frequency part of the record. Yet, as our

understanding of the geomagnetic field behaviour is incomplete, the inferences drawn from these cosmogenic isotope studies could be misleading. In fact, the frequency at which the geomagnetic field intensity stops affecting the production rate of cosmogenic isotopes has never been documented and is therefore an open question for debate.

Here we address some of these issues using a pair of new high-resolution Holocene sediment records from the St. Lawrence Estuary. Located at the transition from the St. Lawrence River to the Gulf of St. Lawrence (Fig. 1), the St. Lawrence Estuary offers a unique archive for paleo-reconstructions from Eastern Canada as recent sedimentation rates vary from about 2 to more than 5 m/kyr [16-17]. These rates allow the recovery and study of sedimentary sequences with decadal to millennial-scale temporal resolution. The successful coring of several high-resolution (>1 m/kyr) Holocene sedimentary sequences, during the IMAGES-V (International Marine Past Global Change Study) oceanographic campaign, in July 1999, on board the *Marion Dufresne II*, offers a unique opportunity to reconstruct Earth's geomagnetic field variations at a temporal resolution rarely matched. We present u-channel-based paleomagnetic records (inclination, declination and relative paleointensity) from cores MD99-2220 and MD99-2221 (hereinafter referred to as cores 2220 and 2221). Comparisons are made to paleomagnetic records from North America and Europe, and to cosmogenic isotope reconstructions from tree rings and ice cores.

3. Geological setting

Cores 2220 (latitude/longitude: 48°38.32N/68°37.93W, water depth 320 m, length 51.6 m) and 2221 (latitude/longitude: 48°10.60N/69°30.35W, water depth 212 m, length 31.0 m) were raised from the Laurentian Channel, a long U-shaped glaciated valley with depths between 200-540 m, in the St. Lawrence Estuary (Fig. 1). Previous work based on high-resolution seismo-stratigraphy and piston cores has defined the tills, glaciomarine sediments and postglacial muds that comprise the regional stratigraphy of the area for the Late Pleistocene to Holocene [18-19]. In recent sediments, fine grained, greenish-grey muds are observed on the deep central parts of the Laurentian Channel, whereas sandy muds are present on the sides and lower slopes as well as on the headward parts of the Laurentian Channel [20].

4. Methods

Low-field volumetric magnetic susceptibility (k) was measured on board the *Marion Dufresne II* using a GEOTEK™ MSCL (Multi Sensor Core Logger) instrument at 2 cm intervals. On shore, the archive halves were sampled using u-channels (rigid u-shaped plastic liners with a square 2-cm cross-section and a length of 1.5 m). The u-channel samples were measured in the Paleomagnetism Laboratory at the University of California in Davis (UCD), using a 2-G Enterprises™ Model 755 cryogenic magnetometer, at 1 cm intervals. However, the width at half-height of the response function of the magnetometer

pick-up coils is ~4.5 cm [21], so that smoothing occurs. Edge effects caused by this smoothing at core breaks was cut from the final data. The natural remanent magnetization (NRM) was studied by progressive alternating field (AF) demagnetization using peak fields of 0, 10, 15, 20, 25, 30, 35, 40, 45 and 50 mT. An anhysteretic remanent magnetization (ARM) was produced using a 100 mT peak AF and a 50 μT direct current (DC) biasing field. This ARM was subsequently demagnetized and measured after peak AF of 0, 20, 25, 30, 35, 40 and 50 mT. The ARM data was also expressed as a susceptibility of the ARM (k_{ARM}) by normalizing the ARM by the strength of the biasing field. Two isothermal remanent magnetizations (IRM) were produced by imparting a DC field of 0.3 T and 1 T. Each IRM was demagnetized and measured at the same peak AF as the ARM. These IRMs were used to construct an S-ratio proxy by dividing the IRM after 30 mT AF demagnetization (IRM_{30mT}) at 0.3 T by the IRM_{30mT} at 1 T. This differs from the classic S-ratio, as defined by Stober and Thompson [22], where after the sample is given an IRM at 1 T, it is given an IRM at 0.3T in reversed orientation. Though our S-ratio proxy deviates from the classical S-ratio and the values are slightly different, the information derived is similar. By using the S-ratio proxy at an AF demagnetization level of 30 mT, the relative importance of the high coercivity component is emphasized. Hysteresis parameters were measured on both cores at 1.5 m intervals using a Princeton Measurements™ alternating gradient magnetometer (MicroMag) at UCD. The saturation magnetization (M_s), saturation remanence (M_{rs}) and the coercive force (H_c) were obtained from hysteresis loops. The coercivity of the remanence (H_{cr}) was determined by backfield experiments. The ratios M_{rs}/M_s and H_{cr}/H_c reflect magnetic grain size and domain state [23].

Grain size measurements on core 2220 were made using a Coulter Counter™ TAII analyzer at the Geological Survey of Canada (Atlantic). Grain size measurements on core 2221 were made on a Fritsch™ Analysette 22 laser diffraction analyzer at the INRS-ETE in Québec City.

5. Stratigraphy

A box core (AH00-2220) containing the sediment water interface was collected from the sampling site of core 2220 in order to evaluate sediment losses due to piston coring. The top ~60 cm of core 2220 organic carbon and $^{13}C_{org}$ contents can be correlated to the box core record, impliying that only the top 14 cm of core 2220 were lost during coring (EPSL Online Background Dataset, Fig. 1a). The top of core 2221 can be correlated to core 2220 using the IRM_{30mT} 0.3T, (EPSL Online Background Dataset, Fig. 1b), suggesting that a similar amount of sediment was lost from core 2221.

Detailed visual description of the cores along with the rock-magnetic and mean grain size data allow the identification of two lithologic units. Unit 1 is observed from the base to 1497 cm in core 2220 (Fig. 2) and from the base to 1353 cm in core 2221 (Fig. 3). Unit 1 consists of grey to dark grey laminated to massive clays, equivalent to the blue-grey, stiff, massive to laminated clays reported in the Estuary by Syvitski and Praeg [18] and to the dark grey to brown clayey mud with faint laminations of Josenhans and Lehman [19] in the Gulf of St. Lawrence. Based on prior work in the region [18-19], we interpret unit 1 to

represent the deposition of glaciomarine sediments from glaciofluvial plumes discharged from the retreating Laurentide Ice Sheet.

Unit 2 is observed from 1497 cm to the top of core 2220 (Fig. 2) and from 1353 cm to the top of core 2221 (Fig. 3). It is composed of dark grey bioturbated silty clays and dark grey bioturbated sandy mud in cores 2220 and 2221, respectively. These bioturbated sediments represent postglacial conditions and are equivalent to the organic-rich bioturbated mud and sands previously reported in the region [18-20]. The postglacial sediments are the focus of this paper.

The transition from unit 1 to unit 2 is very sharp and suggests a major reorganization of Laurentide Ice sheet meltwater routes. The best candidate for this drastic facies change is the major drainage event that occurred at ~7.7 kyr BP or 8.47 cal kyr BP [24] when the rapid collapse of ice in Hudson Bay allowed lakes Agassiz and Ojibway to drain catastrophically into the Labrador Sea through the Hudson Strait, consequently reducing meltwater discharge through the St. Lawrence Estuary. The environmental and climatological interpretation of both lithostratigraphic units will be addressed in a separate paper.

6. Initial chronology

Twenty benthic mollusk shells from cores 2220 and 2221 were sampled and sent for accelerator mass spectrometry (AMS) ^{14}C dating at the IsoTrace laboratory in Toronto (Table 1). The dates are reported using Libby's half-life and corrected for natural and

sputtering fractionation ($\delta^{13}C$ = -25‰ VPDB). To convert the ^{14}C ages to calendar years, the dates were calibrated using CALIB 4.3 [25], assuming a standard reservoir correction of -400 years [26]. In order to compare our results with previous published paleomagnetic records, mostly derived from uncalibrated ^{14}C dates on lacustrine bulk sediments or terrestrial carbon, our data is also reported in reservoir corrected ^{14}C years. An initial age model was constructed for each core (EPSL Online Background Dataset, Fig. 2) by assuming a constant sedimentation rate between the dated material presented in Table 1. These age models reveal similar sediment accumulation rate pattern for both cores. The first ~8500 cal BP are characterized by sedimentation rates ranging from 1.2 to 4.2 m/kyr, whereas the older sediments were deposited at rates possibly higher than 34 m/kyr.

The use of a standard marine reservoir correction of 400 years is supported by the following evidence. First, if we retain the reservoir corrected date of 7570±70 yr BP at 1454 cm in core 2220 and interpolate a sedimentation rate of 0.42 cm/yr from 1454 to 1497 cm (Online Background Data set, Fig. 2), then the transition from unit 1 to unit 2 falls within 30 years of the ~7.7 kyr BP proposed by Barber et al. [24] for the catastrophic drainage of Lake Agassiz. Second, the available calculated reservoir correction for Eastern Canada, which were derived from fish otoliths collected off Newfoundland [27] and a marine pelecypod from Georges Bank (near Nova Scotia) [28], yielded ages of 370±29 and 369±26 years, respectively (CALIB 4.3 on-line database). Third, by using sedimentation rates estimated from ^{210}Pb measurements on box core AH00-2220 (Online Background Dataset, Fig. 3) and interpolated from core 2220 ^{14}C data (Online Background Dataset, Fig. 2), we can determine the age of the uppermost dated pelecypod from the core 2220. This is

done by adding the missing 14 cm of sediment to the depth where the pelecypod was sampled (75 cm) and by applying ^{210}Pb derived sedimentation rates of 0.74 cm/yr from 0-20 cm, 0.28 cm/yr from 20-30 cm and the ^{14}C derived sedimentation rate of 0.15 cm/yr from 30-89 cm. This exercise yields an age of 456 years for the pelecypod horizon compared to the ^{14}C age of 980±50 years, suggesting a reservoir correction of 524 years. These comparisons show that a reservoir correction of 400 years is probably reasonable for the St. Lawrence Estuary during the Holocene. However, considering the offset of ~125 years for the last 1 kyr BP, the assumption of a constant reservoir correction, counting uncertainties inherent to the AMS ^{14}C dating method and interpolation errors, an uncertainty of ±200 years is a reasonable estimate for our age models. Worth noting is that the two-step increase in sedimentation rate from 0.15 to 0.28 cm/yr and finally to 0.74 cm/yr are consistent with the agricultural development linked to the European settlement in Eastern Canada, and the industrial development of the second half of the 20th century [29].

7. Natural remanent magnetization (NRM)

Online Background Dataset Figure 4 shows typical NRM demagnetization behavior of the postglacial sediments from cores 2220 and 2221. Little viscous remanence is observed, and when present, is generally removed by 10 mT peak AF demagnetization. The average NRM intensity prior to demagnetization is 0.07 ± 0.02 A/m which is reduced by 80% on average after 50 mT peak AF demagnetization. In both cores, most samples exhibit a strong stable single component magnetization with medium destructive field (MDF)

between 20 and 30 mT. NRM component directions (Online Background Dataset, Fig. 5) were calculated by principal component analysis [30] using 4 to 9 AF demagnetization steps at peak fields of 10-50 mT. Maximum angular deviation (MAD) values are generally less than 2° and 6° in cores 2220 and 2221, respectively, indicating well defined characteristic remanent magnetization directions (Online Background Dataset, Fig. 5). Except from 1.5 to 5 m in core 2221, the inclination values of the postglacial sediments of both cores are close to the expected inclination (66°) for the coring sites latitude based on a geocentric axial dipole (GAD) model. Due to the lack of azimuthal orientation, the declination of each core section was rotated to fit the end of the overlying core section. The resulting mean declination of the composite record was then set to zero.

8. Magnetic mineralogy and grain size

Mean S-ratio proxy values of core 2220 postglacial sediments are ~ 0.95 (Fig. 2) while ranging from ~0.85 to ~0.95 in core 2221 (Fig. 3). This indicates that much of the magnetic assemblage is saturated at 0.3 T, suggesting magnetite is the dominant magnetic mineral. The slightly lower S-ratio proxy values in core 2221 indicate a higher proportion of high coercivity minerals. It should be noted that the S-ratio proxy was derived from IRM data AF demagnetized at 30 mT and therefore is more sensitive to high coercivity minerals than a standard S-ratio. The shape of the hysteresis loops (Online Background Dataset, Fig. 6), and the hysteresis ratios are consistent with a dominant low coercivity ferrimagnetic component (most likely magnetite) that is of pseudo-single domain (PSD) magnetic grain

size in core 2220 and a coarser assemblage with at least some multi-domain (MD) magnetite in core 2221 (Online Background Dataset, Fig. 7).

9. Construction of a composite record

8.1. IRM correlation

Visual identification of similar lithologic features, best defined from IRM_{30mT} 0.3T downcore profiles of cores 2220 and 2221, provided an initial step toward deriving a common depth-scale for these records (Figs. 2 and 3). Using the common features and core 2220 as the reference series (EPSL Online Background Dataset, Fig. 8), we constructed a new depth-scale for core 2221 with AnalySeries 1.2 software [31] and linear interpolation between correlative features. The adjusted depth scale (Fig. 4) results in a correlation of $r = 0.53$.

8.2. Inclination and declination correlation

Comparison of the component inclination and declination profiles of both cores show offsets that suggest the composite depth-scale could be improved. Figure 5a shows correlative inclination and declination features used jointly to visually adjust the composite depth record without violating any of the rock-magnetic derived stratigraphic constraints. The final tuning was achieved by linear interpolation between correlative features.

Component inclination and declination records from the two cores show many similarities (Fig. 5b). However, inconsistencies are also observed. High amplitude fluctuations within the upper ~150 cm of core 2220 suggest that these sediments could have been disturbed during coring. Another difference between the two records is seen between ~700 to 950 cm, where the data of core 2221 show high frequency variations not observed in core 2220. Maximum MAD values (Online Background Dataset, Fig. 5), coarser magnetic and physical grain sizes (Fig. 3) along with the high frequency variability lead us to suspect that coring deformation may have affected this interval. Because of its strong stable component magnetization (indicated by lower MAD values) and its finer magnetic and physical grain sizes, we believe that core 2220 preserves a more accurate paleomagnetic record.

10. Composite age model

Using the new composite depth-scale for core 2221 (Fig. 5b), we transferred the depths of the AMS ^{14}C dated material of core 2221 to their correlative depths in core 2220 (Table 1). This results in 13 AMS ^{14}C dates within the studied interval (Fig. 6). An age model was constructed from the AMS ^{14}C dates using a third order polynomial fit (r^2=0.996) in the postglacial sediments. A similar age model was also constructed from the uncalibrated, but reservoir corrected ^{14}C dates reported in Table 1 (EPSL Online Background Dataset, Fig. 9).

11. Eastern Canada Holocene paleomagnetic secular variation record

Figure 7 shows the inclination and declination records of core 2220 on the ^{14}C age model presented in EPSL Online Background Dataset Figure 9 along with North American paleomagnetic secular variation (PSV) records from Lake St. Croix [32] and Lake Pepin (Minnesota, USA) [33], Fish Lake (Oregon, USA) [34] and with a recent compilation of lava flows from the western United States [35]. Comparable inclination and declination patterns are observed in all records suggesting that core 2220 preserves Holocene PSV. All the inclination and declination features, as numbered by Lund [36], are recognized. Except for inclination feature 2, these features are temporally consistent between core 2220 and the records from Minnesota (Lake St. Croix and Lake Pepin), from ~850 to 5000 yr BP. Prior to 5000 yr BP, declination features such as 12 and 13 and inclination features such as 10 and 11 in core 2220 are as much as 500 yrs younger than those of the Minnesota lakes. In the first ~5000 yr BP, as previously observed by Hagstrum and Champion [35], the Fish Lake record is systematically older by 280 yrs.

The origin of these temporal offsets between similar features could be due to time transgressive patterns within the directional records (drifting of non-dipole features), different lock-in depths and/or dating inaccuracies. The ^{14}C age models of the various records were derived based on the dating of different material with different techniques (AMS on marine carbonates for cores 2220 and 2221, beta counting on bulk carbon for Lake St.Croix and Fish Lake records, beta counting on terrestrial carbon for the lava flows, constant sedimentation rate and tuning of the inclination record for the Lake Pepin record).

A common problem with radiocarbon dating of bulk carbon from lacustrine sediments is contamination by "old" carbon [3]. This was suggested for the Lake St. Croix record, where Lund and Banerjee [32] systematically subtracted 980 yrs to every date to correct for "old" carbon contamination, even though the consistency of such a contamination is unlikely [37]. Since much of the chronology of Lake Pepin was derived by correlating its inclination record to that of Lake St. Croix, the same potential chronological offset apply. Contamination by "old" carbon was also suggested by Hagstrum and Champion [35] to account for the ~280 yrs offset between the Fish Lake record and the lava flows for the last ~3500 yr BP (Fig. 7). On the other hand, AMS ^{14}C dating of marine carbonates avoids "old" carbon contamination, but often suffer from an unknown dissolved organic carbon reservoir age, that if improperly corrected [26], would lead to errors in the age determination. Furthermore, in all the North American records, the sedimentation rates were assumed constant or estimated with a polynomial fit between the dated material or tie points, leading to another possible source of error. Because of the different dating technique used and the different quality of the chronologies established for the North American records, the offsets between directional features are well within dating uncertainties.

12. Eastern Canada Holocene relative paleointensity record

11.1. Estimation of relative paleointensity

Criteria have been proposed by King et al. [38] and Tauxe [39] to assess the reliability of sediments to record paleointensity variations. These suggest that magnetic concentration variations should not exceed one order of magnitude, the remanence should be carried by stable magnetite in the PSD grain size range, and that the normalized remanence record should not be coherent with the bulk rock-magnetic parameter used for normalization. In previous sections, we have shown that the postglacial sediments of cores 2220 and 2221 were characterized by a strong stable, single component magnetization. The concentration variations in the postglacial sediments, as indicated by k, ARM_{30mT} and IRM_{30mT} values, vary by a factor less than 4, 5 and 4 respectively in core 2220 and less than 4, 6 and 4 respectively in core 2221. The remanence is most likely carried by PSD magnetite assemblage in core 2220 and a coarser PSD to MD magnetite assemblage in core 2221. Because of its coarse grain size, core 2221 is probably not suitable for paleointensity studies. We normalized the NRM_{30mT} of core 2220 by k, ARM_{30mT} and IRM_{30mT} and tested the coherence between these RPI proxies and their normalizers using AnalySeries 1.2 [31] between 750 and 8500 cal BP. Significant coherence above the 95 % confidence limit is observed for both k and ARM_{30mT} normalization, but is significantly reduced when using IRM_{30mT} (Fig. 8). The NRM/IRM ratios show almost identical variations at different demagnetization levels (Fig. 9a), suggesting a similar coercivity spectrum for NRM and

IRM. Therefore, we use the average of three IRM normalizations (20, 30 and 40 mT) as our preferred RPI proxy (Fig. 9b).

Figure 10 shows the power spectra of the inclination, declination and RPI records and the coherence between environmentally sensitive magnetic parameters (k, k_{ARM}/k and ARM_{30mT}) and core 2220 RPI proxy to evaluate the effect of environmental factors on the RPI record. Most of the power in the RPI record is distributed in a relatively sharp band centered at a period of ~1250 yrs along with a broader band centered at a period of ~420 yrs (Fig. 10a). At those two periods, the RPI proxy is not coherent with any of the environmentally sensitive magnetic parameters, implying that much of core 2220 RPI record is free of environmental overprints and may therefore be geomagnetic in origin (Fig. 10b). Coherence above the 95% confidence level is occasionally observed between RPI and environmentally sensitive magnetic parameters, but at higher and lower frequencies than the ones observed in the RPI power spectrum (Fig. 10). No correlation (r=-0.033) between the mean grain size and the RPI records of core 2220 is observed (Online Background Dataset Fig. 10). Similarly, declination has significant power at the period of ~1250 yrs. Spectral power around a period of ~1250 yrs has been previously reported for Holocene declination records (Online Background Dataset Table 1) from North America, South America, Europe and Australia [40-42], suggesting a possible global geomagnetic signal with a possible link between geomagnetic intensity and directional changes.

11.2. Comparison with other North American paleointensity records

Figure 11 shows how the RPI record from core 2220 compares with similar records from Lake Pepin [33] and Lake St. Croix [43], Minnesota (USA) and from Lake LeBoeuf [38], Pennsylvania (USA). The three RPI records are similar in shape and amplitude from ~850 to ~3700 yr BP (Fig. 11b) with a maximum reached around ~2250 yr BP, which is also consistent with global absolute paleointensity estimates derived from archeological material and lava flows [4-6]. Common millennial to sub-millennial-scale features are found in all three sedimentary RPI records (Fig. 11b), suggesting a possible common geomagnetic origin. However, significant differences are observed from ~4500 to ~ 7000 yr BP (Fig. 11a), where a long-term decrease in core 2220 and in the Lake St. Croix records is matched by a long-term increase in the Lake Pepin record. Such a decrease is also observed in Holocene absolute paleointensity estimates [4-6], supporting core 2220 and Lake St. Croix RPI records in that time interval.

Core 2220 RPI record also compares favorably (r=0.67, Online Background Dataset Fig. 11a) with a Finnish lake RPI record derived from varved sediments [44]. Coherence above the 95% confidence level between the two RPI records is observed over a wide range of frequencies including at the period of ~1250 years (Online Background Dataset Fig. 11b), extending the spatial domain of coherent millennial-scale RPI variations.

11.3. Centennial- to millennial-scale modulation of cosmogenic isotopes (^{10}Be and ^{14}C)

Long period geomagnetic modulation of cosmogenic isotopes production rates in the atmosphere has been demonstrated by Mazaud et al. [45] by comparing a Mediterranean derived RPI record [46] with the ^{10}Be data from the Vostok ice core. Several studies have also revealed negative correlations between marine RPI records and cosmogenic isotopes [47-50]. Stoner et al. [7] demonstrated that millennial-scale variations in the flux of cosmogenic isotopes in the GRIP/GISP2 ice cores could be correlated at a global scale to high-resolution marine RPI records. Recently, Snowball and Sandgren [51] showed that a calculated cosmogenic nuclide production rate derived from a Swedish varved lacustrine RPI record could be correlated to the Δ^{14}C tree ring data [25] at millennial timescales during most of the Holocene. These correlations imply changes in the global scale geomagnetic field because the shielding occurs in space far beyond the atmosphere [52]. Similar correlations between core 2220 RPI and cosmogenic isotope production rates should provide a means of assessing whether the high frequency variations observed here reflect variations in the global scale field.

In Figure 12, we compared core 2220 RPI record with the inversed ^{10}Be flux record of the GISP2 ice core from 3300 to 8000 cal BP, the extent of the Holocene ^{10}Be data. The nuclide flux record was calculated with the ^{10}Be concentrations and age model from Finkel and Nishiizumi [53] and by using the Johnsen et al. [54] accumulation rate as suggested by R. Muscheler [pers. com.]. Figure 12a illustrates the correlation ($r = -0.49$) between core 2220 RPI record and the ^{10}Be flux from the GISP2 ice core. This correlation can be further improved ($r = -0.63$) by tuning core 2220 record to the GISP2 record (Fig. 12b), where most of the adjustments are less than 150 years from the original chronology. A maximum

tuning of ~200 years was performed from ~5750 to 6000 cal BP (Online Background Dataset Fig. 12a).

Variations in atmospheric ^{14}C production rate are also related to changes in the strength of Earth's magnetic field [8-11]. Unlike ^{10}Be, atmospheric radiocarbon concentrations are affected by the carbon cycle, which must be accounted for when deriving a ^{14}C production rate record [11]. Moreover, agreement between ^{10}Be and $\Delta^{14}C$ records during the Holocene was used to argue that the changes in the ^{10}Be flux record reflect variations in the global production rate rather than changes in climate [15]. To further assess if the centennial- to millennial-scale RPI variations from core 2220 could be due to global scale changes in geomagnetic field intensity, we compared core 2220 RPI record with the inversed smoothed ^{14}C production rate presented by Bond et al. [14], which was derived from the $\Delta^{14}C$ in tree rings [25] and corrected for marine and terrestrial effects using a four-box carbon cycling model (see [14] for details) from 750 to 8 500 cal BP. A negative correlation of $r = -0.47$ is observed between the two records (Fig. 13), which can be improved to $r = -0.65$ by tuning core 2220 to the ^{14}C production rate record (EPSL Online Background Dataset, Fig. 13). Again, the maximum age adjustments are < 200 years from the original chronology and within the chronological uncertainty of core 2220 (Online Background Dataset Fig. 12b). This can be taken one step further, by comparing core 2220 RPI record, on the tuned chronology, with the unsmoothed ^{14}C production rate where common centennial-scale variability is found in both records (EPSL Online Background Dataset, Fig. 14).

13. Discussion

Based on our present understanding of the geomagnetic role in cosmogenic isotope modulation [e.g., 52, 55], the inverse correlation between the ^{10}Be flux and ^{14}C production rate records with the RPI record suggests that these variations, and therefore the RPI record from core 2220, are reflecting changes in the global scale geomagnetic field. Coherence above the 95% confidence level is observed between core 2220 RPI record and the ^{10}Be flux and the ^{14}C production rate records (Fig. 14) at or very close to the periods of ~1250 and 420 yrs, supporting the geomagnetic origin of those two periods. The similarity between the spectral power in declination and RPI further supports the geomagnetic origin of the RPI signal, but also hints at an alternative possibility where large scale (though not global) features such as the Northern Hemisphere flux patches [e.g., 56-57] could be driving this variability. In either case, if core 2220 RPI record truly reflects changes in Earth's magnetic field intensity, then the assumption that millennial- and even some centennial-scale variations within the cosmogenic isotope production rate records are solely a function of solar variability [e.g., 12-15] may have to be re-examined.

Bond et al. [14] showed that changes in drift-ice proxies within North Atlantic deep-sea cores correlate with changes in the production rate of cosmogenic nuclides (^{10}Be and ^{14}C) during the Holocene. Based on the assumption that nuclide production rates reflect solar variability (e.g., [58]), it was suggested that North Atlantic's millennial scale climate variations were influenced and perhaps forced by solar changes [14]. The data presented here show that the geomagnetic field may be the cause of these cosmogenic

nuclide changes and therefore might play a role in climate, though a correlation between Bond's et al. [14] North Atlantic drift-ice proxy and core 2220 RPI record is only tentative (Online Background Dataset Fig. 15). A connection between cosmic rays and climate, mostly via changes in the cloud condensation nuclei abundance [59-61], is presently being debated [59-65] and provides a possible mechanism by which geomagnetic field intensity may affect climate at centennial to millennial timescales.

14. Acknowledgments

We wish to sincerely thank K. Verosub for the use of his lab at the University of California, Davis. We also thank S. Brachfeld, S.P. Lund, J.T. Hagstrum, G. Bond, R. Muscheler and A. Ojala for generously sharing their data. We are in debt to the captain, officers, crew and scientific participants of Legs 1 and 2 of the IMAGES-V cruise. Thanks are also due to E. Cagnat and B. Long for grain size analyses on core 2221. We also thank D.J.W. Piper, J.E.T. Channell, and C. Laj for their comments on an earlier version of the manuscript and G. Bond, C. Bourlès and an anonymous reviewer for constructive reviews. This study was supported by the IMAGES and the Climate System History and Dynamics (CSHD) programs and by the Canadian Climate Action Fund (CCAF). GS was supported by postgraduate scholarships from NSERC, le Fonds québécois de la recherche sur la nature et les technologies, Natural Resources Canada and by Fisheries and Oceans Canada. Laboratory work at UCDavis and J.S.S. contribution were supported by NSF OCE-9911698.

15. References

[1] K.M. Creer, P. Tucholka, C.E. Barton (Eds.), Geomagnetism of baked clays and sediments, Elsevier, Amsterdam, 1983, pp. 324.

[2] R. Merrill, M. McElhinny, P. McFadden, The magnetic field of the Earth, Academic Press, San Diego, 1996. pp. 531.

[3] R. Thompson, ^{14}C dating and magnetostratigraphy, Radiocarbon 25 (1983) 229-238.

[4] M.W McElhinny, W.E. Senanayake, Variations in the geomagnetic dipole 1, the past 50 000 years, J. Geomag. Geoelectr. 34 (1982) 39-51.

[5] N. Teanby, D. Gubbins, The efects of aliasing and lock-in processes on palaeosecular variation records from sediments, Geophys. J. Int. 142 (2000) 563-570.

[6] S. Yang, H. Odah, J. Shaw, Variations in the geomagnetic dipole moment over the last 12 000 years, Geophys. J. Int. 140 (2000) 158-162.

[7] J.S. Stoner, J.E.T. Channell, C. Hillaire-Marcel, C. Kissel, Geomagnetic paleointensity and environmental record from Labrador Sea core MD95-2024: global marine sediment and ice core chronostratigraphy for the last 110 kyr, Earth Planet. Sci. Lett. 183 (2000) 161-177.

[8] W. Elsaesser, E.P. Ney, J.R. Winckler, Cosmic-ray intensity and geomagnetism, Nature 178 (1956) 1226-1227.

[9] D. Lal, B. Peters, Cosmic ray produced radioactivity on the Earth, In: S. Flügge (Ed.), Handbook of physics 46 (2), Springer, Berlin, 1967, pp.551-612.

[10] D. Lal, Theoretically expected variations in the terrestrial cosmic-ray production rates of isotopes, Soc. Ital. Fis. Bologna 95 (1988) 216-233.

[11] E. Bard, Geochemical and geophysical implications of the radiocarbon calibration, Geochimi Cosmochimi Acta 62 (1998) 2025-2038.

[12] E. Bard, G.M. Raisbeck, G.M. Yiou, J. Jouzel, Solar modulation of cosmogenic nuclide production over the last millennium: comparison between C-14 and Be-10 records, Earth and Planet. Sci. Lett. 150 (1997) 453-462.

[13] B. van Geel, O.M. Raspopov, H. Renssen, J. van der Plicht, V.A. Dergachev, H.A.J. Meijer, The role of solar forcing upon climate change, Quat. Sci. Rev. 18 (1999) 331-338.

[14] G. Bond, B. Kromer, J. Beer, R. Muscheler, M.N. Evans, W. Showers, S. Hoffmann, R. Lotti-Bond, I. Hajdas, G. Bonani, Persistent solar influence on North Atlantic climate during the Holocene, Science 294 (2001) 2130-2136.

[15] R. Muscheler, J. Beer, G. Wagner, R.C. Finkel, Changes in deep-water formation during the Younger Dryas event inferred from ^{10}Be and ^{14}C records, Nature, 408 (2000) 567-570.

[16] J.N. Smith, C.T. Schafer, Sedimentation, bioturbation and Hg uptake in the sediments of the Estuary and Gulf of St. Lawrence, Limnol. Oceanogr. 44 (1999) 207-219.

[17] D. Zhang, Fluxes of short-lived radioisotopes in the marginal marine basins of Eastern Canada, Ph.D. thesis, UQÀM, Montréal, 2000, pp. 193.

[18] J.P.M. Syvitski, D.B. Praeg, Quaternary sedimentation in the St. Lawrence Estuary and adjoining areas, Eastern Canada: An overview based on high-resolution seismo-stratigraphy, Géogr. Phys. Quat. 43 (1989) 291-310.

[19] H. Josenhans, S. Lehman, Late glacial stratigraphy and history of the Gulf of St. Lawrence, Canada, Can. J. Earth Sci. 36 (1999) 1327-1345.

[20] D.H. Loring, D.J.G. Nota, Morphology and Sediments of the Gulf of St. Lawrence, Bull. Fish. Res. Board Can. 182, 1973, pp. 147.

[21] R. Weeks, C. Laj, L. Endignoux, M. Fuller, A. Roberts, R. Manganne, E. Blanchard, W. Goree, Improvements in long-core measurement techniques: applications in palaeomagnetism and palaeoceanography, Geophys. J. Int. 114 (1993) 651–662.

[22] J.C. Stober, R. Thompson, Magnetic remanence acquisition in Finnish lake sediments, Geophys. J. R. Astron. Soc. 57 (1979) 727-739.

[23] R. Day, M. Fuller, V.A. Schmidt, Hysteresis properties of titanomagnetites: grain-size compositional dependence, Phys. Earth Planet. Inter. 13 (1977) 260-267.

[24] D.C. Barber, A. Dyke, C. Hillaire-Marcel, A.E. Jennings, J.T. Andrews, M.W. Kerwin, G. Bilodeau, R. McNeely, J. Southon, M.D. Morehead, J.-M. Gagnon, Forcing of the cold event of 8,200 years ago by catastrophic drainage of Laurentide lakes, Nature 400 (1999) 344-348.

[25] M. Stuiver, P. J. Reimer, E. Bard, J. W. Beck, G.S. Burr, K. A. Hughen, B. Kromer, G. McCormac, J. van Der Plicht, M. Spurk, INTCAL98 radiocarbon age calibration, 24,000-0 cal BP, Radiocarbon 40 (1998) 1041-1083.

[26] E. Bard, Correction of AMS ^{14}C ages measured in planktonic foraminifera: paleoceanographic implications, Paleoceanography 3 (1988) 635-645.

[27] S.E. Campana, Use of radiocarbon from nuclear fallout as a dated marker in the otoliths of haddock *Melanogrammus aeglefinus*, Mar. Eco. Progr. Ser. 150 (1997) 49-56.

[28] C.R.Weidman, G.A. Jones, A shell-derived time history of bomb ^{14}C on Georges Bank and its Labrador Sea Implications, J. Geophys. Res. 98 (1993) 14577-14588.

[29] A. de Vernal, C. Hillaire-Marcel, B. Ghaleb, G. St-Onge, J. Leduc, V. Loucheur, D. Zhang, A. Gamache-Rochette, F. Saucier, High frequency climate oscillations in the lower St. Lawrence estuary during the last millenia, EURESCO meeting, 2001, Abstract volume.

[30] J.L. Kirschvink,. The least-squares line and plane and the analysis of paleomagnetic data, Geophys. J. R. Astron. Soc., 62 (1980) 699-718.

[31] D. Paillard, L. Labeyrie, P. Yiou, Macintosh program performs time-series analysis, Eos Trans. AGU, 77 (1996) 379.

[32] S.P. Lund, S.K. Banerjee, Late Quaternary paleomagnetic field secular variation from two Minnesota Lakes, J. Geophys. Res. 90 (1985) 803-825.

[33] S. Brachfeld, S.K Banerjee, A new high-resolution geomagnetic relative paleointensity record for the North American Holocene: A comparison of sedimentary and absolute intensity data, J. Geophys. Res. 105 (2000) 821-834.

[34] K.L. Verosub, P.J. Mehringer Jr., P. Waterstraat, Holocene secular variation in western North America: paleomagnetic record from Fish Lake, Harney County, Oregon, J. Geophys. Res. 91 (1986) 3609–3623.

[35] J.T. Hagstrum, D.E. Champion, A Holocene paleosecular variation record from ^{14}C-dated volcanic rocks in western North America, J. Geophy. Res. 107 (2002) 10.1029/2001JB000524.

[36] S.P. Lund, A comparison of paleomagnetic secular variation records from North America, J. Geophys. Res. 101 (1996) 8007-8024.

[37] J.K. Child, A. Werner, Evidence for a hardwater radiocarbon dating effect, Wonder Lake, Denali National Park and Preserve, Alaska, U.S.A., Géogr. Phys. Quat. 53 (1999) 407-411.

[38] J.W. King, S.K. Banerjee, J.A. Marvin, A new rock magnetic approach to selecting sediments for geomagnetic paleointensity studies: application to paleointensity for the last 4000 years, J. Geophys. Res. 88 (1983) 5911–5921.

[39] L. Tauxe, Sedimentary records of relative paleointensity: theory and practice, Rev. Geophys. 31 (1993) 319–354.

[40] K.M. Creer, P. Tucholka, On the current state of lake sediment palaeomagnetic research, Geophys. J. R. Astron. Soc. 74 (1983) 223-238.

[41] C. Itota, M. Hyodo, K. Yaskawa, Long-term features of drifting and standing non-dipole field as determined from Holocene secular variations, Geophys. J. Int. 130 (1997) 390-404.

[42] C.S.G. Gogorza, A.M. Sinito, J.F. Vilas, K.M. Creer, H. Nunez, Geomagnetic secular variations over the last 6500 years as recorded by sediments from lakes of south Argentina, Geophys. J. Int. 143 (2000) 787-498.

[43] S.P. Lund, M. Schwartz, Environmental factors affecting geomagnetic field palaeointensity estimates from sediments, In: B.A. Maher, R. Thompson (Eds.), Quaternary Climates, Environments and Magnetism, Cambridge University Press, Cambridge, 1999, pp. 323-351.

[44] A. Ojala, T. Saarinen, Palaeosecular variation of the Earth's magnetic field during the last 10 000 years based on the annually laminated sediment of Lake Nautajärvi, central Finland, The Holocene 12 (2002) 391-400.

[45] A. Mazaud, C. Laj, M. Bender, A geomagnetic chronology for Antarctic ice accumulation, Geophys. Res. Lett. 21 (1994) 337-340.

[46] E. Tric, J.-P. Valet, P. Tulcholka, M. Paterne, L. Labeyrie, F. Guichard, L. Tauxe, M. Fontugne, Paleointensity of the geomagnetic field during the last 80,000 years, J. Geophys. Res. 97 (1992) 9337-9351.

[47] M. Frank, B. Schwarz, S. Baumann, P.W. Kubik, M. Suter, A. Mangini, A 200 kyr record of cosmogenic radionuclide production rate and geomagnetic field intensity from ^{10}Be in globally stacked deep-sea sediments, Earth Planet. Sci. Lett. 149 (1997) 121-129.

[48] S. Baumgartner, J. Beer, J. Masarik, G. Wagner, L. Meynadier, H.-A. Synal, Geomagnetic Modulation of the ^{36}Cl Flux in the GRIP Ice Core, Greenland, Science 279 (1998) 1330-1332.

[49] C. Laj, C. Kissel, A. Mazaud, J.E.T. Channell, J. Beer, North Atlantic paleointensity stack since 75 ka (NAPIS-75) and the duration of the Laschamp event. Philos, Trans. R. Soc. Ser. A 358 (2000) 1009-1025.

[50] G. Wagner, J. Beer, C. Laj, C. Kissel, J. Masarik, R. Muscheler, H.-A. Synal, Chlorine-36 evidence for the Mono Lake event in the Summit GRIP ice core, Earth Planet. Sci. Lett 181(2000) 1-6.

[51] I. Snowball, P. Sandgren, Geomagnetic field variations in northern Sweden during the Holocene from varved lake sediments and their implications for cosmogenic nuclide production rates, The Holocene 12 (2002) 517-530.

[52] J. Beer, R. Muscheler, G. Wagner, C. Laj, C. Kissel, P.W. Kubik, H.-A. Synal, Cosmogenic nuclides during Isotope Stages 2 and 3, Quat. Sci. Rev. 21 (2002) 1129-1139.

[53] R.C. Finkel, K. Nishiizumi, Beryllium 10 concentrations in the Greenland Ice Sheet Project 2 ice core from 3 to 40 ka, J. Geophys. Res. 102 (1997) 26699-26706.

[54] S.J. Johnsen, D. Dahl-Jensen, W, Dansgaard, N. Gundestrup, Greenland palaeotemperatures derived from the GRIP bore hole temperature and ice core isotope profiles, Tellus 47B (1995) 624-629.

[55] G. Wagner, C. Laj, J. Beer, C. Kissel, R. Muscheler, J. Masarik, H.-A. Synal, Reconstruction of the paleoaccumulation rate of central Greenland during the last 75 kyr using the cosmogenic radionuclides ^{36}Cl and ^{10}Be and geomagnetic field intensity data, Earth Planet. Sci. Lett. 193 (2001) 515-521.

[56] A. Jackson, A.R.T. Jonkers, Four centuries of geomagnetic secular variations from historical records, Phil. Trans. R. Soc. Lond. A 358 (2000) 957-990.

[57] C. G. Constable, C.L. Johnson, S. Lund, Global geomagnetic field models for the past 3000 years: transient or permanent flux lobes?, Phil. Trans. R. Soc. Lond. A 358 (2000) 991-1008.

[58] J. Masarik, J. Beer, Simulation of particle fluxes and cosmogenic nuclide production in the Earth's atmosphere, J. Geophys. Res. 104 (1999) 12099-13012.

[59] N. Marsh, H. Svensmark, Low cloud properties influenced by cosmic rays, Phys. Rev. Lett. 85 (2000) 5004-5007.

[60] N. Marsh, H. Svensmark, Cosmic rays, clouds and climate, Space Sci. Rev. 94 (2000) 215-230.

[61] F. Yu, Altitude variations of cosmic ray induced production of aerosols: Implications for global cloudiness and climate, J. Geophy. Res. 107 (2002) 10.1029/2001JA000248.

[62] H. Svensmark, H., E. Friis-Christensen, Variation of cosmic ray flux and global cloud coverage-a missing link in solar-climate relationships, J. Atmos. Sol. Terr. Phys. 59 (1997) 1225-1232.

[63] G. Wagner, D.M. Livingstone, J. Masarik, R. Muscheler, J. Beer, Some results relevant to the discussion of a possible link between cosmic rays and the Earth's climate J. Geophy. Res. 106 (2001) 3381-3387.

[64] B. Sun, S. Bradley, Solar influences on cosmic rays and cloud formation: A reassessment, J. Geophy. Res. 107 (2002) 10.1029/2001JD000560.

[65] K.S. Carslaw, R.G. Harrison, J. Kirkby, Cosmic rays, clouds, and climate, Science 298 (2002) 1732-1737.

[66] J. Shaw, P. Gareau, R.C. Courtney, Palaegeography of Atlantic Canada 13-0 kyr, Quat. Sci. Rev. 21 (2002) 1861-1878.

[67] S.J. Blott, K. Pye, Gradistat: A grain size distribution and statistics package for the analysis of unconsolidated sediments, Earth Surf. Proces. Landf. 26 (2001) 1237-1248.

Table 1
Radiocarbon dates from cores 2220 and 2221

Depth (cm)	Composite depth (cm)[a]	AMS ^{14}C Age (yr BP)	Corrected AMS ^{14}C Age (yr BP)[b]	Calibrated Age (cal BP)[c]	Dated material	IsoTrace Lab number
Core 2220						
*41		1020±50	620±50	545 (614) 641	*Lacuna pallidula*	TO-8759
75		980±50	580±50	523 (551) 620	*Portlandia lenticula*	TO-8760
318-319		2290±50	1890±50	1838 (1891) 1947	Mollusc shell	TO-8761
*521.5		640±50	240±50	259 (282) 309	Pelecypod valve	TO-8762
586-587		3930±60	3530±60	3826 (3897) 3977	*Astarte striata*	TO-8763
647		4270±60	3870±60	4293 (4392) 4435	*Nuculana sp.*	TO-8764
1119-1120		7140±70	6740±70	7557 (7602) 7662	Pelecypod valve	TO-8765
1454		7970±70	7570±70	8355 (8401) 8481	*Portlandia lenticula*	TO-8766
4535		8730±70	8330±70	9169 (9283) 9426	Pelecypod valve	TO-8767
Core 2221						
50-51	40.9	540±50	140±50	106 (151) 259	*Macoma balthica*	TO-8748
95-96	91.3	960±50	560±50	513 (540) 606	*Nuculana pernula*	TO-8749
225	258.8	1830±60	1430±60	1299 (1357) 1418	*Mytilus edulis*	TO-8750
363	486.1	2810±60	2410±60	2444 (2549) 2690	Pelecypod valve	TO-8751
615	771.6	4720±100	4320±100	4827 (4946) 5065	*Yoldia myalis*	TO-8752
755	927	5630±60	5230±60	5928 (5989) 6174	Mollusc shell	TO-8753
*980.5	1081.5	3470±90	3070±90	3247 (3384) 3443	*Astarte montagui*	TO-8754
1187-1188	1303.7	7530±70	7130±70	7921 (7964) 8032	Pelecypod valve	TO-8755
1315-1316	1455.1	8200±70	7800±70	8583 (8686) 8845	Pelecypod valve	TO-8756
1606	1868.8	8250±70	7850±70	8632 (8772) 8881	Pelecypod valve	TO-8757
2067-2068	2504.6	8220±170	7820±170	8496 (8719) 8911	*Nuculana pernula*	TO-8758

All ages were measured by the AMS method and corrected to a base of $\delta^{13}C$=-25‰. Errors represent 68.3 % (1σ) confidence limits. [a]Composite depth interpolated from the IRM_{30mT}, inclination and declination correlations. [b]Corrected by –400 years to account for the apparent age of the dissolved inorganic carbon reservoir in surface waters of the North Atlantic [26].[c]Calibrated with CALIB4.3 [25] assuming a standard marine reservoir correction of –400 years [26]; the first and last ages represent the 1σ cal age range, whereas the ages in parentheses are the calibrated ages using the intercept method [25]. Dated material at depths marked with an asterisk are considered invalid and were not used to construct the age models.

Figure captions

Fig. 1 Shaded relief image of Eastern Canada digital elevation model along with the location of cores 2220 and 2221 sampling sites in the St. Lawrence Estuary. Modified from Shaw et al. [66]. P.E.I. Prince Edward Island.

Fig. 2. High-resolution rock-magnetic stratigraphy of core 2220. A -400 year reservoir correction was applied to the AMS ^{14}C dates. Unit 1 was deposited prior to ~7700 yr BP and corresponds mostly to glaciomarine laminated clays. Unit 2 is composed mostly of postglacial bioturbated silty clays. The grain size data were processed with the Gradistat program [67].

Fig. 3. High-resolution rock-magnetic stratigraphy of core 2221. A -400 years reservoir correction was applied to the AMS ^{14}C dates. Unit 1 as in Figure 2. Unit 2 is composed mostly of postglacial bioturbated sandy mud.

Fig. 4. New composite depth-scale for core 2221 based on the IRM_{30mT} 0.3T correlation.

Fig. 5. Comparison of inclination and declination features in cores 2220 and 2221 postglacial sediments. A) Top, inclination record of core 2221 on the adjusted depth-scale as in Figure 4 compared to core 2220. Bottom, declination record of core 2221 on the adjusted depth-scale. Stippled lines indicate proposed correlative features. This was done

without violating any of the previous IRM_{30mT} 0.3T lithostratigraphic constraints. B) Inclination (top) and declination (bottom) of core 2221 on the optimized depth–scale.

Fig. 6. New composite age model for the St. Lawrence Estuary cores. Depths of the dated material from core 2221 were transferred on core 2220 using the IRM_{30mT} 0.3T, inclination and declination correlations as in Figures 4 and 5. A third order polynomial fit was used to construct the final age model for the postglacial sediments

Fig. 7. Comparison of North American Holocene geomagnetic PSV records. A) Inclination and B) Declination profiles of core 2220 along with the Lake St. Croix [32], Lake Pepin [33] and Fish Lake records [34], and a compilation of lava flows from the western United States transformed into directional space at the Fish Lake location (diamonds) [35]. Declination data were not published for Lake Pepin. Distinctive inclination and declination features are numbered according to Lund [36].

Fig. 8. Coherence of the RPI proxies with the normalization parameters from ~750 to 8500 cal BP. A Blackman-Tuckey cross-spectral analysis with a Bartlett window [31] was applied. The solid line represents the 95 % confidence level. A) NRM_{30mT}/k vs k, B) NRM_{30mT}/ARM_{30mT} vs ARM_{30mT} and C) NRM_{30mT}/IRM_{30mT} vs IRM_{30mT}.

Fig. 9. Relative paleointensity proxy. A) NRM/IRM at demagnetization level of 20, 30 and 40 mT. B) The arithmetic mean of the three paleointensity proxies along with the corresponding standard deviation (grey curves).

Fig. 10. Power spectrum of core 2220 component inclination, declination and RPI from ~750 to 8500 cal BP. The power spectra were calculated with the Blackman-Tuckey method with a Bartlett window [31]. B) Coherence between environmentally sensitive magnetic parameters (k, k_{ARM}/k and ARM_{30mT}) and the RPI proxy. The coherence was calculated with a Blackman-Tuckey cross-spectral analysis with a Bartlett window [31]. The solid line represents the 95 % confidence level.

Fig. 11. Comparison of core 2220 RPI record with the RPI records of Lake Pepin [32], Lake St. Croix [43] and Lake LeBoeuf [38] from A) 0 to 8000 yr BP and from B) 0 to 4000 yr BP. The Lake LeBoeuf record was normalized by its mean.

Fig. 12. Comparison of core 2220 RPI record with the GISP2 inversed ^{10}Be flux record [53-54] from ~3300 to 8000 cal BP. A) Both records are on their own chronology. B) Core 2220 RPI record was tuned to the GISP2 record.

Fig. 13. Comparison of core 2220 RPI record with the smoothed inversed ^{14}C production rate record of [14] from 750 to 8 500 cal BP. The ^{14}C production rate data were corrected for marine and terrestrial effects using a four-box carbon-cycling model (see [14] for

details). A 9-point running mean was used to smooth the ^{14}C record. Both records are on their own chronology.

Fig. 14. Coherence between core 2220 RPI and the ^{14}C production rate [14] and ^{10}Be flux [53-54] records. The RPI, ^{14}C and ^{10}Be data are as in Figs 12a and 13. The grey zones represent the two main periods (~1250 and 420 yrs) identified from the power spectrum of core 2220 RPI record (see Fig.10). The coherence was calculated with a Blackman-Tuckey cross-spectral analysis with a Bartlett window [31]. The solid line represents the 95 % confidence level.

EPSL Online Background Dataset Table and figure captions

Table 1
Spectral analysis results of Holocene declination records with periods close to ~1250 years.

Region	Time interval (yrs)	Declination (yrs)	Reference
North America	0-10000	1245	[40]
	0-8520	1150	[41]
South America	0-6000	1050	[40]
	0-6500	1200	[42]
Europe	0-10000	1155	[40]
Australia	0-10000	1080	[40]

The periods were rounded.

Fig. 1. Core top correlation. A) Correlation of the organic carbon and $^{13}C_{org}$ contents of core 2220 with a box core record (core AH00-2220; latitude/longitude: 48°38.33N/68°37.82W, water depth 324 m, length 0.51 m) from the same site. The correlation between the box core and the long core indicates that only the first 14 cm are missing from core 2220. C_{org} contents were obtained by calculating the difference between the total carbon (C_{tot}) and the inorganic carbon (C_{inorg}) contents. C_{tot} contents were measured with a Carlo-Erba™ elemental analyzer, whereas C_{inorg} contents were measured using a UIC coulometer. ^{13}C contents were measured on acidified aliquots loaded on the carousel of a Carlo-Erba™ elemental analyzer on-line with a Micromass IsoPrime™ instrument. B) Correlation of the $IRM_{30mT}0.3T$ between core 2220 and core 2221 first 100 cm.

Fig. 2. Initial age model based on AMS ^{14}C dating for cores 2220 and 2221. SR = sedimentation rate.

Fig. 3. Sedimentation rates (SR) derived from ^{210}Pb measurements in the first 30 cm of box core AH00-2220 (latitude/longitude: 48°38.33N/68°37.82W, water depth 324 m, length 0.51 m). Using the regional ^{210}Pb supported value of [17], we calculated a mean sedimentation rate of 0.74 cm/yr from 0-20 cm and 0.28 cm/yr from 20-30 cm. The ^{210}Pb measurements were made after chemical treatment, purification and deposition on a silver disk following routine procedures at GEOTOP [17] by alpha counting of the daughter ^{210}Po.

Fig. 4. Typical vector endpoint diagrams and decay of the normalized intensity during AF demagnetization for postglacial sediments of A) core 2220 (942 cm) and B) core 2221 (168 cm). Closed squares represent north and east components, whereas open squares represent vertical and east components.

Fig. 5. Component inclination and declination with corresponding MAD values for the postglacial sediments of A) core 2220 and B) core 2221. The vertical lines correspond to the expected inclination for the sites latitude based on a GAD model.

Fig. 6. Typical hysteresis loops for postglacial sediments of A) core 2220 and B) core 2221.

Fig. 7. Hysteresis parameters for cores 2220 and 2221 postglacial sediments plotted on a Day et al. [23] diagram.

Fig. 8. Comparison between IRM_{30mT} in core 2220 and 2221. Each record is shown on its own depth scale. Stippled lines indicate common features observed in both cores.

Fig. 9. New composite age model, based on uncalibrated reservoir corrected AMS ^{14}C dates, for the St. Lawrence Estuary cores. Depths of the dated material from core 2221 were transferred on core 2220 using the IRM_{30mT} 0.3T, inclination and declination correlations. A third order polynomial fit was used to construct the age model for the postglacial sediments.

Fig. 10. Comparison of the RPI and mean grain size records from core 2220. A third order polynomial fit was subtracted from both records to remove a long-term trend.

Fig. 11. A) Comparison of core 2220 RPI with a varved RPI record derived from Lake Nautajärvi, central Finland [44] from 750 to 8500 cal BP. The Lake Nautajärvi original chronology was in AD/BC. For comparison purposes, we converted the AD/BC ages in cal BP by subtracting 1950 years from the AD/BC ages. B) Coherence between core 2220 and Lake Nautajärvi RPI records. The coherence was calculated with a Blackman-Tuckey cross-spectral analysis with a Bartlett window [31]. The solid line represents the 95 %

confidence level. The grey zone represents the period of ~1250 yrs identified from the power spectrum of core 2220 RPI record (see Fig. 10).

Fig. 12. Comparison of core 2220 original vs. tuned chronology for the A) ^{10}Be flux correlation [53, 54] and B) ^{14}C production rate correlation [14].

Fig. 13. Comparison of core 2220 RPI record with the inversed smoothed ^{14}C production rate record of [14] from 750 to 8 500 cal BP. The ^{14}C production rate data were corrected for marine and terrestrial effects using a four-box carbon cycling model (see [14] for details). A 9-point running mean was used to smooth the ^{14}C record. Core 2220 RPI record was tuned to the ^{14}C production rate record.

Fig. 14. Comparison of the unsmoothed ^{14}C production rate record [14] with core 2220 RPI from A) 2000-4000 cal BP and from B) 7000-8500 cal BP. The ^{14}C production rate data were corrected for marine and terrestrial effects using a four-box carbon cycling model (see [14] for details). Core 2220 RPI chronology was tuned to the 9-point running mean ^{14}C production rate record as in Online Background Dataset Fig. 13.

Fig. 15. Comparison of core 2220 detrended RPI record with the detrended percent of hematite-stained grains from core MC52-VM29-191 [14] from 750 to 8500 cal BP. A third order polynomial fit and a linear fit to the data were subtracted from cores MD99-2220 and MC52-VM29-191, respectively, to remove long-term trends.

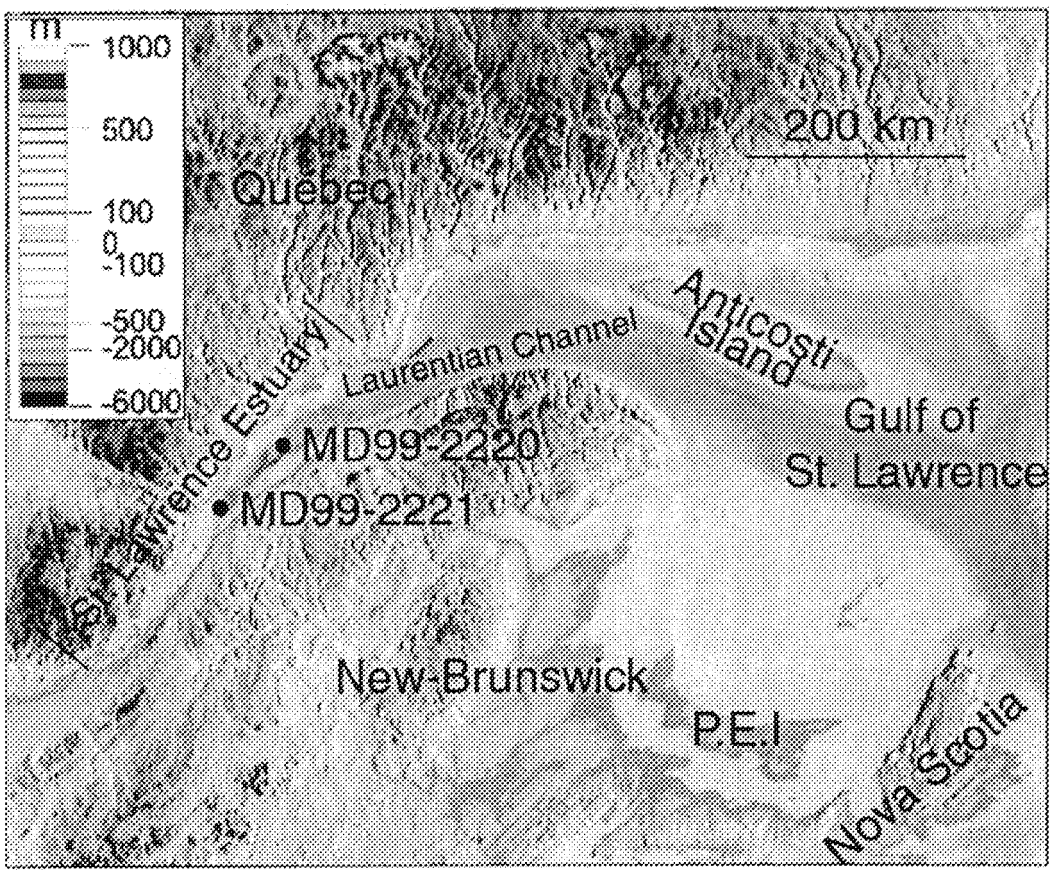
m
1000
500
100
0
-100
-500
-2000
-6000
200 km
Quebec
Anticosti Island
Laurentian Channel
St. Lawrence Estuary
MD99-2220
MD99-2221
Gulf of St. Lawrence
New-Brunswick
P.E.I
Nova Scotia

Fig. 1

Core 2220

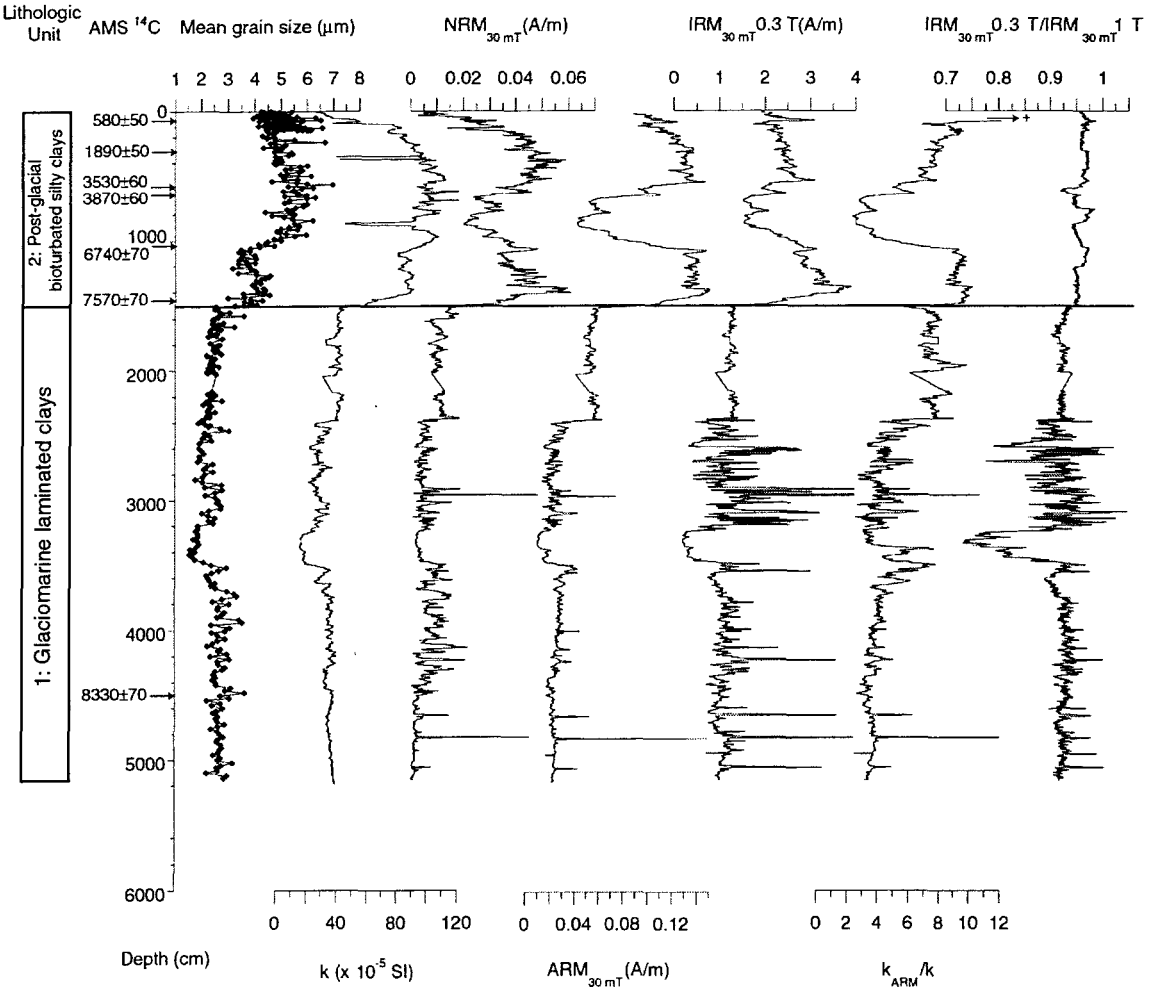

Fig. 2

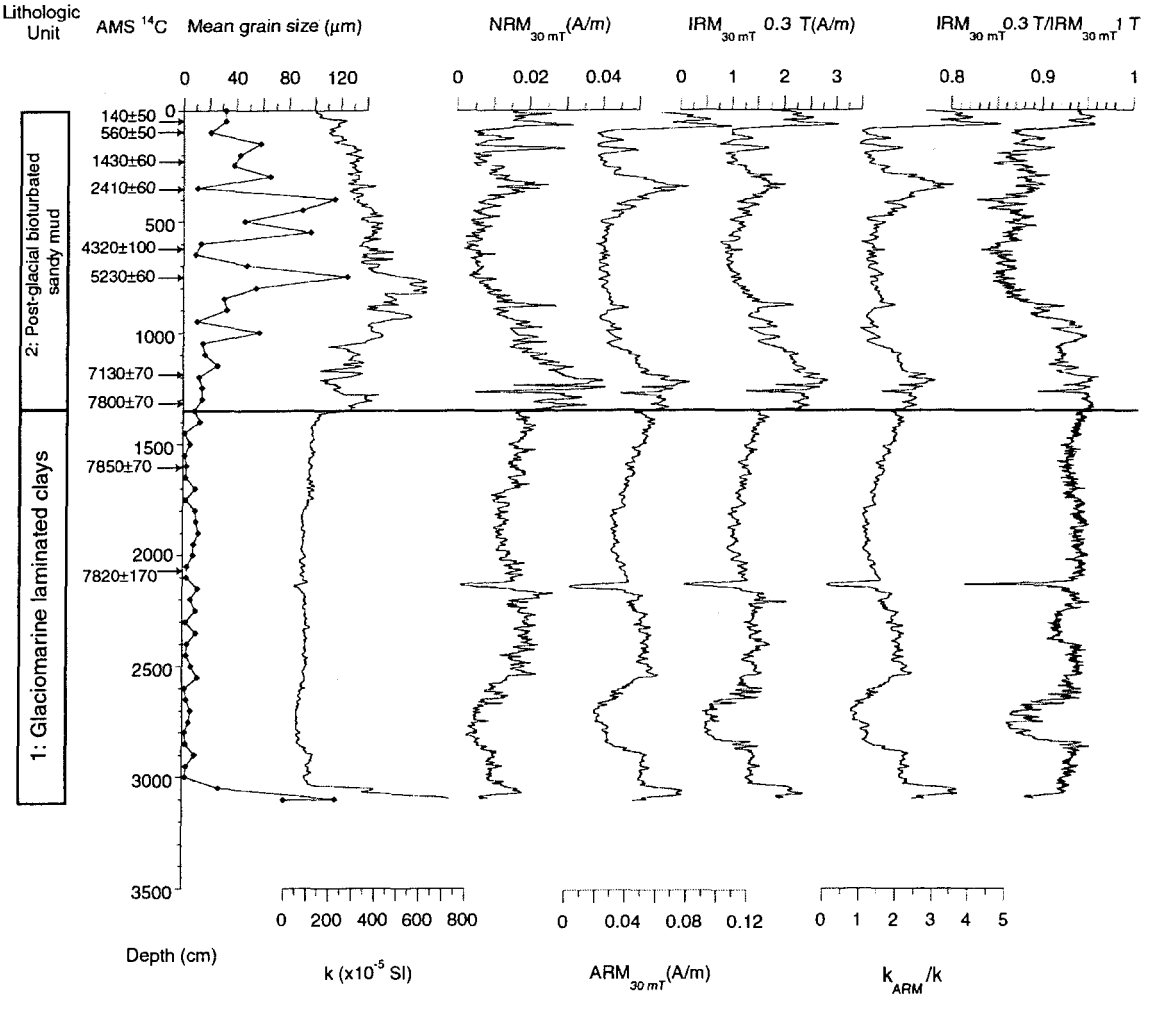
Core 2221
Lithologic Unit
AMS ^{14}C
Mean grain size (μm)
$NRM_{30\ mT}$(A/m)
$IRM_{30\ mT}$ 0.3 T(A/m)
$IRM_{30\ mT}$ 0.3 T/$IRM_{30\ mT}$ 1 T
2: Post-glacial bioturbated sandy mud
1: Glaciomarine laminated clays
140±50
560±50
1430±60
2410±60
4320±100
5230±60
7130±70
7800±70
7850±70
7820±170
Depth (cm)
k (x10^{-5} SI)
$ARM_{30\ mT}$(A/m)
k_{ARM}/k

Fig. 3

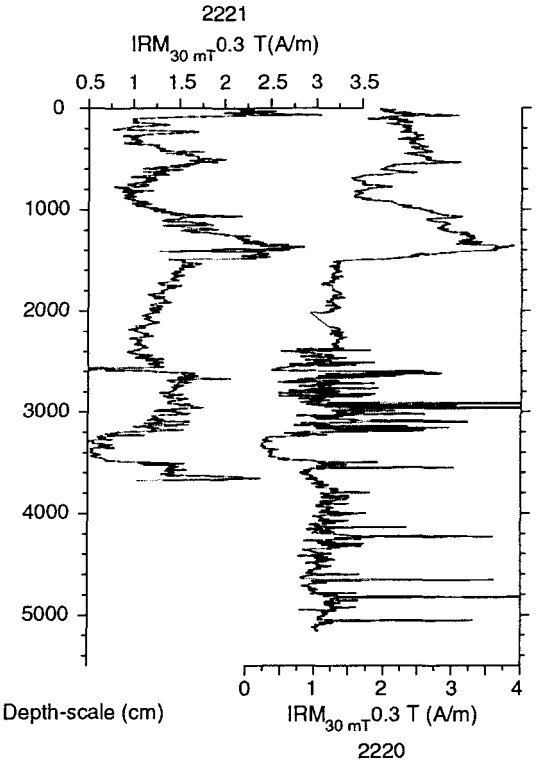
2221
IRM30 mT0.3 T(A/m)
0.5 1 1.5 2 2.5 3 3.5
0
1000
2000
3000
4000
5000
Depth-scale (cm)
0 1 2 3 4
IRM30 mT0.3 T (A/m)
2220

Fig. 4

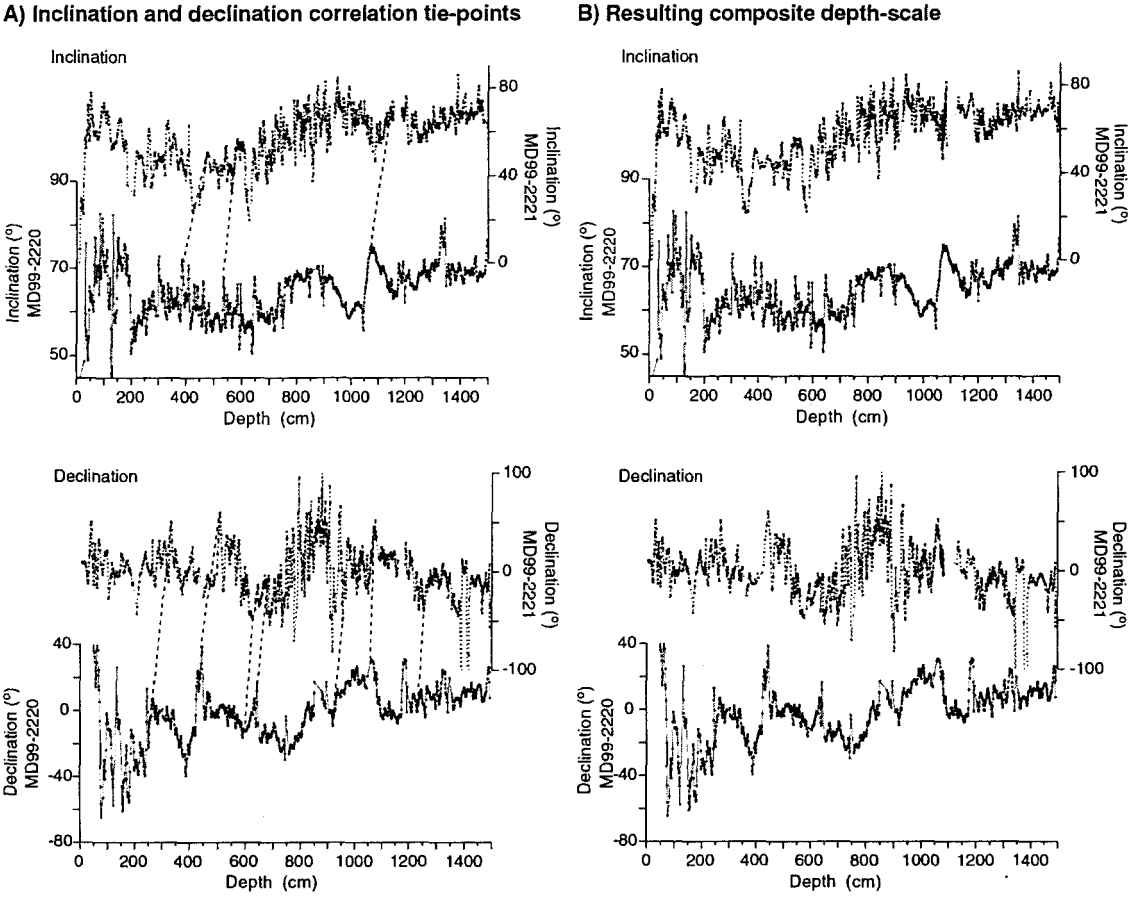
A) Inclination and declination correlation tie-points
B) Resulting composite depth-scale
Inclination
Declination
Inclination (°) MD99-2220
Inclination (°) MD99-2221
Declination (°) MD99-2220
Declination (°) MD99-2221
Depth (cm)
0
200
400
600
800
1000
1200
1400
50
70
90
0
40
80
-80
-40
-100
100

Fig. 5

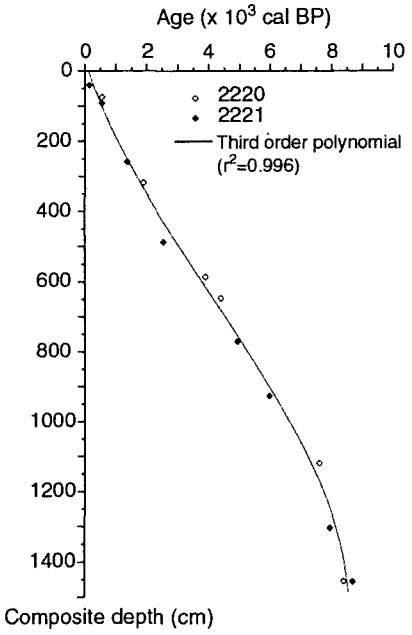
Age (x 10^3 cal BP)
0
2
4
6
8
10
0
200
400
600
800
1000
1200
1400
2220
2221
Third order polynomial
(r^2=0.996)
Composite depth (cm)

Fig. 6

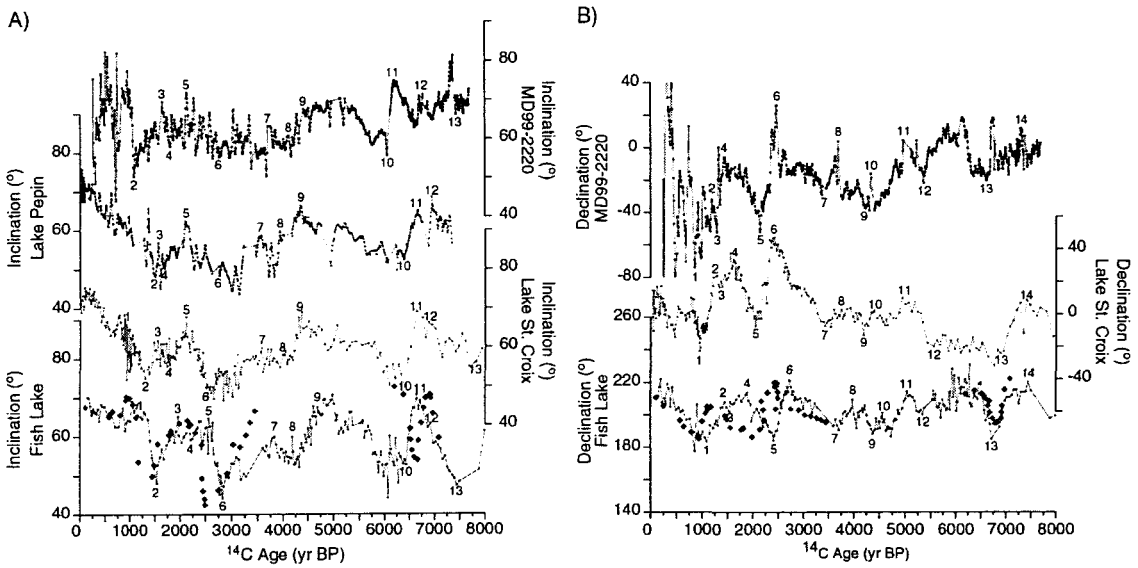
A)
B)
Inclination (°)
Lake Pepin
Inclination (°)
Fish Lake
Inclination (°)
MD99-2220
Inclination (°)
Lake St. Croix
Declination (°)
MD99-2220
Declination (°)
Fish Lake
Declination (°)
Lake St. Croix
14C Age (yr BP)
14C Age (yr BP)

Fig. 7

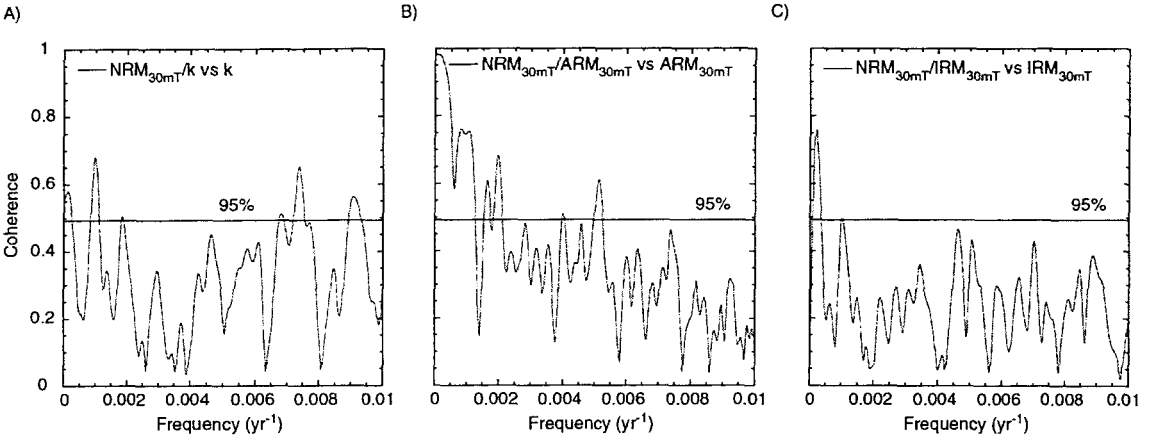
A)
B)
C)
NRM30mT/k vs k
NRM30mT/ARM30mT vs ARM30mT
NRM30mT/IRM30mT vs IRM30mT
95%
Coherence
Frequency (yr-1)
0
0.2
0.4
0.6
0.8
1
0.002
0.004
0.006
0.008
0.01

Fig. 8

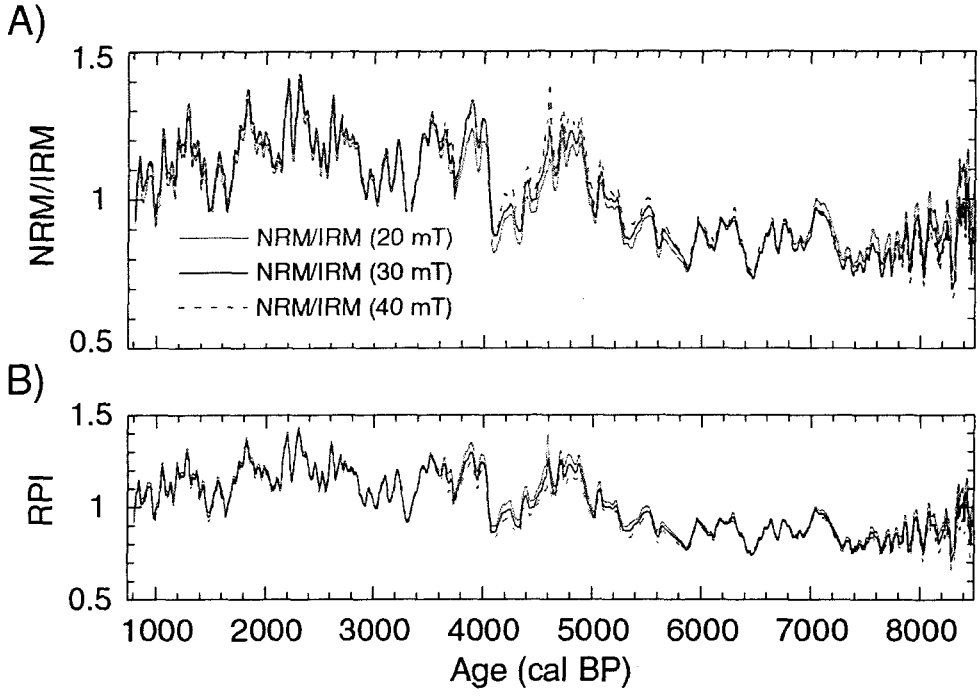
A)
1.5
1
0.5
NRM/IRM
NRM/IRM (20 mT)
NRM/IRM (30 mT)
NRM/IRM (40 mT)
B)
1.5
1
0.5
RPI
1000
2000
3000
4000
5000
6000
7000
8000
Age (cal BP)

Fig. 9

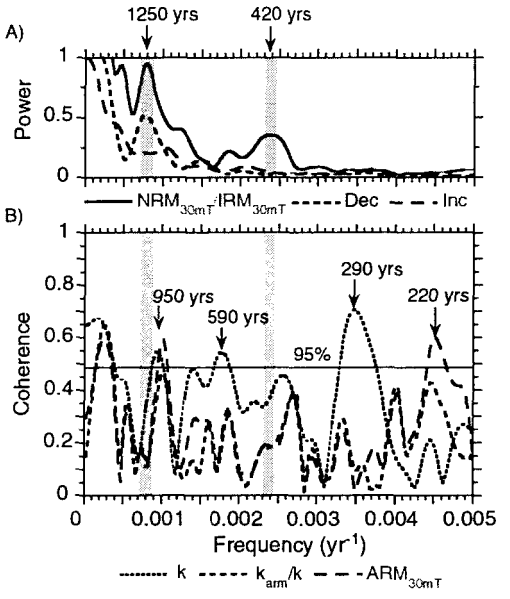
A)
1250 yrs
420 yrs
Power
1
0.5
0
NRM30mT/IRM30mT
Dec
Inc
B)
290 yrs
220 yrs
950 yrs
590 yrs
95%
Coherence
1
0.8
0.6
0.4
0.2
0
0
0.001
0.002
0.003
0.004
0.005
Frequency (yr-1)
k
karm/k
ARM30mT

Fig. 10

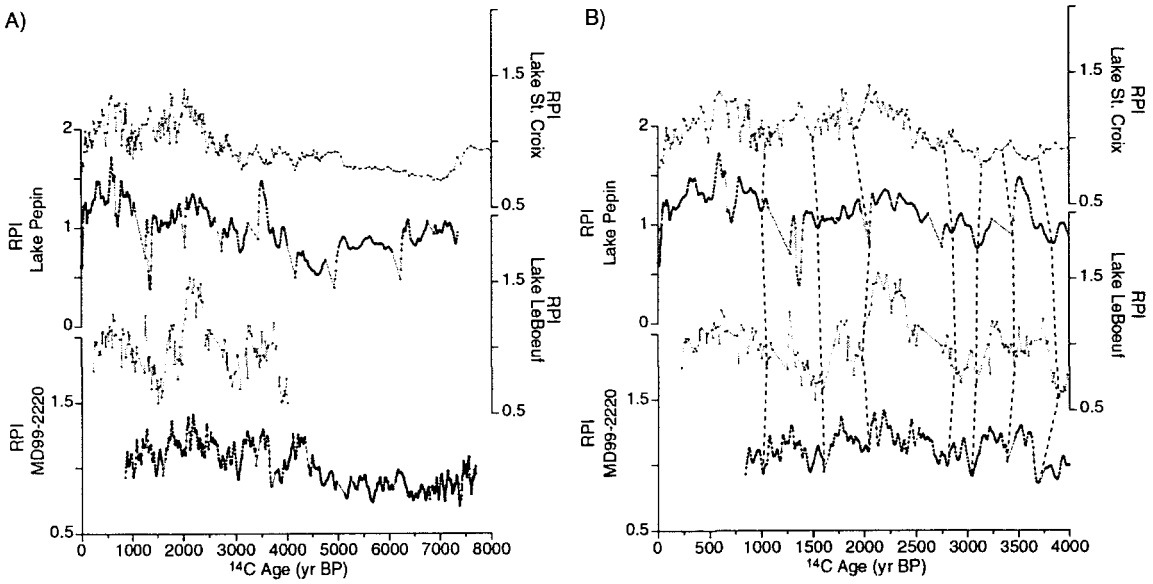
A)
RPI Lake Pepin
RPI MD99-2220
RPI Lake St. Croix
RPI Lake LeBoeuf
0 1000 2000 3000 4000 5000 6000 7000 8000
14C Age (yr BP)
B)
RPI Lake Pepin
RPI MD99-2220
RPI Lake St. Croix
RPI Lake LeBoeuf
0 500 1000 1500 2000 2500 3000 3500 4000
14C Age (yr BP)

Fig. 11

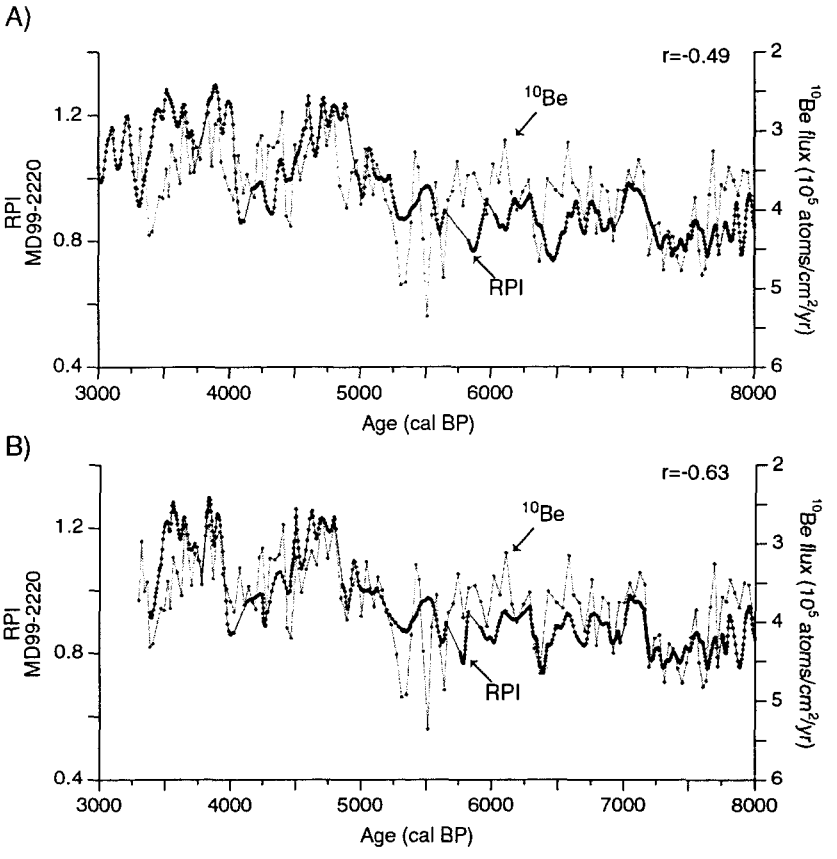
A)
r=-0.49
^{10}Be
RPI
RPI MD99-2220
^{10}Be flux (10^5 atoms/cm^2/yr)
Age (cal BP)
B)
r=-0.63
^{10}Be
RPI
RPI MD99-2220
^{10}Be flux (10^5 atoms/cm^2/yr)
Age (cal BP)

Fig. 12

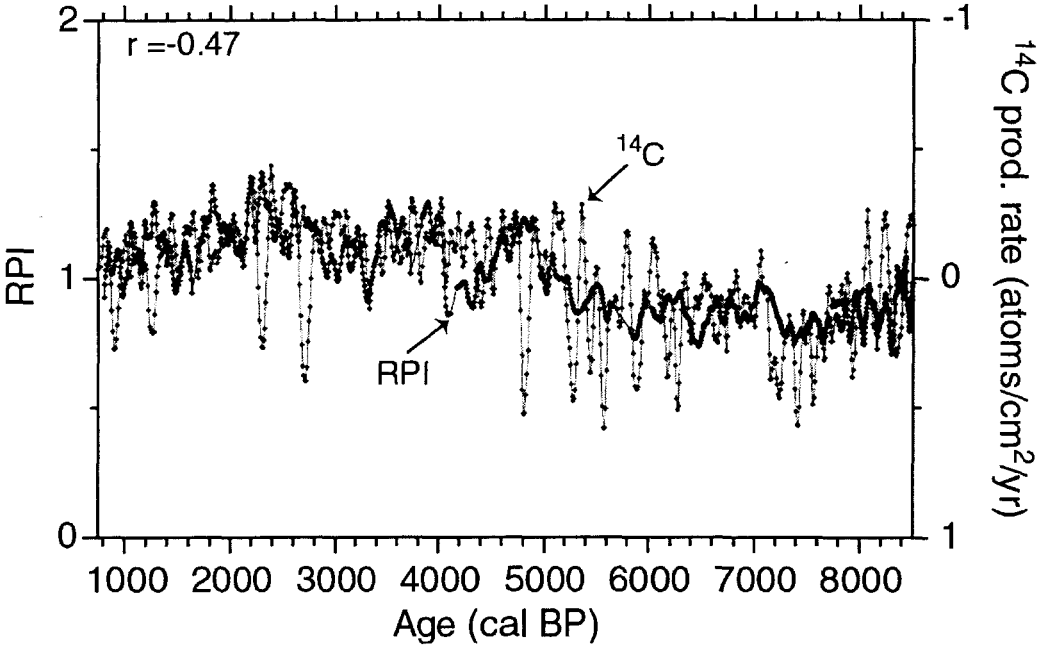
r =-0.47
^{14}C
RPI
RPI
2
1
0
-1
0
1
1000 2000 3000 4000 5000 6000 7000 8000
Age (cal BP)
^{14}C prod. rate (atoms/cm^2/yr)

Fig. 13

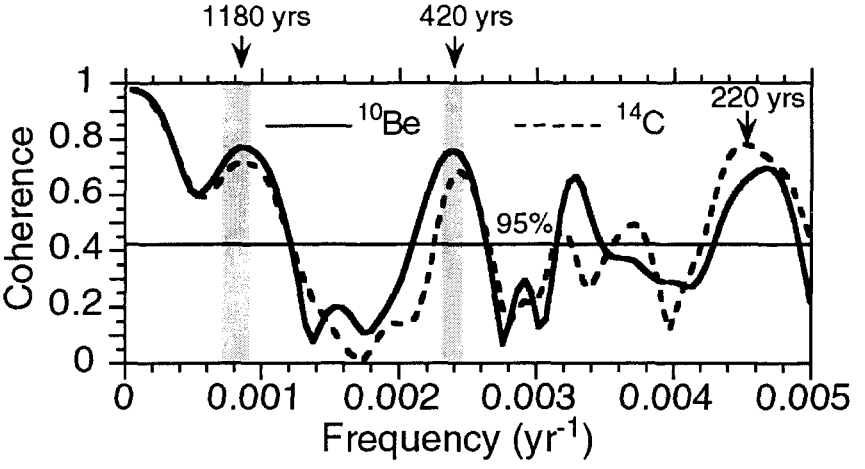
1180 yrs
420 yrs
220 yrs
^{10}Be
^{14}C
95%
Coherence
1
0.8
0.6
0.4
0.2
0
0
0.001
0.002
0.003
0.004
0.005
Frequency (yr^{-1})

Fig. 14

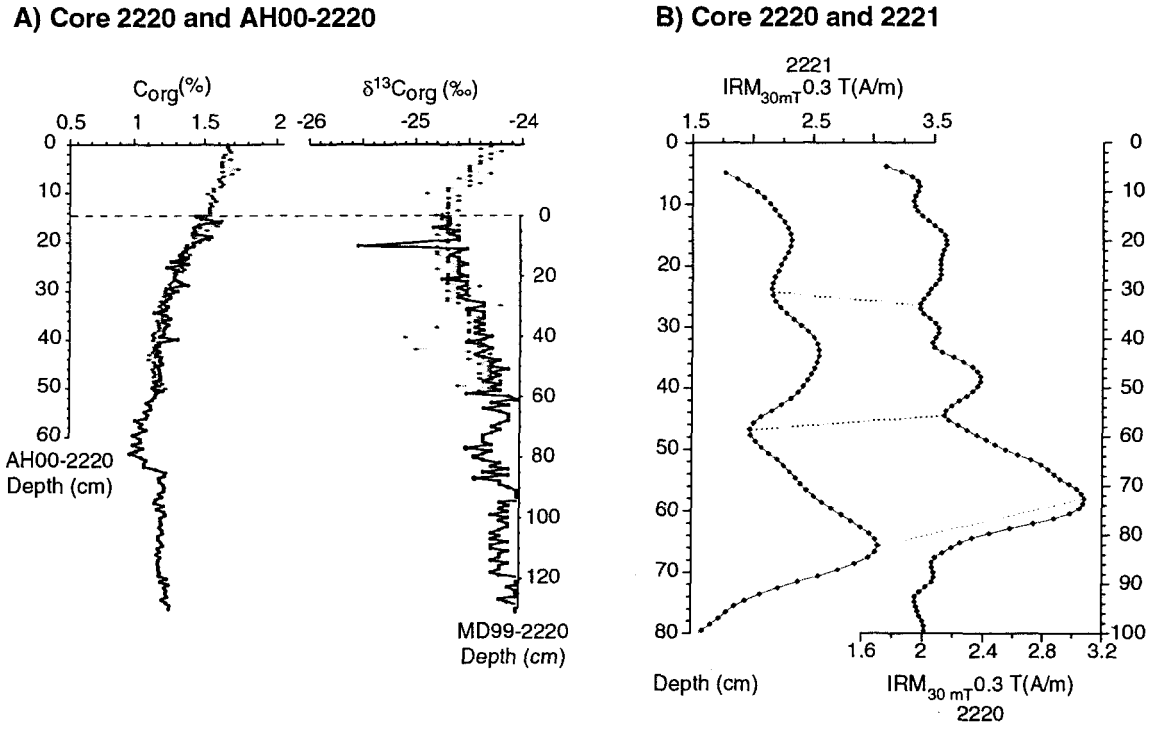

Online Background Dataset Fig. 1

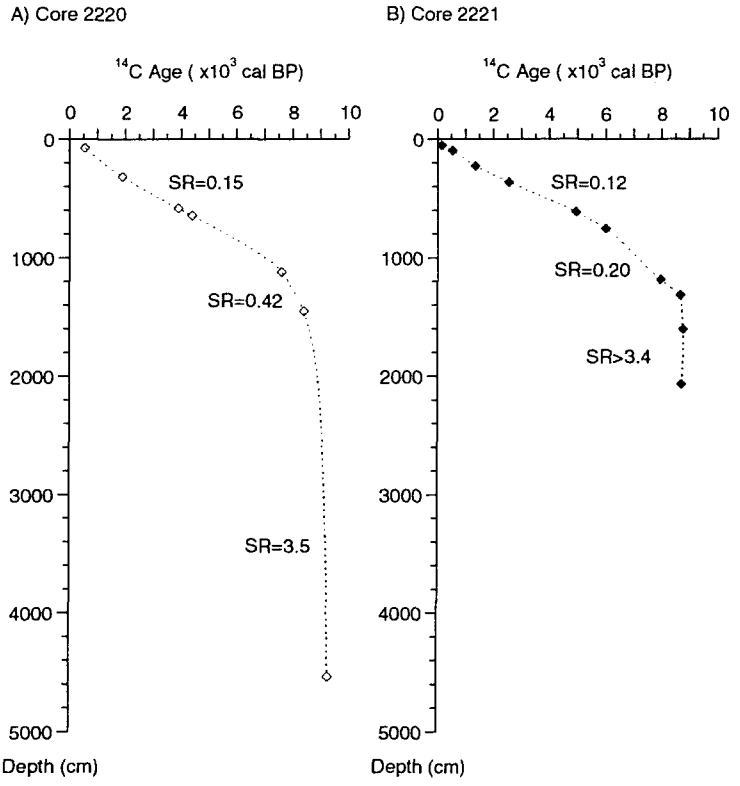

Online Background Dataset Fig. 2

AH00-2220

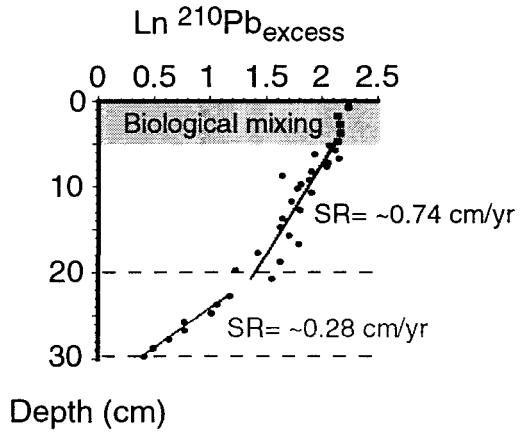

Online Background Dataset Fig. 3

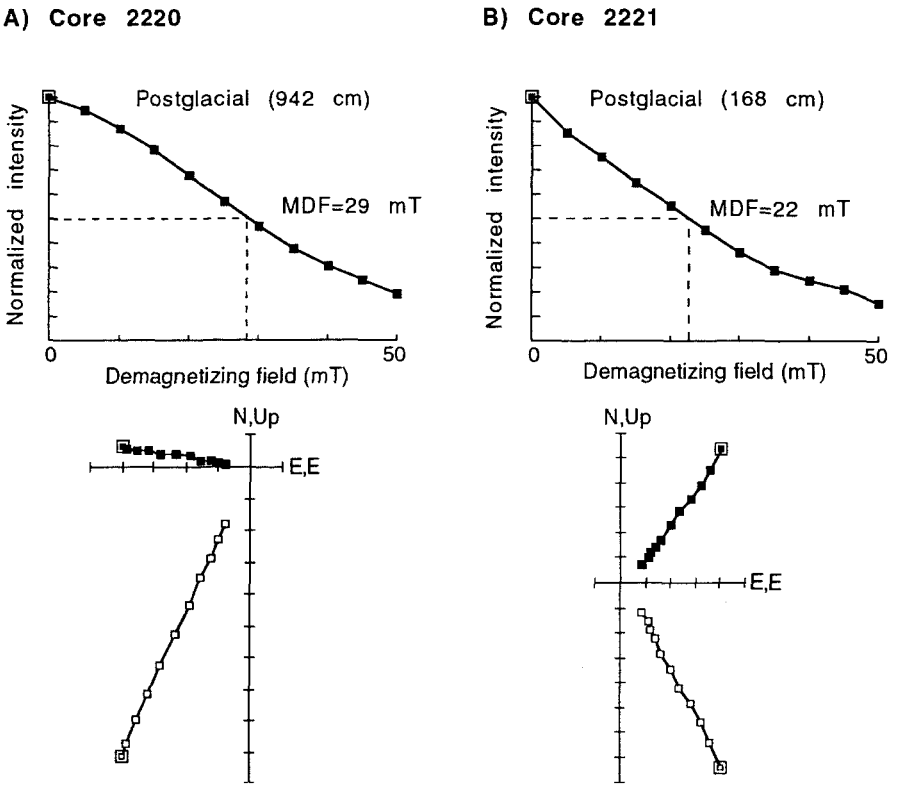

Online Background Dataset Fig. 4

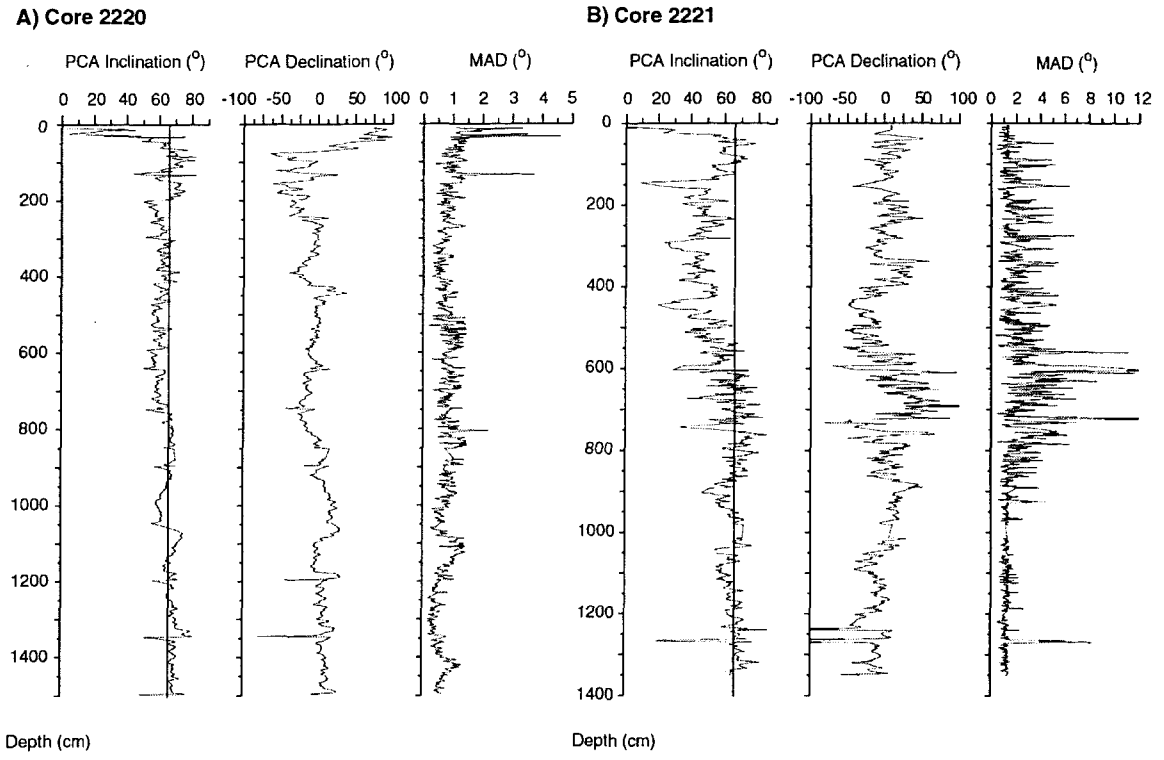

Online Background Dataset Fig. 5

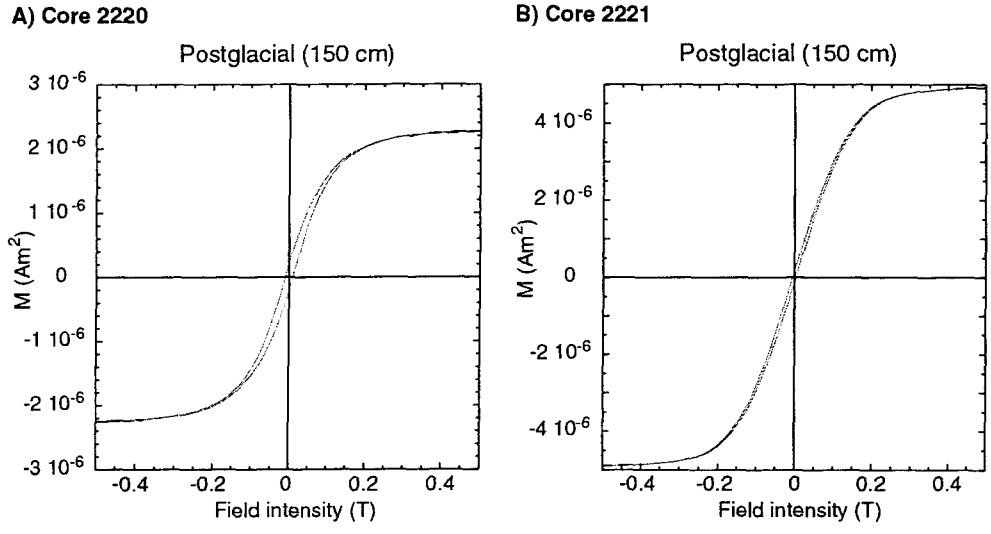

Online Background Dataset Fig. 6

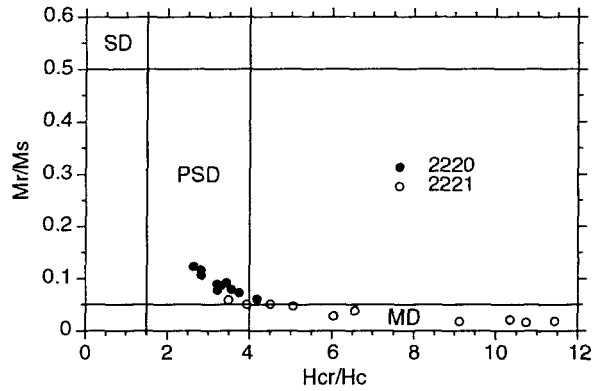

Online Background Dataset Fig. 7

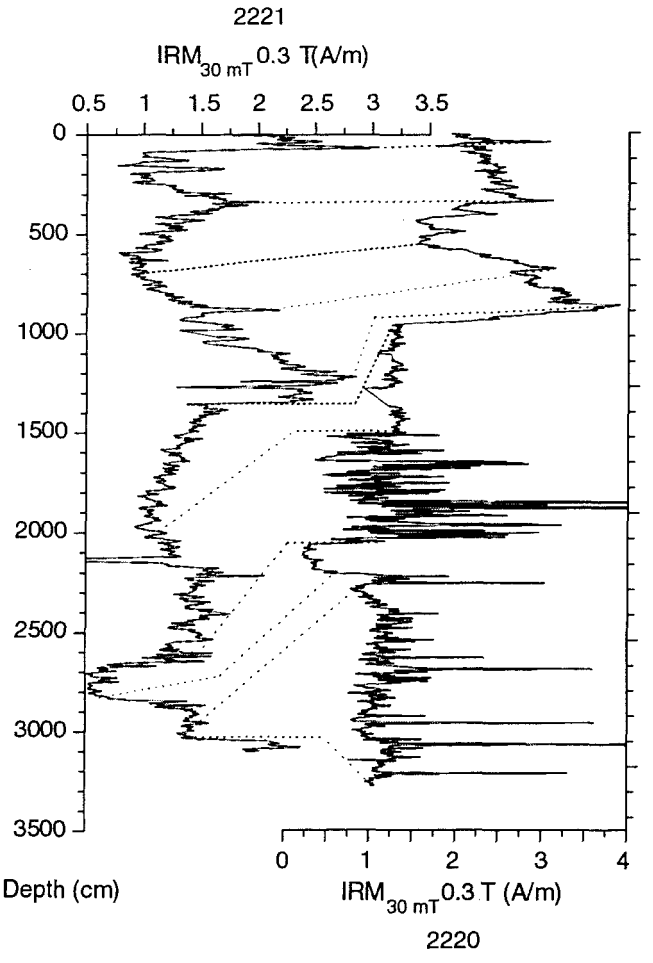

Online Background Dataset Fig. 8

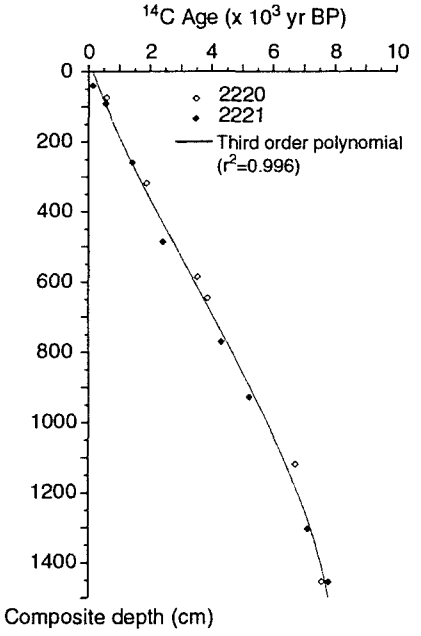

Online Background Dataset Fig. 9

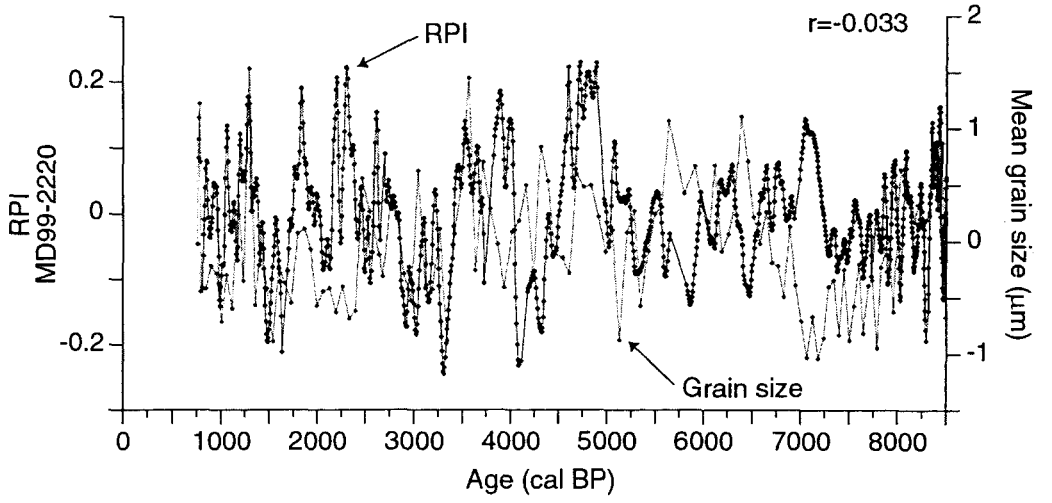

Online Background Dataset Fig. 10

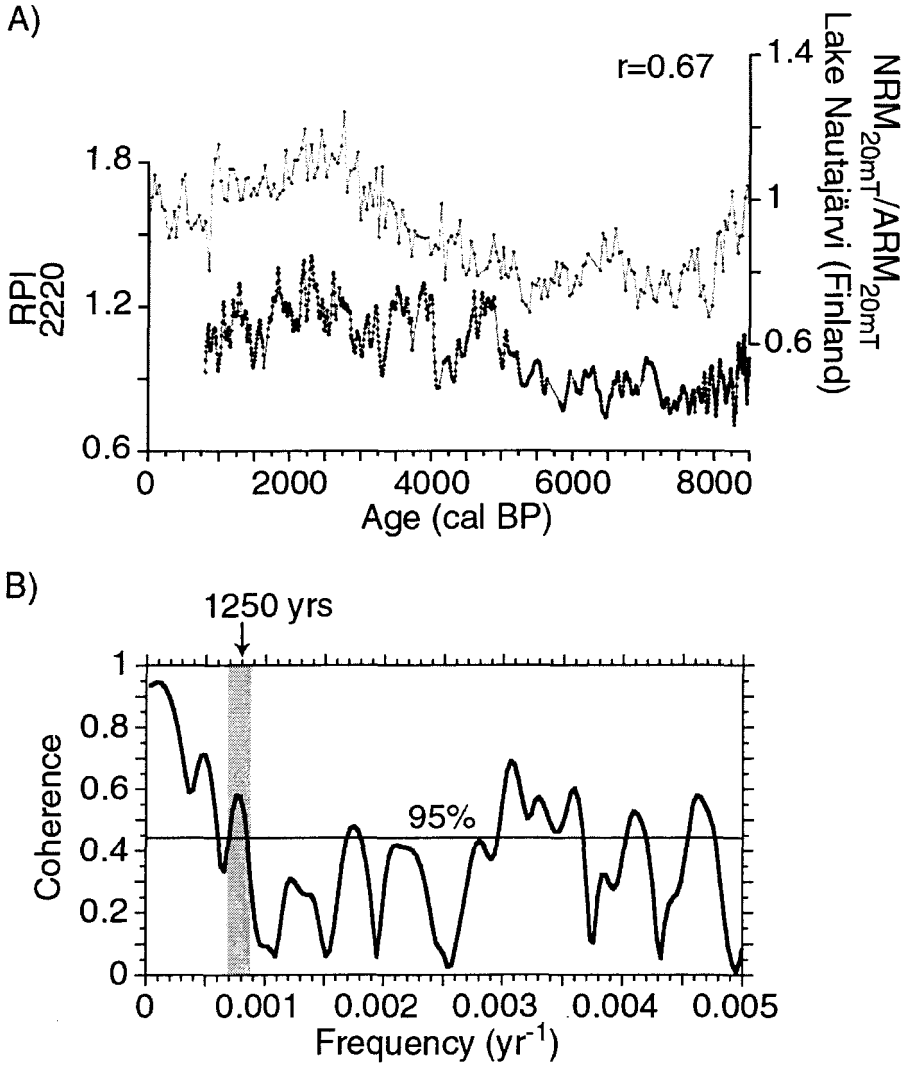

Online Background Dataset Fig. 11

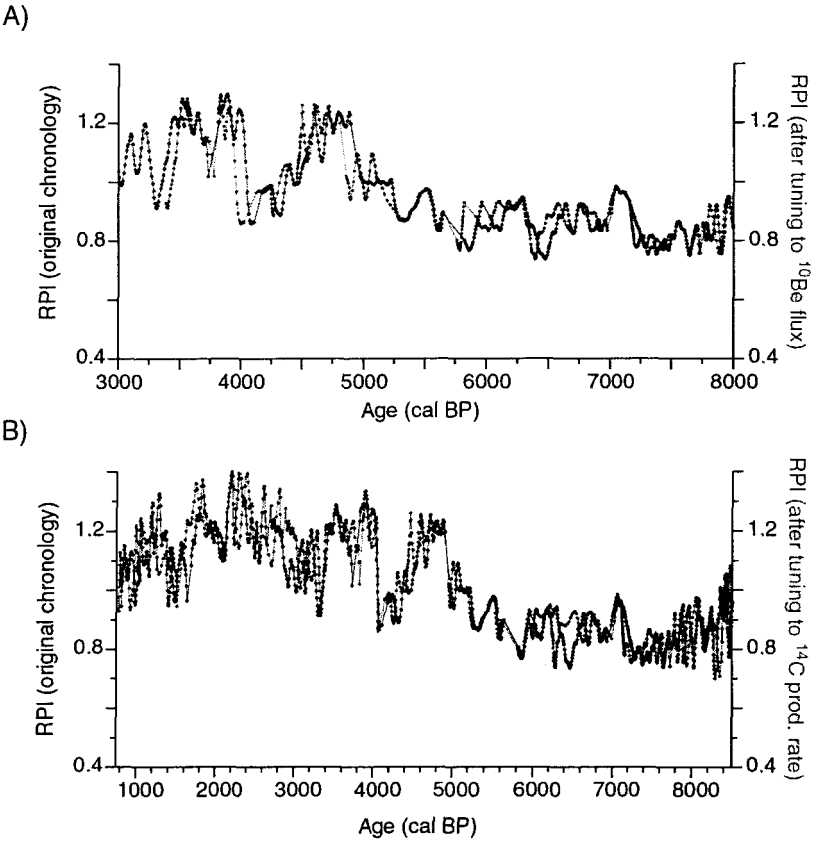

Online Background Dataset Fig. 12

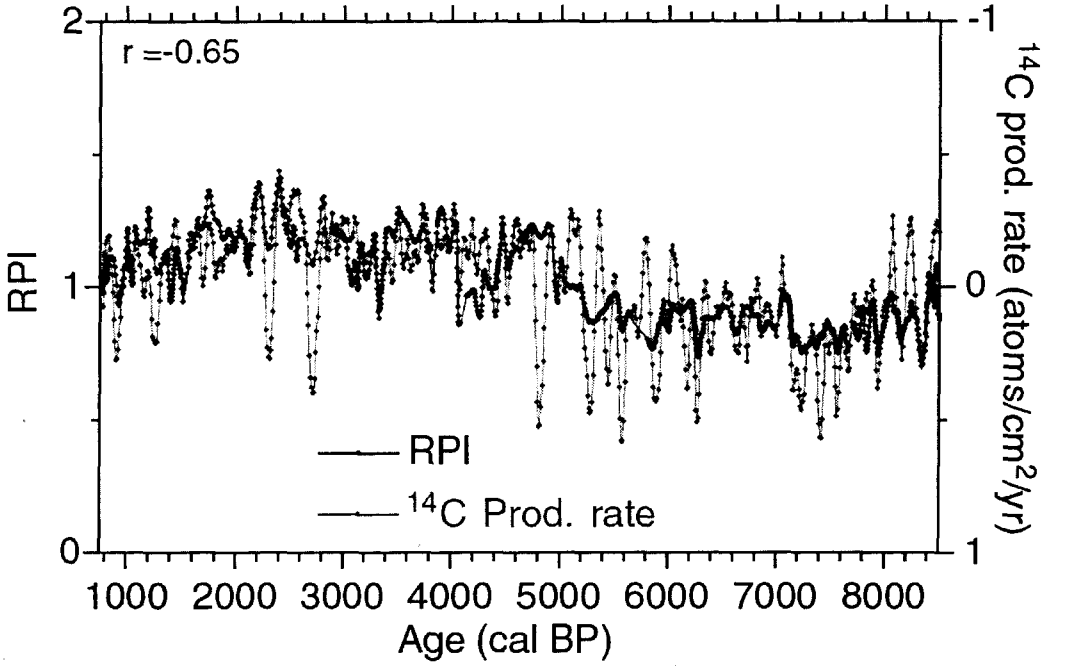

Online Background Dataset Fig. 13

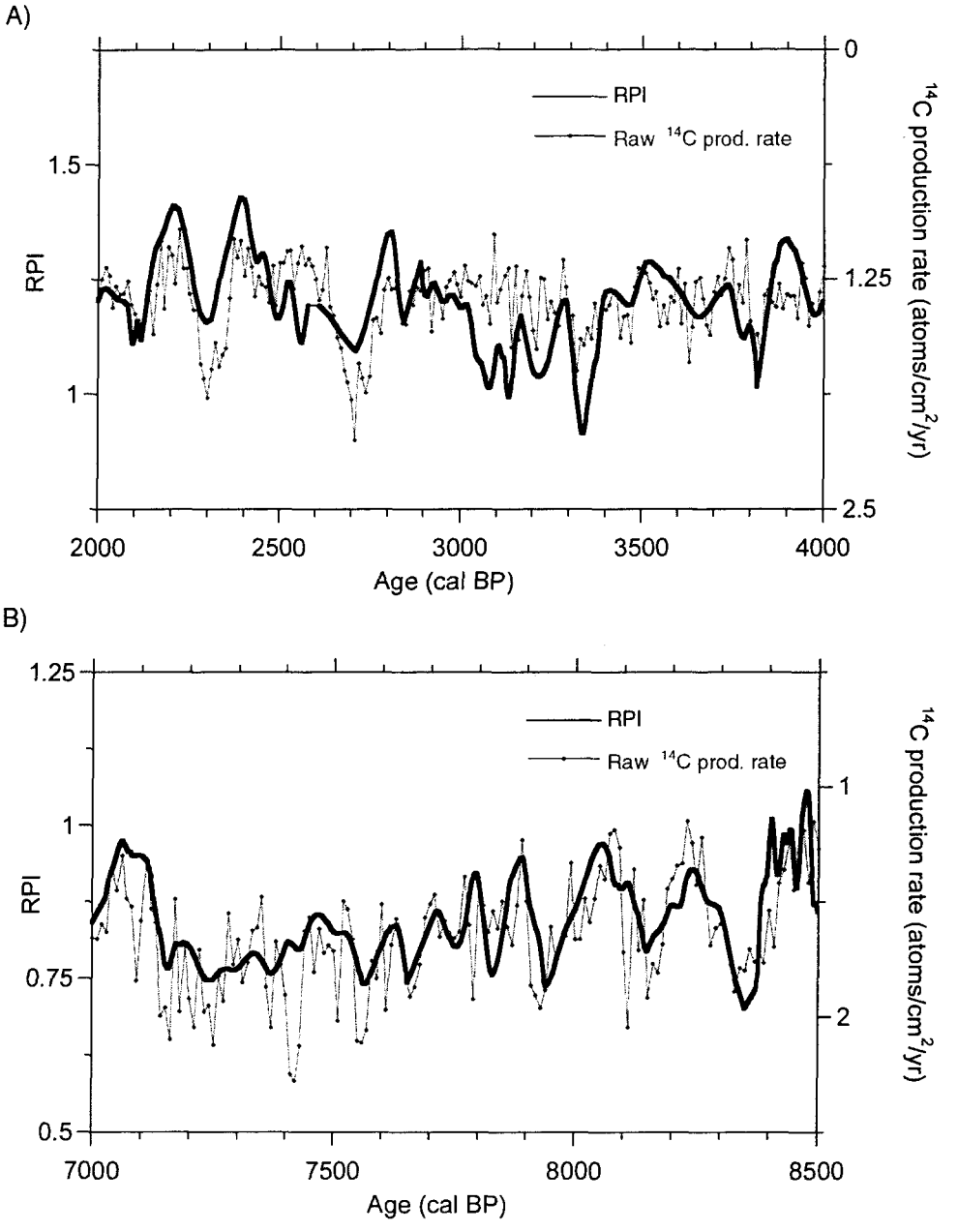

Online Background Dataset Fig. 14

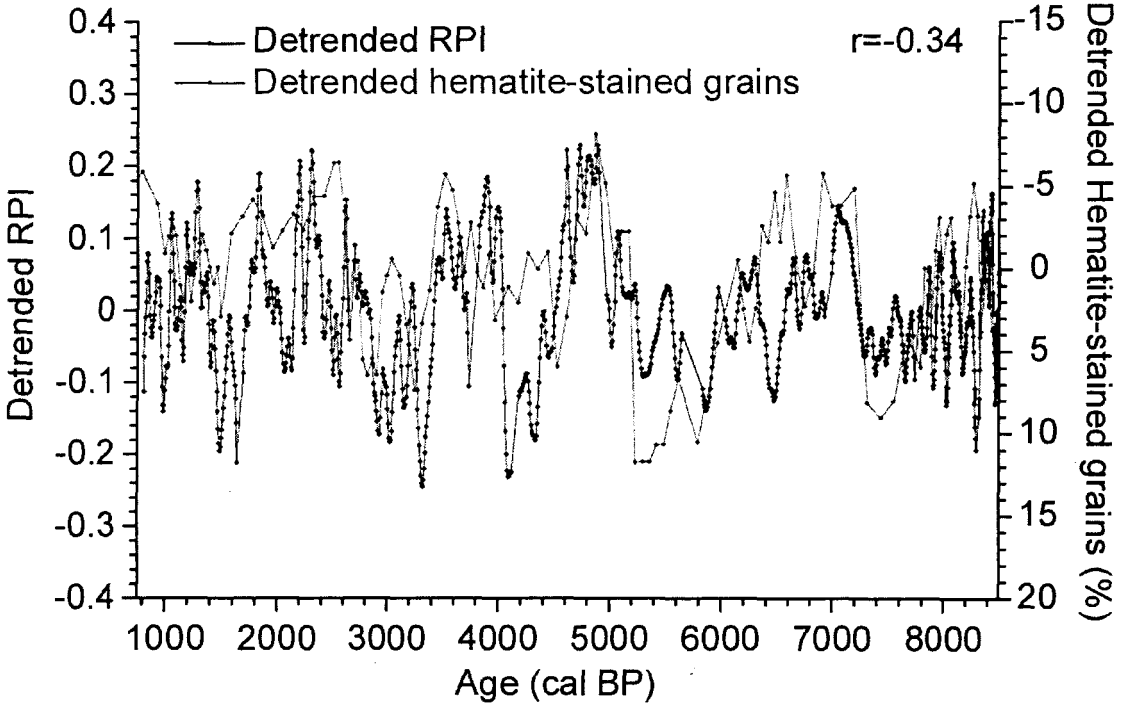

Online Background Dataset Fig. 15

CHAPITRE III

EARTHQUAKE AND FLOOD-INDUCED TURBIDITES IN THE SAGUENAY FJORD (QUÉBEC): A HOLOCENE PALEOSEISMICITY RECORD

Guillaume St-Onge[2,*], Thierry Mulder [b], David J.W. Piper [c], Claude Hillaire-Marcel [a], Joseph S. Stoner[d]

Sous presse dans *Quaternary Science Reviews*

---

[2]Centre de recherche en géochimie et géodynamique (GEOTOP-UQÀM-McGill), Case postale 8888, Succursale Centre-Ville, Montréal, Québec, H3C 3P8, Canada
[b]Université Bordeaux 1, DGO, UMR EPOC 5805, Avenue des facultés, 33405 Talence Cedex, France
[c]Geological Survey of Canada (Atlantic),1 Challenger Drive, Box 1006, Dartmouth, Nova Scotia, B2Y 4A2, Canada
[d]Institute of Arctic and Alpine Research (INSTAAR), University of Colorado, Campus Box 450, Boulder, CO 80309-0450, USA
*Corresponding author. Tel.: +418-654-3704; fax: +418-654-2615.
E-mail address: guillaume_st-onge@inrs-ete.uquebec.ca (G. St-Onge), now at INRS-ETE, C.P. 7500, Ste-Foy, Québec, G1V 4C7, Canada
For electronic supplement see http://www.elsevier.com/locate/quascirev

Abstract

A 38 m-long piston core from the deep basin of the Saguenay Fjord, Québec, recorded rapidly deposited layers (RDL) interpreted to represent major floods and earthquakes over the past ~ 7200 years. High-resolution physical, magnetic and sedimentological analyses revealed at least 14 RDL, generally with a sandy base and a light grey color, interbedded with hemipelagic sediments. Digital X-radiography and grain size analyses at < 1 cm spacing showed that six RDL have normal grading and likely resulted from earthquake-triggered slumps. Six other RDL have a similar normally graded basal bed, overlain by a coarsening-upward unit that underlies a fining-upward unit, interpreted as a deposit of flood-induced hyperpycnal flow. By analogy with the deposits that followed the 1663 AD earthquake, such beds are inferred to result from the breaching and rapid draining of a natural dam generated by an earthquake-triggered landslide. Based on this interpretation, the chronology derived from paleomagnetic secular variation, paleointensity and one accelerator mass spectrometry (AMS) ^{14}C date suggests that earthquake frequency was dramatically reduced at ~ 4 ka, consistent with ice-load modeling for deglaciation in Eastern Canada. This study demonstrates that hyperpycnal and slump-generated turbidites can be readily distinguished in small basins such as the Saguenay Fjord and that hyperpycnal turbidites tend to be much thicker, because of greater flow duration and constriction.

1. Introduction

A few rapidly deposited layers (RDL), with a thickness ranging from few centimeters to several meters, were deposited during the last 350 years in the deep basin of the Saguenay Fjord, an intracratonic basin in eastern Canada (Fig. 1). Some of these RDL were related to the 1663 AD ($M \approx 7$) earthquake, the 1971 AD St-Jean-Vianney and the 1924 AD Kénogami landslides and to the flood of 1996 (Smith and Walton, 1980; Syvitski and Schafer, 1996; Urgeles et al., 2002). This record of historic catastrophic events is extended to the early Holocene in a new 38 m-long core (MD99-2222) recovered during the 1999 IMAGES V (International Marine Past Global Change Study) cruise on the RV *Marion Dufresne II*. The study includes high-resolution physical (density, digital X-radiography and color reflectance), magnetic (magnetic susceptibility, paleomagnetic secular variation and paleointensity) and sedimentological analyses (detailed description, carbonate content and grain size). The purpose is to identify RDL prior to 1663 AD and to determine the frequency of natural hazards such as floods and earthquakes in the Fjord area during the Holocene.

2. Geological setting

The Saguenay Fjord (Québec) is a long (90 km) and narrow (1-6 km) glacially excavated valley that lies in an ancient graben in the Precambrian Canadian Shield (Drainville 1968; Fig. 1). It is adjacent to the seismically active region of Charlevoix (Fig.

1), where five M > 6 earthquakes occurred during the last 350 years (Lamontagne, 2000). The Fjord receives sediment from the Saguenay-Lac-Saint-Jean watershed (78 000 km^2), which has a mean monthly discharge of 1500 m^3/s, but can reach 5000 m^3/s during the spring freshet (Syvitski and Schafer, 1996). Average mean suspended particulate matter (SPM) concentration is 3 mg/l with a maximum of 24 mg/l (Hébert, 1995). The Fjord contains a ~10 m-thick brackish (0-10) surface layer separated by a sharp pycnocline that overlies the penetrating saline (30.5) waters of the Lower St. Lawrence Estuary (Syvitski and Schafer, 1996).

Seismic-reflection profiles in the Fjord show a 800-m-thick Quaternary sediment sequence filling the Fjord and reaching 1300 m thickness in the intermediate basin (Praeg and Syvitski, 1991). Following deglaciation at around 10 kyr BP, saline waters of the Laflamme Sea flooded the Saguenay depression with a relative sea level 198 m higher than present (Lasalle and Tremblay, 1978) and deposited a thick draping layer of slightly calcareous clays, the Laflamme Sea Clays (Lasalle and Tremblay, 1978). Holocene sediments are a few meters to tens of meters in thickness in the Fjord. Modern sedimentation rates range from 7 cm/yr at the head of the Fjord to less than 0.1 cm/yr in the deepest part of the deep basin (Smith and Walton, 1980; Zhang, 2000).

3. Methods

3.1. Coring site and core processing

Core MD99-2222 was raised from the deepest part of the deep basin of the Saguenay Fjord (48°18.28N, 70°15.44'W, water depth 271 m; Fig. 1) using the Calypso piston coring device on board the RV *Marion Dufresne II*. Wet bulk density and low-field volumetric magnetic susceptibility (k) were measured on board using a GEOTEK™ MSCL (Multi Sensor Core Logger) at 2 cm intervals. Archive halves were then photographed, described and measured for spectral reflectance using a hand-held Minolta™ spectrophotometer at 5 cm intervals. In this paper, we use L* which ranges from 0 (black) to 100 (white) and was previously used to identify reworked material from the Laflamme Sea Clays in Saguenay Fjord sediments (St-Onge and Hillaire-Marcel, 2001).

3.2. Grain size analyses and digital X-radiographs

Grain size analyses were made at the Université Bordeaux 1 with a Malvern™ Supersizer "S" with a sampling interval ≤ 1 cm in each RDL and at 5 cm intervals between the RDL. The grain size data were then processed with the Gradistat program (Blott and Pye, 2001). Digital X-radiographs were made on sediment slabs in an aluminum holder (1.5-m-long, 7-cm wide and 0.5-cm-thick) or on u-channels (rigid u-shaped plastic liners

with a square 2-cm cross-section and a length of 1.5 m) using the SCOPIX system at the Université Bordeaux 1 (Migeon et al., 1999).

3.3. Inclination and declination determination

The u-channel samples were measured in the Paleomagnetism Laboratory at the University of California in Davis, using a 2-G Enterprises™ Model 755 cryogenic magnetometer, at 1 cm intervals. Inclinations and declinations were calculated by principal component analysis (Kirschvink, 1980) using 4 to 10 alternating field (AF) demagnetization steps at peak fields of 10-80 mT. Because of a lack of azimuthal orientation, the declination of each core section was rotated to fit the end of the overlying core section. Declination below each RDL was also rotated to fit the declination above it. Following these procedures, a long-term linear trend likely resulting from core twisting was removed. This twisting was probably due to the coarse basal layers of the numerous RDL.

3.4. Geochemical and isotopic analyses

$CaCO_3$ contents were analyzed with an automatic Bernard calcimeter at 10 cm intervals. The $^{210}Pb_{ex}$ measurements were made after chemical treatment, purification and deposition on a silver disk following routine procedures at GEOTOP (Zhang, 2000) by alpha counting of the daughter ^{210}Po.

4. Rapidly deposited layers (RDL)

Based on physical, magnetic and sedimentological data, we identified at least 14 RDL in core MD99-2222 (Fig. 2). These layers contrast sharply from the dark grey bioturbated "background" sediments and are visually recognizable by their light color due to higher $CaCO_3$ content resulting from the incorporation of light grey, slightly calcareous, Laflamme Sea Clays (St-Onge and Hillaire-Marcel, 2001). Most RDL have a sandy base with corresponding peaks in density and magnetic susceptibility, along with generally lower paleomagnetic inclinations that indicate an energetic depositional process where the magnetic particles are plastered horizontally because of high flow velocity and rapid sediment accumulation. Homogeneous, light grey, clayey silt beds generally overlie the sandy bases.

We identified two types of RDL based on digital X-radiographs and high-resolution grain size analyses. The first type (RDL 2, 5, 6, 8, 12 and 13; Figs. 2-3) consists of ~7 cm to 1 m-thick fining-upward beds interpreted as Bouma-type turbidites (Bouma, 1962). Each consists of sharp-based laminated sand or silt underlying homogeneous unbioturbated clayey silt. The second type (RDL 1, 3, 7, 9, 10 and 11; Figs. 2, 4-5) is recognized by a sharp-based fining-upward basal bed underlying an upper bed composed of a laminated coarsening-upward unit, separated by a gradational contact, and followed by a thick fining-upward unit. These RDL are ~40 cm to 16 m thick.

The higher $CaCO_3$ content and lighter color of RDL 4 and 14 (only partially cored) are indicative of reworked Laflamme Sea Clays (Fig. 2), but the absence of characteristic

grain size trend (Fig. 6) or sedimentary structures prevent any clear interpretation on their depositional process. Nonetheless, because of its thickness and homogeneity, we infer that RDL 14 represents the upper part of a fining-upward bed, as in the two types of RDL presented above.

Kneller (1995) and Kneller and Branney (1995) showed that a basal coarsening-upward unit can be deposited by a depletive waxing flow, i.e. a flow decelerating with distance but accelerating with time, whereas Mulder and Syvitski (1995) showed that such flows can be generated by flooding rivers if the suspended matter concentration at the river mouth is above a threshold value. Beds composed of coarsening- and then fining-upward units have been interpreted as deposits from hyperpycnal turbidity currents or hyperpycnites (Mulder et al., 2002), where the coarsening-upward basal unit is deposited during the rising limb of the flood hydrograph and the top fining-upward unit during the falling limb (Mulder et al., 2001a; 2001b).

5. Possible RDL trigger mechanisms

Three trigger mechanisms could be responsible for the RDL deposition: floods, landslides initiated by overloading or oversteepening, and earthquake-triggered slumps. In 1996, a major flood caused by heavy rainfalls and the destruction of several dykes produced intense erosion and delivered more than 15 x 10^6 m^3 tons of sediments into the Baie des Ha!Ha! and the Northern Arm of the Fjord (Lapointe et al., 1998). The resulting bed was several decimeters thick at the head of the Fjord, but only a few centimeters thick

in more distal areas and no related deposit was detected in the deepest part of the deep basin, where core MD99-2222 was retrieved (St-Onge and Hillaire-Marcel, 2001; Urgeles et al., 2002).

Mulder and Syvitski (1995) showed that the Saguenay River is too "clean" to generate a hyperpycnal flow even during a major flood. The highest annual discharge (1928 AD) recorded from 1900-1979 AD (Smith and Schafer, 1987) deposited only a 4- cm-thick sandy bed at the head of the Fjord. This suggests that spring freshet or heavy rainfall alone cannot produce the decimeter to meter-thick turbidites that are observed distally in core MD99-2222.

Similar conclusions can be derived from the study of historical terrestrial landslides such as the 1971 St-Jean-Vianney and the 1924 Kénogami slides, which were respectively triggered by heavy rainfalls and the release of liquid industrial waste (Schafer et al., 1990). The 1971 landslide displaced more than 7.5 x 10^6 m^3 of sediments (Lasalle and Tremblay, 1978). It deposited a centimeter to decimeter-thick homogeneous light grey clayey bed in the Northern Arm, but nothing in the deepest part of the Fjord (Smith and Walton, 1980; St-Onge and Hillaire-Marcel, 2001). The 1924 landslide displaced about 1.9 x 10^6 m^3 of sediment (Smith and Schafer, 1987), but deposited only a 4 cm-thick light grey clayey layer in the Northern Arm of the Fjord (Smith and Schafer, 1987), suggesting that terrestrial landslides alone cannot generate the thicker turbidites observed more distally in core MD99-2222.

The 1988 AD earthquake (M=6) (Lamontagne, 2000; Fig. 1), did not produce any significant landslides or submarine slides in the deep basin of the Fjord (Urgeles, 2002).

However, a major earthquake (M ≈ 7) that occurred on February 5, 1663 AD near the mouth of the Saguenay Fjord (Lamontagne, 2000) or in the Saguenay area (Locat et al., 2003), generated about 3 km^3 of landslides and submarine slides over most of the deep basin of the Fjord (Syvitski and Schafer, 1996). A landslide at the head of the Fjord possibly dammed the river with about 0.2 km^3 of material (Syvitski and Schafer, 1996). Syvitski and Schafer (1996) interpreted that this dam was breached during the following spring freshet, contributing to very high suspended particulate matter concentrations, which generated an estimated 28-day-long hyperpycnal flow. They concluded that the turbidite observed in sediment cores or in seismic reflection profiles throughout the Fjord was deposited by this hyperpycnal flow and that the underlying debris flow was triggered by the initial earthquake shock.

6. Earthquake and flood-induced RDL

6.1. The 1663 AD event

Previous core, seismic reflection and multibeam bathymetry investigations in the Saguenay Fjord have identified and linked a meter-thick RDL to the 1663 AD earthquake (Schafer and Smith, 1987, Locat and Leroueil, 1988; Perret et al. 1995; Syvitski and Schafer, 1996; Locat et al., 2000; St-Onge and Hillaire-Marcel, 2001). In cores sampled in the deepest part of the deep basin, this RDL is the first meter-thick unbioturbated and

homogeneous light grey layer observed downcore. It is a fining-upward turbidite with a low organic carbon content and an increase in inorganic carbon content (Perret et al., 1995; Syvitski and Schafer, 1996; St-Onge et al., 2001). The top of this RDL was observed at depths of ~ 70 cm (Perret et al., 1995; St-Onge et al., 2001), 50 cm and 70 cm (Syvitski and Schafer, 1996) in cores collected in the proximity of core MD99-2222. On the basis of its similar downcore depth, thickness, sediment texture, color and $CaCO_3$ content (Figs. 2, 4-5), we assign the uppermost RDL of core MD99-2222 to the 1663 AD earthquake.

In core MD99-2222, we interpret the basal fining-upward turbidite of RDL 1 as the result of the initial earthquake shaking and the overlying coarsening- and then fining-upward units as a result of a hyperpycnal turbidity current generated by the spring freshet. The very thin basal unit compared to the top unit implies a strongly asymmetric flood hydrograph, such as that during glacier outburst floods (Björnson, 1992), consistent with breaching and rapid draining of the landslide dam. A numerical model of the transport and deposit of the inferred hyperpycnal flow (Mulder et al., 1998) correctly reproduced the formation of the basal inversely graded and top normally graded units.

6.2. Other earthquake and flood-induced RDL

By analogy to the 1663 AD RDL, the five other sequences composed of a fining-upward turbidite underlying a coarsening- and fining-upward sequence (Figs. 2 and 4) are considered to have been deposited through a similar series of events. The succession from the basal turbidite to the hyperpycnite seems continuous for all these RDL with no visible

traces of "background" hemipelagic sedimentation or bioturbation between the two units. This indicates that the flood-induced turbidite was deposited very shortly after the deposition of the basal fining-upward turbidite.

7. Earthquake-triggered RDL

The individual fining-upward turbidites (Figs. 2-3) all have similar characteristics suggesting that they were deposited by similar events. The absence of thick turbidites in the deepest part of the Fjord associated with historical floods or terrestrial landslides and the similarity of the beds with the lowest unit of the RDL couplets described above suggest that the most likely explanation for their deposition is that they were produced by earthquake-triggered terrestrial and/or submarine slides, that transformed into a debris flow and then to a turbidity current (e.g., Piper et al., 1999). However, in this type of RDL, no slides dammed the river upstream and the top hyperpycnite is lacking.

8. Chronology

Because of $CaCO_3$ dissolution (St-Onge et al., 1999), little material is available for radiocarbon dating. One benthic mollusk shell at 2090 cm yielded an AMS radiocarbon age of 3790 ± 60 yr BP, corresponding to 3636 (3709) 3816 calendar years using CALIB4.3 (Stuiver et al., 1998), assuming a marine reservoir correction of -400 yrs. The correction

was recently shown to be appropriate for the St. Lawrence Estuary waters, which composes the bottom waters of the Fjord (St Onge et al., 2003). The interval of hemipelagic sediment between this date and the base of the 1663 AD RDL accumulated at a rate of 0.15 cm/yr. This estimate is consistent with a sedimentation rate of 0.18 cm/yr determined by extrapolation of $^{210}Pb_{ex}$ activities on top of core MD99-2222 (Fig. 7) and with rates calculated using ^{137}Cs and $^{210}Pb_{ex}$ activities in box-cored sediments from surrounding sites (Smith and Walton, 1980; Zhang, 2000; St-Onge and Hillaire-Marcel, 2001). Using the 0.15 cm/yr sedimentation rate, we then correlated the full magnetic vector of core MD99-2222 "background" sediments with the Holocene paleomagnetic record of core MD99-2220, raised from the St. Lawrence Estuary (48°38.32N, 68°37.93W, water depth: 320 m; St-Onge et al., 2003). This exercise resulted in a good correlation to core MD99-2220 inclination (r=0.47; Fig. 8), declination (r=0.53; Fig. 8) and relative paleointensity proxy (r=0.71; see Electronic supplement, Figs. S1-S4) records. Core MD99-2220 chronology is primarily based on thirteen ^{14}C AMS dates and is in good agreement with the Greenland Ice Sheet Project (GISP2) chronology (Meese et al., 1994) and the tree-ring chronology of Stuiver et al. (1998) for the last ~8500 cal BP (St-Onge et al., 2003). The resulting chronology reveals that the base of core MD99-2222 is about 7200 cal BP (Fig. 8).

9. Earthquake recurrence during the Holocene

Doig (1998) described seven unusual silt layers in organic-rich lake sediments from the Saguenay area that he interpreted as the result of resuspension after local earthquakes of

magnitude ≥ 6. Dating control was based on extrapolation of the appearance of ^{137}Cs at 1943 +/-6 AD, suggesting a maximum age of ~ 3 ka for the lake cores. Based on this chronology, Doig (1998) estimated a recurrence interval in the range of one earthquake every 350 to 1000 years. However, because there are no chronological constraints beyond 1943 AD, pre-anthropogenic sedimentation rates are unknown, making this estimate highly speculative.

Earthquakes that produced RDL in the Saguenay Fjord are likely to have a magnitude higher than 6.75 (Urgeles et al., 2002) if their epicenter was located near the epicenter of the M = 6 1988 AD earthquake (Fig. 1), an earthquake which did not produce any significant landslides or submarine slides in the Fjord (Urgeles et al., 2002). The epicentral area of the 1988 AD earthquake as the source of moderate to strong earthquakes in the Saguenay region is supported by the following evidence. First, prior to 1988 AD, no M > 3 earthquake was recorded or reported in the Saguenay area (Du Berger et al., 1991). Second, a cluster of deep seismic events is now observed around the area of the 1988 AD earthquake (Urgeles et al., 2002) and third, there is no apparent link between earthquakes and surface geologic features such as the Saguenay graben (Du Berger et al., 1991). The high magnitude threshold necessary to trigger a RDL in the Saguenay Fjord is consistent with the long mean recurrence interval of 2000 years calculated in this study over the past 4 ka (two RDL in 4 ka), which is longer than the estimate of Doig (1998) for the last 3 ka. The shorter recurrence interval of Doig (1998) for M ≥ 6 earthquakes may result from the lack of chronological control and/or the recording of lower magnitude earthquakes such as the M = 6 1988 AD earthquake.

Based on our chronology and excluding RDL 4, the frequency of RDL and hence that of large earthquakes in the Saguenay region appeared to have been substantially higher in the mid-Holocene, prior to 4 ka, with a recurrence interval of approximately 300 years (Fig. 8). There is no direct relationship between seismicity and the rate of crustal rebound determined from raised shorelines (e.g. summarized by Shaw et al. 2002), as crustal rebound was fast from 10-6 ka and much slower thereafter. However, the core MD99-2222 RDL record is consistent with the ice-load modeling of Wu (1998), who predicted that the greatest fault instability would be expected in the 7-4 ka period in Eastern Canada, possibly activating pre-existing faults from numerous zones of weakness in the Saguenay area (Du Berger et al., 1991). The well-dated record from core MD99-2222 thus substantially improves the record of Eastern Canadian paleoseismicity (Adams, 1996).

10. The impact of earthquakes on sedimentation

The turbidites in the Saguenay Fjord are probably all related, either directly or indirectly, to earthquake activity, as no other mechanism could account for the decimeter- to meter-thick turbidites observed distally in core MD99-2222. However, the cumulative thickness of those directly derived from slope failure is only about 10% of those that resulted from hyperpycnal flow. Thick turbidites are most readily generated by hyperpycnal flow because of the much longer duration of such turbidity currents (days) compared with those generated by slumps (hours). Large turbidity currents on continental margins gain much of their sediment load from remobilizing sediment stored in canyons (conduit

flushing of Normark and Piper, 1991), so that duration of flow is a critical factor in determining the ultimate size of a turbidite bed. Indeed, during high magnitude floods, the concentration of suspended particulate matter increases exponentially with increasing discharge and long duration events associated with high sediment load suggest hyperpycnal flows could be responsible for a considerable amount of the fluvial terrigenous inputs into the oceans (Mulder et al., 2003; Syvitski, 2003).

Acknowledgements

We are in debt to the IPEV, Y. Balut, the captain, officers, crew and scientific participants of Legs 1 and 2 of the IMAGES-V cruise. We wish to sincerely thank K. Verosub for the use of his lab at the University of California Davis (UCD) for the paleomagnetic measurements. Thanks are also due to O. Weber, J. Saint-Paul and G. Chabaud for laboratory assistance at the Université Bordeaux 1 and to C. Goldfinger and B. Normark for their constructive reviews. Discussions with J.-C. Mareschal were greatly appreciated. This study was supported by the IMAGES and CSHD programs, the CCAF and CFCAS and by NSERC "Saguenay post-déluge" strategic grant. G. St-Onge acknowledges postgraduate scholarships from NSERC, FCAR, Natural Resources Canada and Fisheries and Oceans Canada. Laboratory measurements at UCD and J.S. Stoner contribution were supported by NSF OCE-9911698.

References

Adams, J., 1996. Paleoseismology in Canada: a dozen years of progress. Journal of Geophysical Research 101, 6193-6207.

Björnson, H., 1992. Jökulhlaups in Iceland: characteristics, prediction and simulation. Annals of Glaciology 16, 95-106.

Blott, S.J., Pye, K., 2001. Gradistat: A grain size distribution and statistics package for the analysis of unconsolidated sediments. Earth Surface Processes and Landforms 26, 1237-1248.

Bouma, A.H., 1962. Sedimentology of some flysch deposits. A graphic approach to facies interpretation. Elsevier, Amsterdam.

Doig, R., 1998. 3000-year paleoseismological record from the region of the 1988 Saguenay, Quebec, earthquake. Bulletin of the Seismological Society of America 88, 1198-1203.

Drainville, G., 1968. Le fjord du Saguenay: contribution à l'océanographie. Le Naturaliste canadien 95, 809-855.

Du Berger, R., Roy, D.W., Lamontagne, M., Woussen, G., North, R.G., Wetmiller, R.J., 1991. The Saguenay (Quebec) earthquake of November 25, 1988: seismological data and geological setting. Tectonophysics, 186, 59-74.

Hébert, S., 1995. Qualité des eaux du Saguenay-Lac-Saint-Jean. 1979-1992. Ministère de l'Environnement et de la Faune. Québec.

Kirschvink, J.L., 1980. The least-squares line and plane and the analysis of paleomagnetic data. Geophysical Journal of the Royal Astronomical Society 62, 699-718.

Kneller, B.C., 1995. Beyond the turbidite paradigm: physical models for deposition of turbidites and their implications for reservoir prediction. In Hartley, A.J., Prosser, D.J. (Eds.), Characterization of deep marine clastic systems. Geological Society [London] Special Publication 94, pp. 31-49.

Kneller, B.C., Branney, M.J., 1995. Sustained high-density turbidity currents and the deposition of thick massive beds. Sedimentology 42, 607-616.

Lamontagne, M., 2000. Geotechnical impact of Eastern and Northern Canadian earthquakes. In Couture, R. Evans S.G. (Eds.), Canadian workshop on geotechnique and natural hazards: an IDNDR perspective. Proceedings of the 53rd Canadian Geotechnical Conference, Montréal, Québec, pp. 43-49.

Lapointe, M.F., Secretan, Y., Driscoll, S.N., Bergeron, N., Leclerc, M., 1998. Response of the Ha!Ha! River to the flood of July 1996 in the Saguenay Region of Quebec: Large-scale avulsion in a glaciated valley. Water Resources Research 34, 2383-2392.

Lasalle, P., Tremblay, G., 1978. Dépôts meubles Saguenay Lac Saint-Jean. Rapport 191, Ministère des Richesses naturelles du Québec, Québec city, Québec, 61 pp.

Locat, J., Leroueil, S., 1988. Physicochemical and geotechnical characteristics of recent Saguenay Fjord sediments. Canadian Geotechnical Journal 25, 382-388.

Locat, J., Urgeles, R., Schmitt, T., Martin, F., Hoareau, L., Hill, P., Long, B., Kammerer, E., Sanfaçon, R., 2000. The morphological signature of natural disasters in the Upper

Saguenay Fjord area, Québec, Canada. Proceedings of the 53rd Canadian Geotechnical Conference, Montréal, Québec, pp. 109-116.

Locat, J., Martin, F., Locat, P., Leroueil, S., Levesque, C., Konrad, J.-M., Urgeles, R., Canals, M., Duchesne, M.J., 2003. Submarine mass movements in the upper Saguenay Fjord, (Québec, Canada), triggered by the 1663 earthquake. In: Locat, J., Mienert, J. (Eds.), Submarine Mass Movements and Their Consequences, 1st International Symposium, Kluwer Academic Publishers, Dordrecht, pp. 509-519.

Meese, D.A., Alley, R.B., Fiacco, R.J., Germani, M.S., Gow, A.J., Grootes, P.M., Illing, M., Mayewski, P.A., Morrison, M.C., Ram, M., Taylor, K.C., Yang, Q., and Zielinski, G.A., 1994. Preliminary depth-age scale of the GISP2 ice core: Special CRREL Report 94-1, US.

Migeon, S., Weber, O., Faugères, J.-C., Saint-Paul, J., 1999. SCOPIX: a new X-ray imaging system for core analysis. Geo-Marine Letters 18, 251-255.

Mulder, T., Syvitski, J.P.M., 1995. Turbidity currents generated at river mouths during exceptional discharges to the world oceans. Journal of Geology 103, 285-299.

Mulder, T., Syvitski, J.P.M., Skene, K.I., 1998. Modeling of erosion and deposition by turbidity currents generated at river mouths. Journal of Sedimentary Research 68, 124-137.

Mulder, T., Migeon, S., Savoye, B., Jouanneau, J.-M., 2001a. Twentieth century floods recorded in deep Mediterranean sediments. Geology 29, 1011-1014.

Mulder, T., Migeon, S., Savoye, B., Faugères, J.-C., 2001b. Inversely graded turbidite sequences in the deep Mediterranean: a record of deposits from flood-generated turbidity currents?. Geo-Marine Letters 21, 86-93.

Mulder, T., Migeon, S., Savoye, B., Faugères, J.-C., 2002. Inversely graded turbidite sequences in the deep Mediterranean: a record of deposits from flood-generated turbidity currents? Reply. Geo-Marine Letters 22, 112-120.

Mulder, T., Syvitski, J.P.M., Migeon, S., Faugères, J.-C., Savoye, B., 2003. Marine hyperpycnal flows: initiation, behavior and related deposits. A review. Marine and Petroleum Geology 20, 861-882.

Normark, W.R, Piper, D.J.W., 1991. Depositional consequences of turbidity currents reflecting initiation processes and flow evolution. Society of Economic Paleontologists and Mineralogists Special Publication 46, 207-230.

Perret, D., Locat, J., Leroueil, S., 1995. Strength development with burial in fine-grained sediments from the Saguenay Fjord, Quebec. Canadian Geotechnical Journal 32, 247-262.

Piper, D.J.W., Cochonat, P., Morrison, M., 1999. Sidescan sonar evidence for progressive evolution of submarine failure into a turbidity current: the 1929 Grand Banks event. Sedimentology 46, 79-97.

Praeg, D.B., Syvitski, J.P.M., 1991. Marine geology of Saguenay Fjord. Geological Survey of Canada, Open File 2395, 14 sheets.

Schafer, C.T., Smith, J.N., 1987. Hypothesis for a submarine landslide and cohesionless sediment flows resulting from a 17th century earthquake-triggered landslide in Quebec, Canada. Geo-Marine Letters 7, 31-37.

Schafer, C.T., Smith, J.N., Côté, R., 1990. The Saguenay Fjord: A major tributary to the St. Lawrence Estuary, p. 378-420. In Sabh, M.I., Silverberg, N. (Eds.), Oceanography of a Large-Scale Estuarine System. The St.-Lawrence. Springer-Verlag, New York, pp. 378-420.

Shaw, J., Gareau, P., Courtney, R.C., 2002. Paleogeography of Atlantic Canada 13-0 kyr. Quaternary Science Reviews 21, 1861-1878.

Smith, J.N., Schafer, C., 1987. A 20th-century record of climatologically modulated sediment accumulation rates in a Canadian fjord. Quaternary Research 27, 232-247.

Smith, J.N., Walton, A., 1980. Sediment accumulation rates and geochronologies measured in the Saguenay Fjord using Pb-210 dating method. Geochimica et Cosmochimica Acta 44, 225-240.

St-Onge, G., Leduc, J., Bilodeau, G., de Vernal, A., Devillers, R., Hillaire-Marcel, C., Loucheur, V., Marmen, S., Mucci, A., Zhang, D., 1999. Caractérisation des sédiments récents du fjord du Saguenay à partir de traceurs physiques, géochimiques, isotopiques et micropaléontologiques. Géographie physique et Quaternaire 53, 339-350.

St-Onge, G., Hillaire-Marcel, C., 2001. Isotopic constraints of sedimentary inputs and organic carbon burial rates in the Saguenay Fjord, Quebec. Marine Geology 176, 1-22.

St-Onge, G., Stoner, J.S., Hillaire-Marcel, C., 2003. Holocene paleomagnetic records from the St. Lawrence Estuary, Eastern Canada: centennial- to millennial-scale geomagnetic modulation of cosmogenic isotopes. Earth and Planetary Science Letters 209, 113-130.

Stuiver, M., Reimer, P.J., Bard, E., Beck, J. W., Burr, G.S., Hughen, K.A., Kromer, B., McCormac, G., van der Plicht, J., Spurk, M., 1998. INTCAL98 radiocarbon age calibration, 24,000-0 cal BP. Radiocarbon 40, 1041-1083.

Syvitski, J.P.M., Schafer, C.T., 1996. Evidence for earthquake-triggered basin collapse in Saguenay Fjord, Canada. Sedimentary Geology 104, 127-153.

Syvitski, J.P.M., 2003. Sediment fluxes and rates of sedimentation. In Middleton, G.V. (Ed.), Encyclopedia of Sediments and Sedimentary Rocks. Kluwer Academic Publishers, Dordrecht, Netherlands, pp. 600-606.

Urgeles, R. Locat, J., Lee, H.J., Martin, F., 2002. The Saguenay Fjord, Quebec, Canada: integrating marine geotechnical and geophysical data for seismic slope stability and hazard assessment. Marine Geology 185, 319-340.

Wu, P., 1998. Intraplate earthquakes and post-glacial rebound in eastern Canada and Northern Europe, In Wu, P. (Ed.), Dynamics of the Ice Age Earth, a modern perspective. Zurich, Trans Tech Publications, pp. 603-628.

Zhang, D., 2000. Flux de radio-isotopes à courte période dans les bassins marins marginaux de l'est canadien. Ph.D. thesis, Université du Québec à Montréal, Montréal, Québec.

Figure captions

Fig. 1. The Saguenay Fjord (Québec). Upper panel: Location of core MD99-2222 sampling site. Also illustrated are the location of the 1988 AD earthquake epicenter and the approximate location of the Charlevoix seismic zone (CSZ). Lower panel: Longitudinal transect along the Saguenay Fjord showing the bottom morphology and salinity gradients. Modified from St-Onge and Hillaire-Marcel (2001).

Fig. 2. Rapidly deposited layers (RDL) in core MD99-2222. RDL 1 is linked to the 1663 AD earthquake. The fining-upward turbidites are in yellow, the sequences composed of a basal fining-upward turbidite underlying a succession of coarsening and fining beds are in orange, whereas RDL 4 and 14 are in grey (see text for details).

Fig. 3. Grain size trend for the fining-upward turbidites.

Fig. 4. Grain size trend for the fining-upward turbidite and hyperpycnal deposit sequences.

Fig. 5. Digital X-radiographs and grain size data of the two thickest fining-upward turbidite and hyperpycnite sequences. A: RDL 1 (1663 AD). B: RDL 11. Digital X-radiographs were made on sediment slabs in an aluminum holder for RDL 11 and on the u-channels for RDL 1. Small fissures in the sediment are indicated by arrows.

Fig. 6. Mean grain size for (A) RDL 4 and (B) RDL 14. The base of RDL 14 was not cored.

Fig. 7. $^{210}Pb_{ex}$ measurements in the surface sediments of core MD99-2222. Using the regional $^{210}Pb_{ex}$ supported value of 1.0 dpm/g (Zhang, 2000), we estimated a sedimentation rate (SR) of 0.18 cm/yr.

Fig. 8. Core MD99-2222 tuned chronology. A) Inclination. B) Declination. Core MD99-2220 magnetic inclination and declination records are from St-Onge et al. (2003). Arrows indicate the estimated age of each RDL. The correlation coefficients were calculated from 750 to 7200 cal BP.

Electronic supplement

Figure S1. Comparison of core MD99-2222 normalized remanence record with core MD99-2220 (St. Lawrence Estuary). The natural remanent magnetization (NRM) and the isothermal remanent magnetization (IRM) were measured at 1cm intervals on u-channel samples using a 2-G Enterprises™ Model 755 cryogenic magnetometer at the University of California, Davis. The NRM was obtained by progressive alternating field (AF) demagnetization using peak fields of 0, 10, 20, 25, 30, 35, 40, 50, 60, 70 and 80 mT. The IRM was produced by imparting a DC field of 0.3 T and was subsequently demagnetized and measured at peak AF fields of 0, 20, 30, 40 and 50 mT. The normalized remanence record presented here was obtained by dividing the NRM_{30mT} with the IRM_{30mT} and is believed to primarily reflect changes in the intensity of the Earth's magnetic field. Core MD99-2222 record is based on the chronology presented in this paper, whereas core MD99-2220 chronology is from St-Onge et al. (2003). The correlation coefficient was calculated from 750 to 7200 cal BP.

Reference for the electronic supplement

St-Onge, G., Stoner, J.S., Hillaire-Marcel, C., 2003. Holocene paleomagnetic records from the St. Lawrence Estuary, Eastern Canada: centennial- to millennial-scale geomagnetic modulation of cosmogenic isotopes. Earth and Planetary Science Letters 209, 113-130.

Figure S2. Rock-magnetic properties of core MD99-2222. The RDL are highlighted in color as in Fig. 2 (see figure 2 and main text for details). The magnetic concentration variations in the "background sediments", as indicated by changes in k, ARM_{30mT} and IRM_{30mT} values, vary by a factor less than 10. The natural remanent magnetization (NRM) was studied by progressive alternating field (AF) demagnetization using peak fields of 0, 10, 20, 25, 30, 35, 40, 50, 60, 70 and 80 mT at 1 cm intervals on u-channel samples using a 2-G Enterprises™ Model 755 cryogenic magnetometer at the University of California, Davis. An anhysteretic remanent magnetization (ARM) was produced using a 100 mT peak AF and a 50 μT direct current (DC) biasing field. This ARM was subsequently demagnetized and measured after peak AF of 0, 20, 30, 40 and 50 mT. The ARM data were also expressed as a susceptibility of the ARM (k_{ARM}) by normalizing the ARM by the strength of the biasing field. The isothermal remanent magnetization (IRM) was produced by imparting a DC field of 0.3 T. Each IRM was demagnetized and measured at the same peak AF as the ARM.

Figure S3. Hysteresis parameters for core MD99-2222 sediments. Typical hysteresis loops for "background" sediments sampled at A) 1650 cm and B) 3600 cm. C) Hysteresis parameters plotted on a Day et al. (1977) diagram. The shape of the hysteresis loops and the hysteresis ratios of most samples are consistent with a dominant low coercivity ferrimagnetic component such as magnetite that is of pseudo-single domain (PSD) magnetic grain size. The three highest Hcr/Hc values were measured on samples from the sandy base of RDL 1. Hysteresis parameters were measured at 1.5 m intervals using a

Princeton Measurements™ alternating gradient magnetometer (MicroMag) at the University of California, Davis. The saturation magnetization (M_s), saturation remanence (M_{rs}) and the coercive force (H_c) were obtained from hysteresis loops. The coercivity of the remanence (H_{cr}) was determined by backfield experiments.

Reference for the electronic supplement

Day, R., Fuller, M., Schmidt, V.A., 1977. Hysteresis properties of titanomagnetites: grain-size compositional dependence. Physics of the Earth and Planetary Interiors 13, 260-267.

Figure S4. Paleomagnetic directional data of core MD99-2222 sediments. A) Component inclination and declination with corresponding MAD values. The RDL are highlithed in color as in Fig. 2 (see figure 2 and main text for details). Typical vector endpoint diagrams and decay of the normalized intensity during alternating field (AF) demagnetization for "background" sediments sampled at B) 1653 cm and C) 3601 cm. These graphs illustrate that the "background" sediments are characterized by a well-defined, strong stable single component magnetization. MDF=Medium Destructive Field.

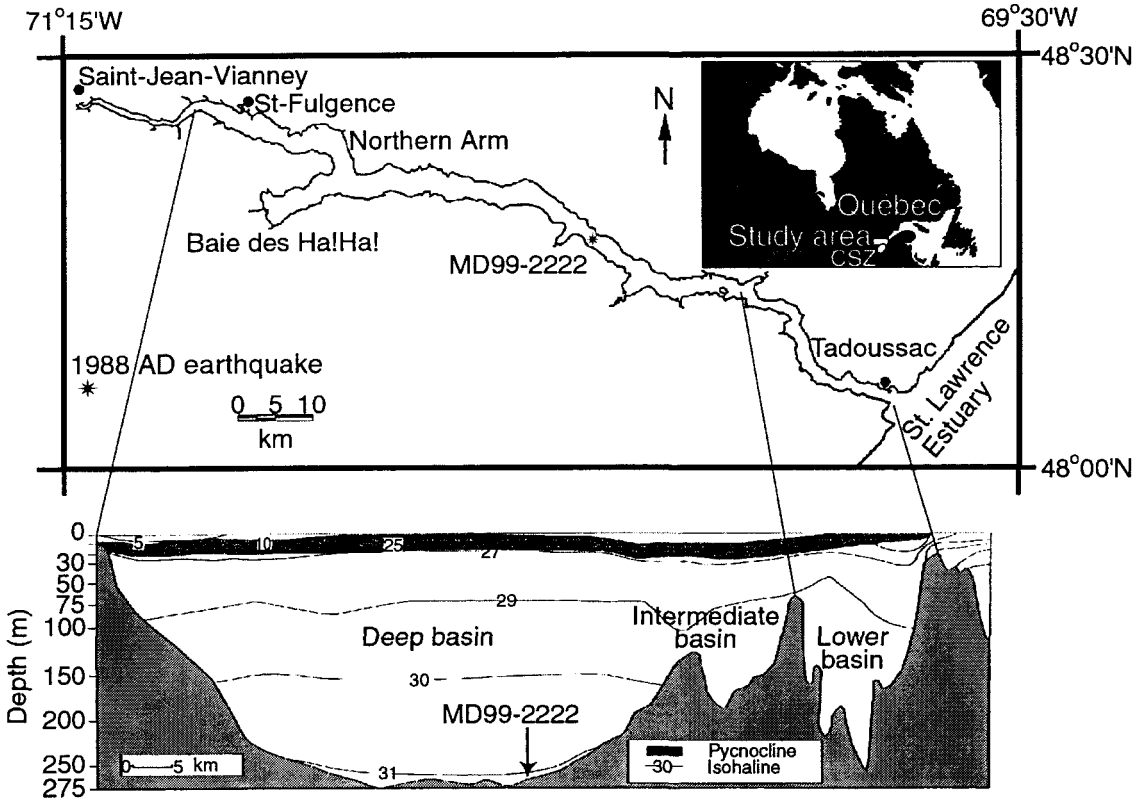
71°15'W
69°30'W
48°30'N
48°00'N
Saint-Jean-Vianney
St-Fulgence
Northern Arm
Baie des Ha!Ha!
MD99-2222
N
Québec
Study area
CSZ
Tadoussac
St. Lawrence Estuary
1988 AD earthquake
0 5 10
km
Depth (m)
0
30
50
75
100
150
200
250
275
5
10
25
27
29
30
31
Deep basin
Intermediate basin
Lower basin
MD99-2222
0 5 km
Pycnocline
30 Isohaline

Fig. 1

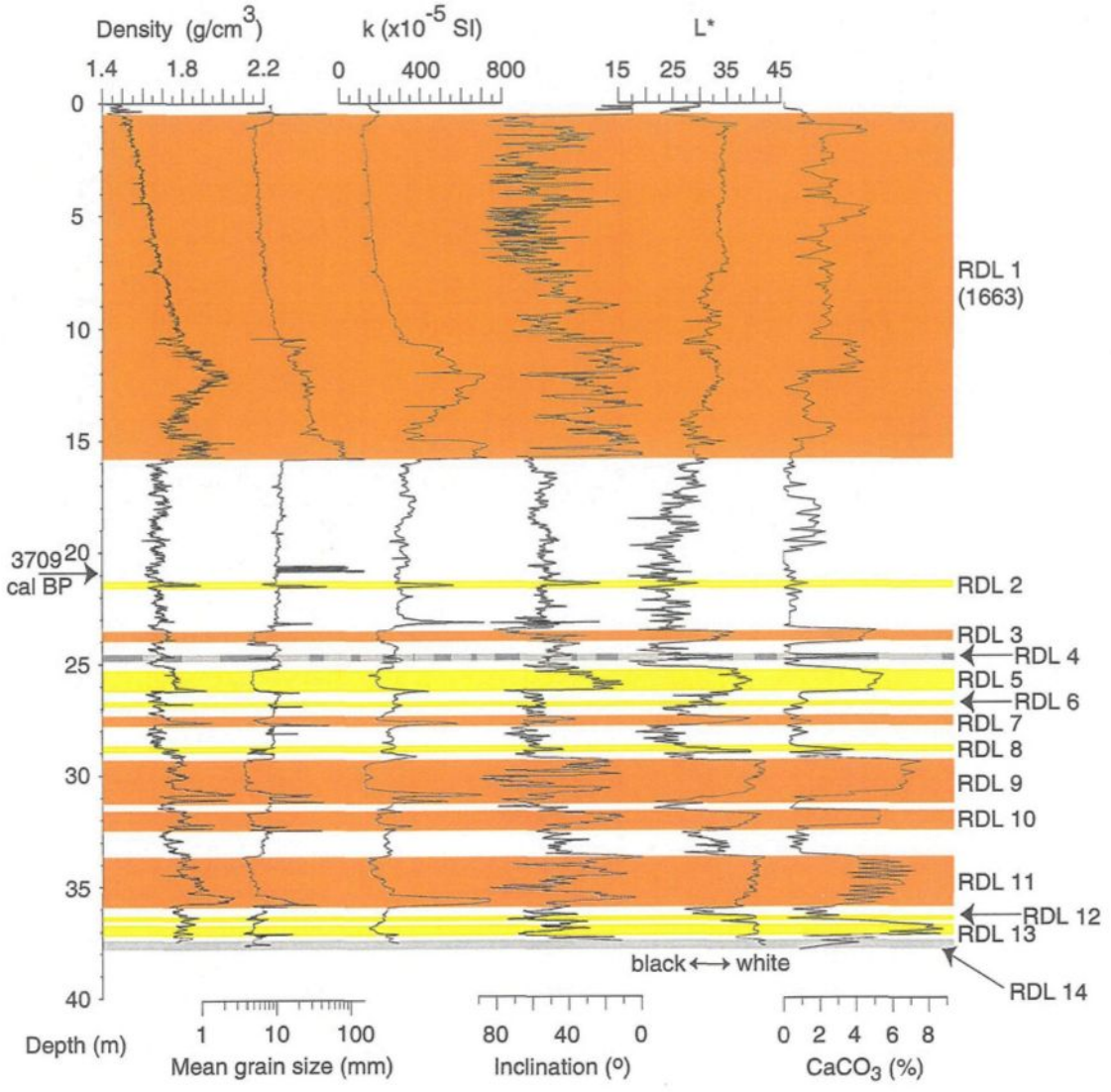
Density (g/cm3)
k (x10-5 SI)
L*
1.4 1.8 2.2
0 400 800
15 25 35 45
0
5
10
15
20
25
30
35
40
3709 cal BP
RDL 1 (1663)
RDL 2
RDL 3
RDL 4
RDL 5
RDL 6
RDL 7
RDL 8
RDL 9
RDL 10
RDL 11
RDL 12
RDL 13
black ↔ white
RDL 14
Depth (m)
1 10 100
Mean grain size (mm)
80 40 0
Inclination (°)
0 2 4 6 8
CaCO3 (%)

Fig. 2

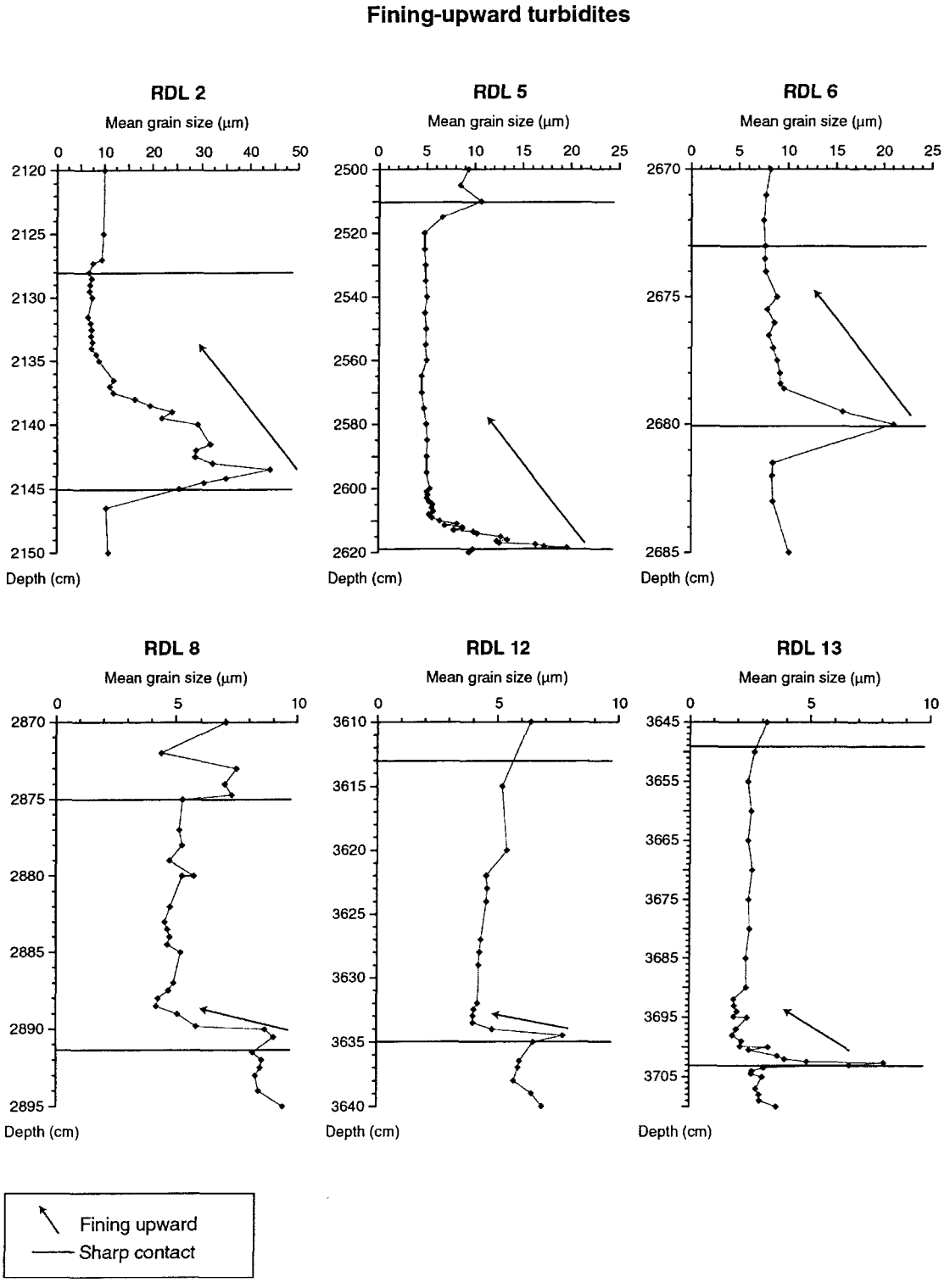
Fining-upward turbidites
RDL 2
Mean grain size (μm)
0 10 20 30 40 50
2120 2125 2130 2135 2140 2145 2150
Depth (cm)
RDL 5
Mean grain size (μm)
0 5 10 15 20 25
2500 2520 2540 2560 2580 2600 2620
Depth (cm)
RDL 6
Mean grain size (μm)
0 5 10 15 20 25
2670 2675 2680 2685
Depth (cm)
RDL 8
Mean grain size (μm)
0 5 10
2870 2875 2880 2885 2890 2895
Depth (cm)
RDL 12
Mean grain size (μm)
0 5 10
3610 3615 3620 3625 3630 3635 3640
Depth (cm)
RDL 13
Mean grain size (μm)
0 5 10
3645 3655 3665 3675 3685 3695 3705
Depth (cm)
Fining upward
Sharp contact

Fig. 3

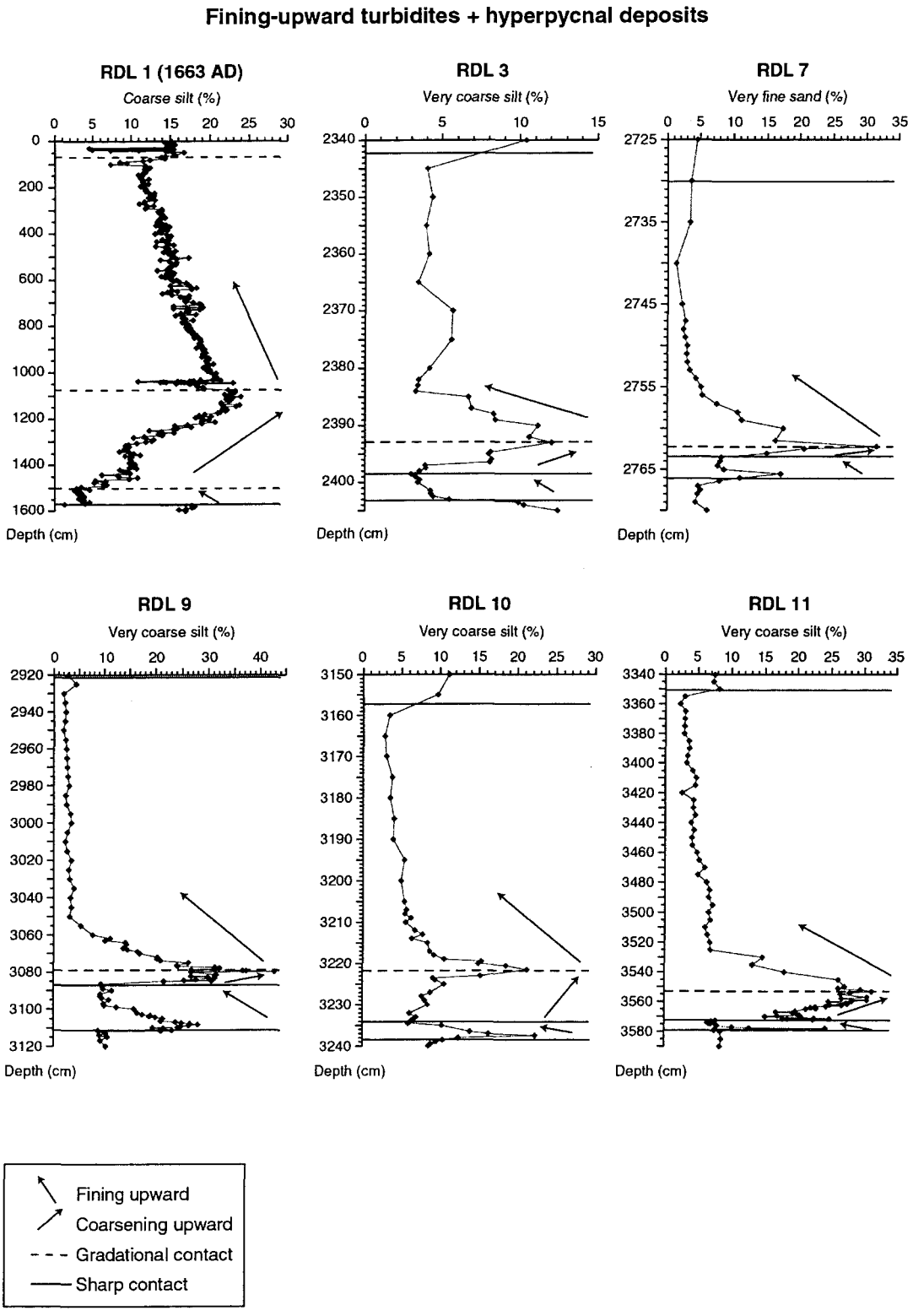
Fining-upward turbidites + hyperpycnal deposits
RDL 1 (1663 AD)
Coarse silt (%)
Depth (cm)
RDL 3
Very coarse silt (%)
Depth (cm)
RDL 7
Very fine sand (%)
Depth (cm)
RDL 9
Very coarse silt (%)
Depth (cm)
RDL 10
Very coarse silt (%)
Depth (cm)
RDL 11
Very coarse silt (%)
Depth (cm)
Fining upward
Coarsening upward
Gradational contact
Sharp contact

Fig. 4

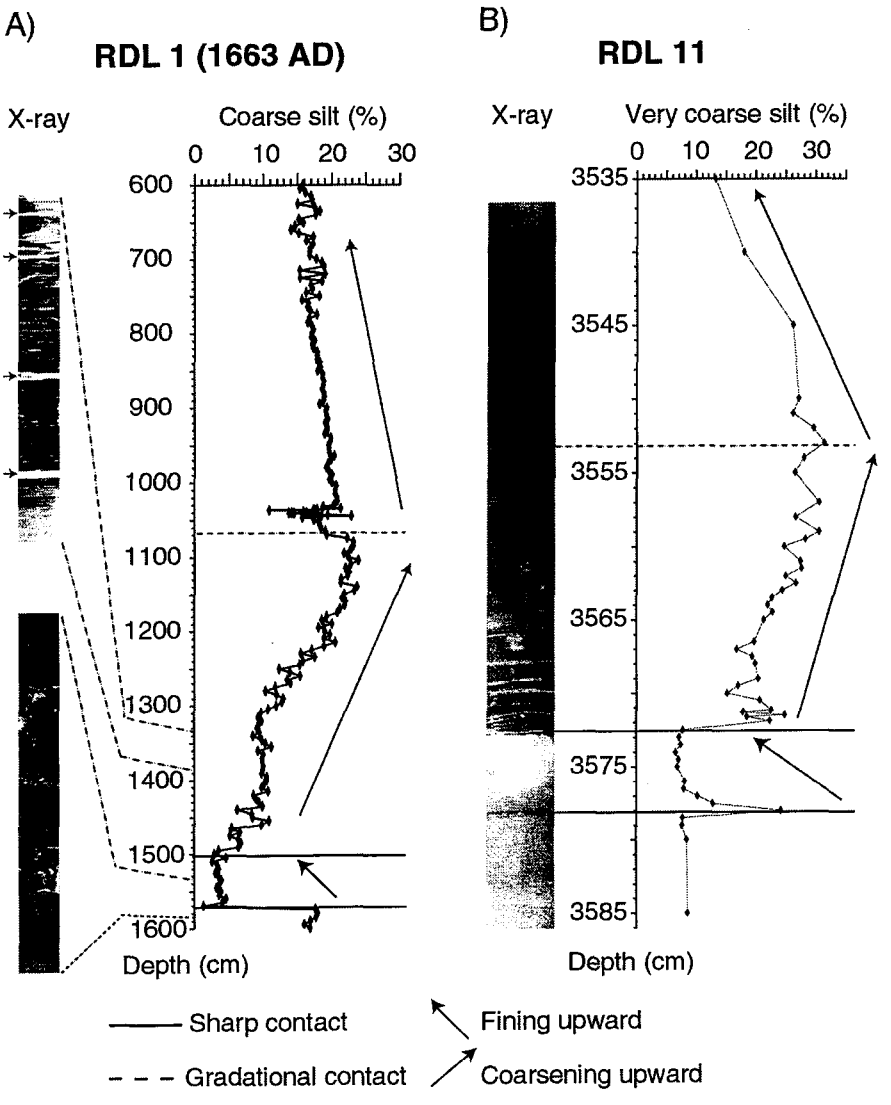
A)
RDL 1 (1663 AD)
X-ray
Coarse silt (%)
0 10 20 30
600
700
800
900
1000
1100
1200
1300
1400
1500
1600
Depth (cm)
B)
RDL 11
X-ray
Very coarse silt (%)
0 10 20 30
3535
3545
3555
3565
3575
3585
Depth (cm)
Sharp contact
Gradational contact
Fining upward
Coarsening upward

Fig. 5

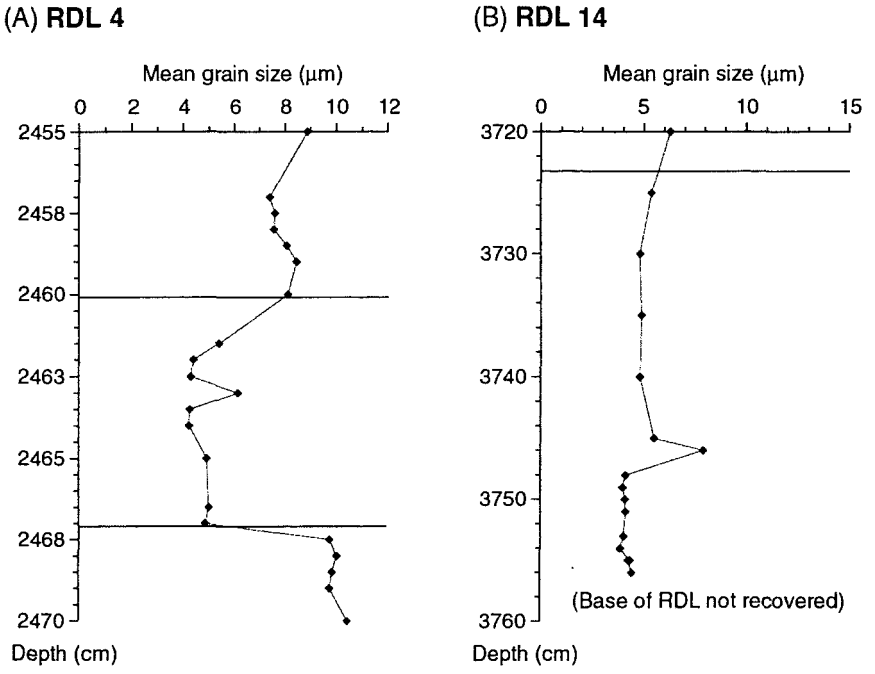
(A) RDL 4
Mean grain size (μm)
0
2
4
6
8
10
12
2455
2458
2460
2463
2465
2468
2470
Depth (cm)
(B) RDL 14
Mean grain size (μm)
0
5
10
15
3720
3730
3740
3750
3760
(Base of RDL not recovered)
Depth (cm)

Fig. 6

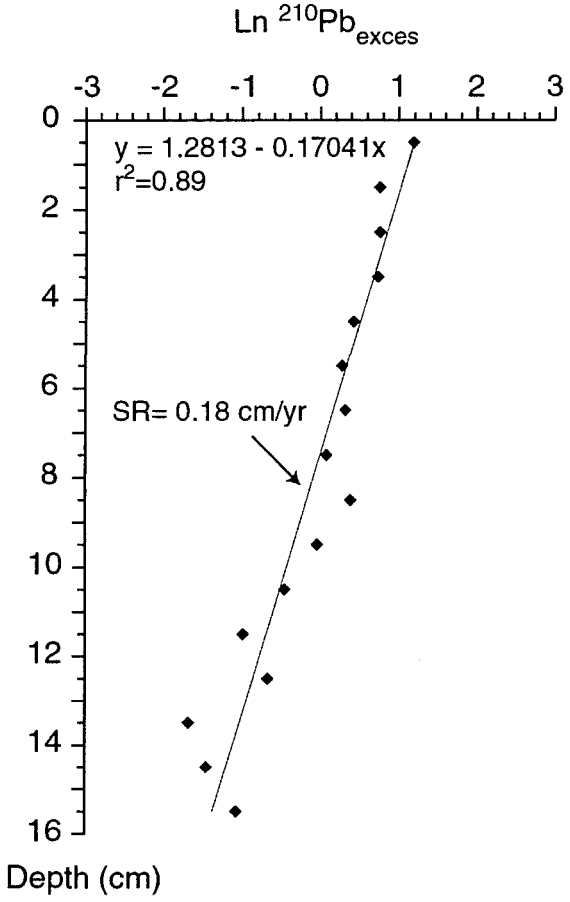
Ln 210Pbexces
-3
-2
-1
0
1
2
3
0
2
4
6
8
10
12
14
16
y = 1.2813 - 0.17041x
r2=0.89
SR= 0.18 cm/yr
Depth (cm)

Fig. 7

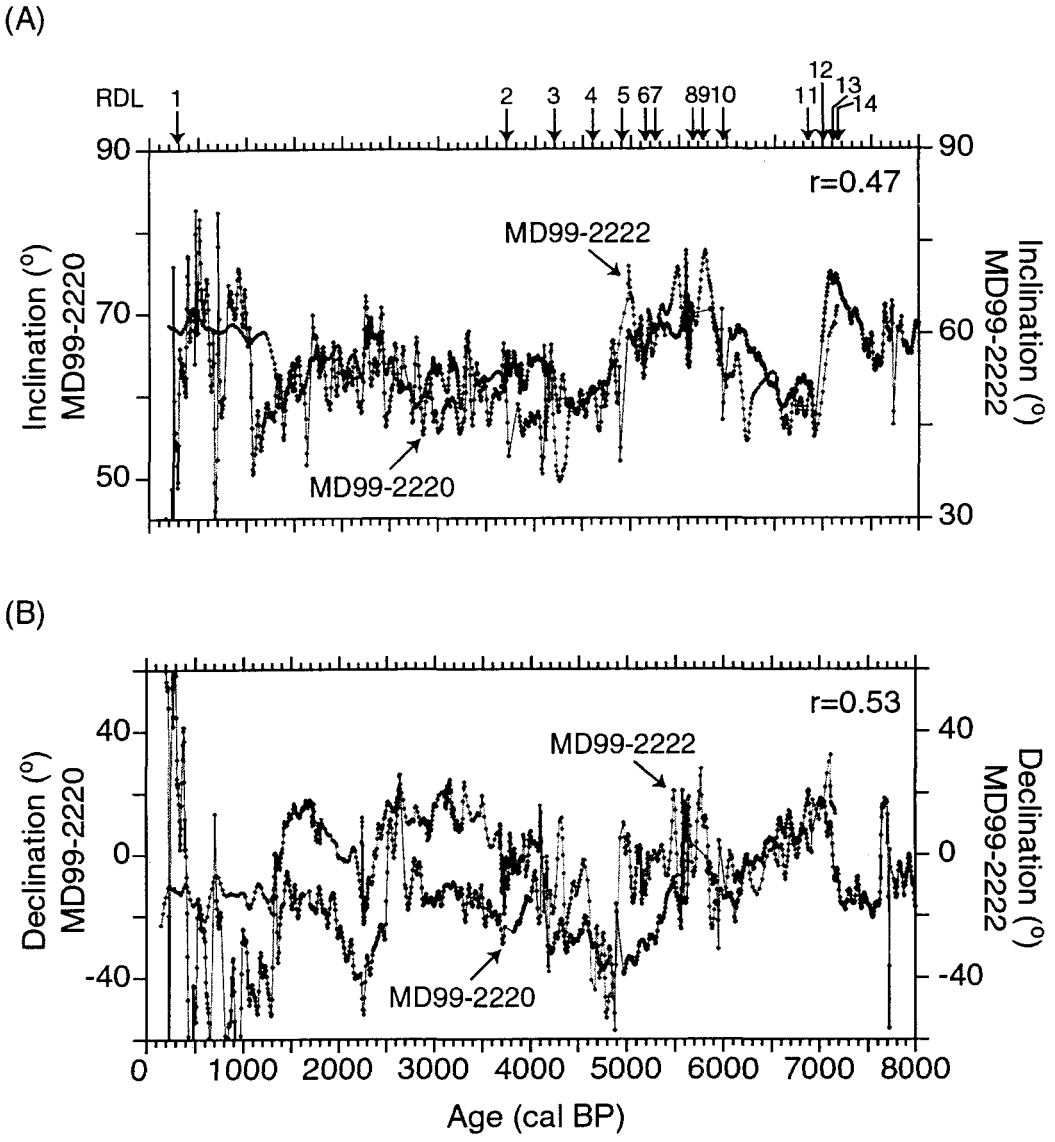
(A)
RDL
1
2
3
4
5
67
8910
11
12
13
14
90
70
50
r=0.47
MD99-2222
MD99-2220
Inclination (°) MD99-2220
Inclination (°) MD99-2222
60
30
(B)
r=0.53
40
0
-40
Declination (°) MD99-2220
Declination (°) MD99-2222
0
1000
2000
3000
4000
5000
6000
7000
8000
Age (cal BP)

Fig. 8

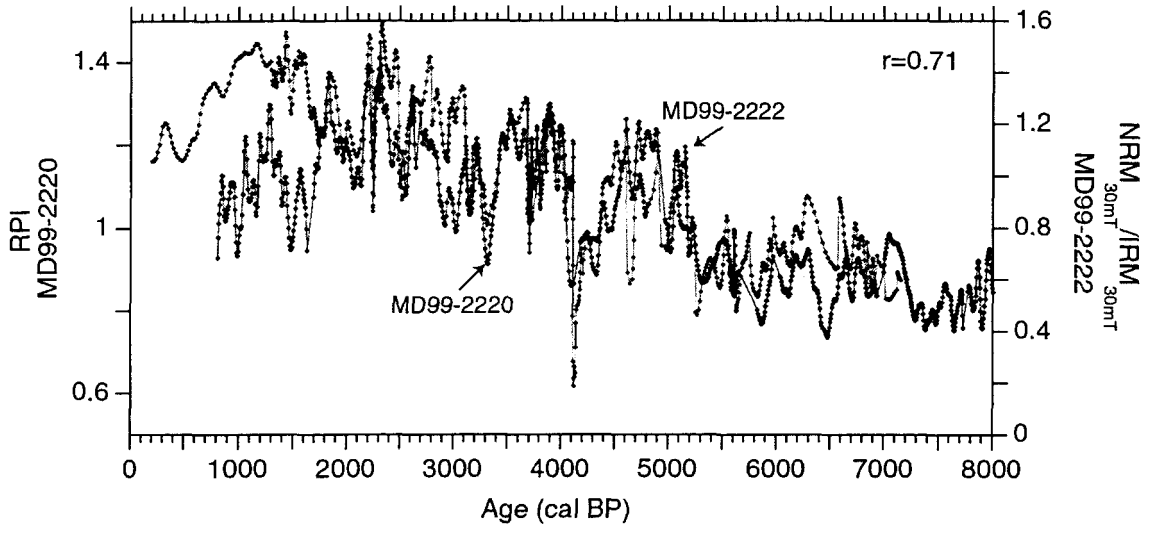

Electronic Supplement Figure S1

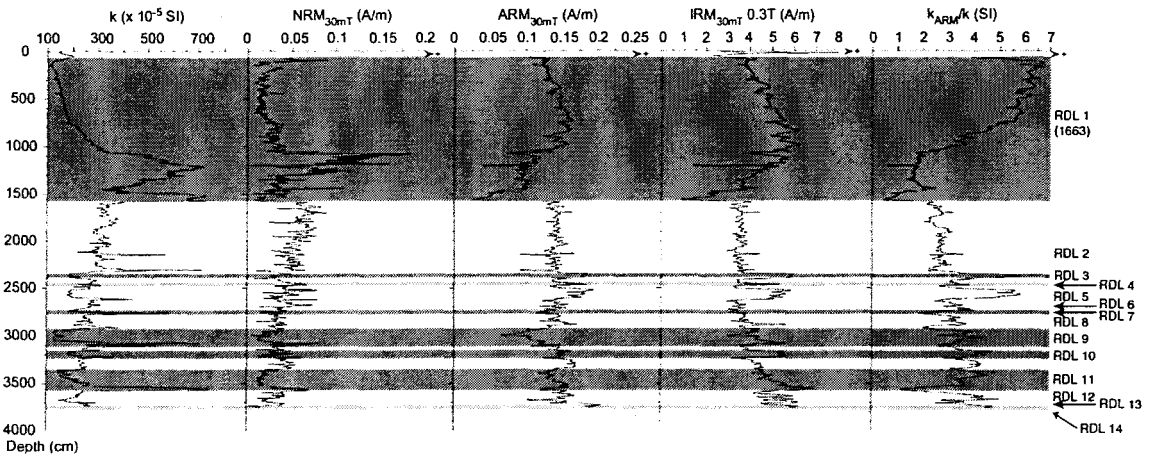

Electronic Supplement Figure S2

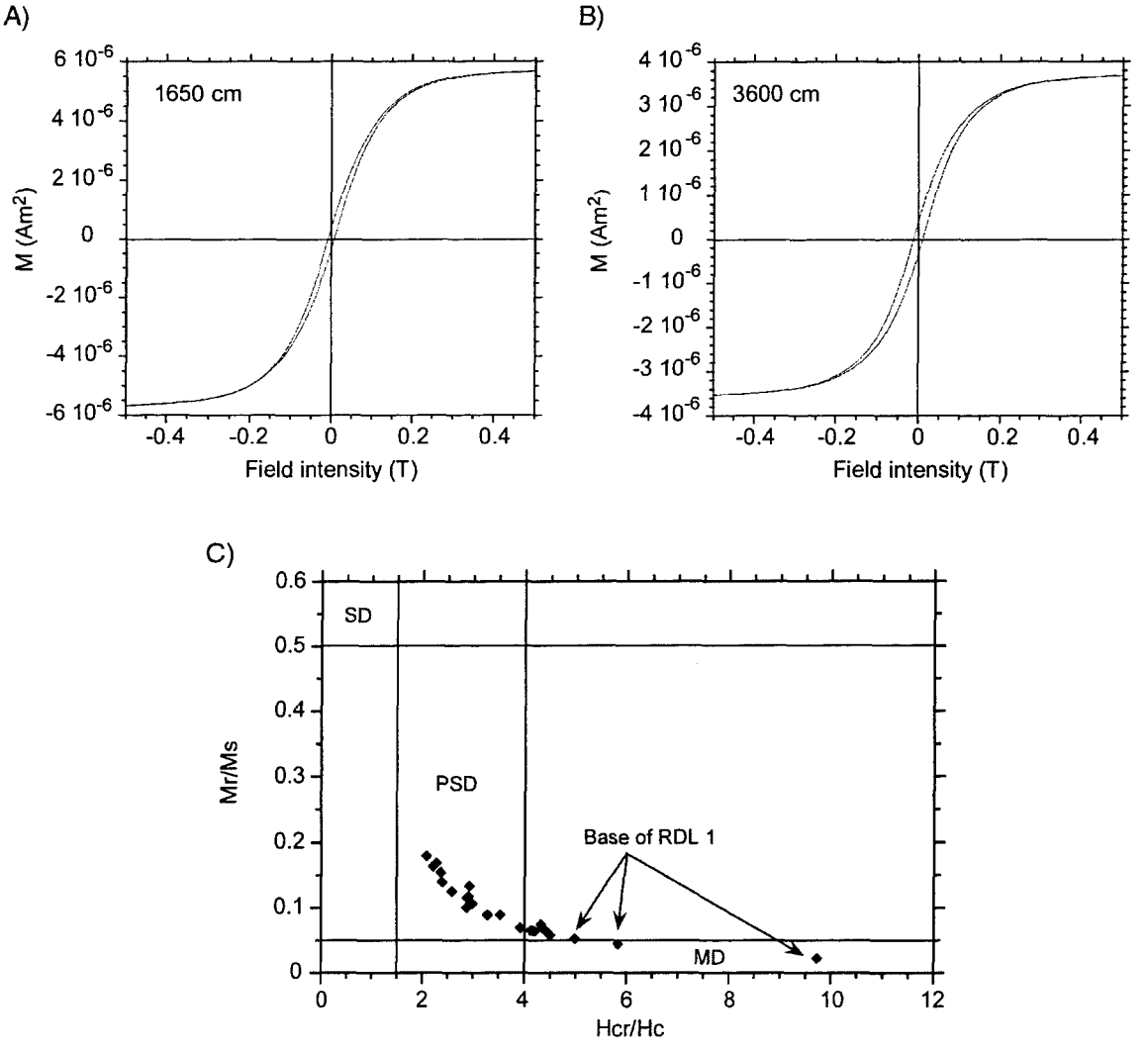

Electronic Supplement Figure S3

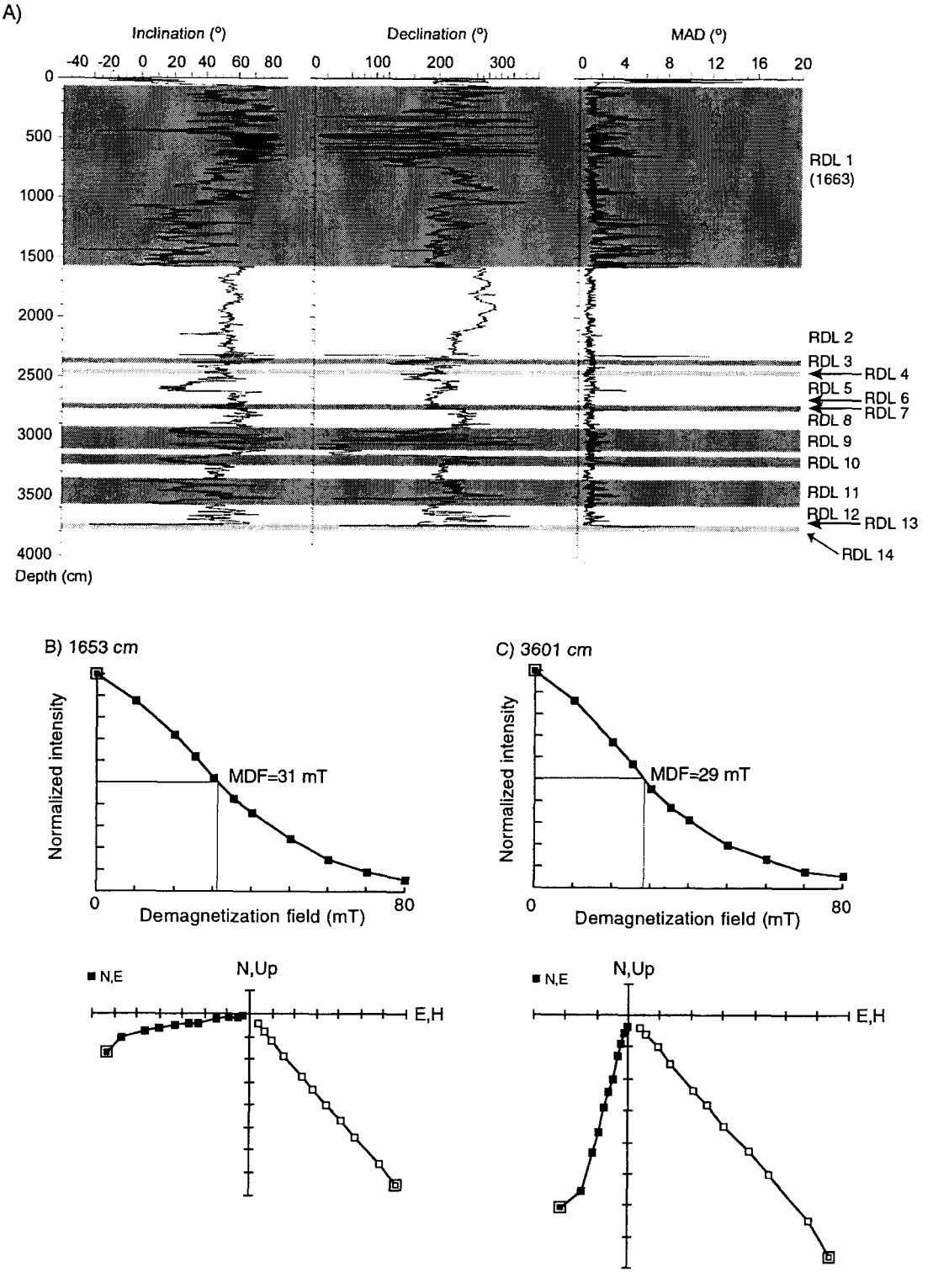

Electronic Supplement Figure S4

CHAPITRE IV

DECADAL-SCALE PRECIPITATION VARIATIONS IN THE GREAT LAKES/ST. LAWRENCE RIVER WATERSHED AS REVEALED BY A 800-YEAR PALEODISCHARGE PROXY RECORD

Guillaume St-Onge[3,*], David J.W. Piper [2], Claude Hillaire-Marcel [1], Anne de Vernal [1] and Joseph S. Stoner[3]

Sera soumis pour publication dans *Geology* ou *Marine Geology*

Keywords: St. Lawrence River, Great Lakes, grain size, discharge, North Atlantic Oscillation (NAO).

[3] Centre en recherche en géochimie et géodynamique (GEOTOP-UQÀM-McGILL), Case postale 8888, Succursale Centre-Ville, Montréal, Québec, H3C 3P8, Canada
[2] Geological Survey of Canada (Atlantic), 1 Challenger Drive, Box 1006, Dartmouth, Nova Scotia, B2Y 4A2, Canada
[3] Institute of Arctic and Alpine Research (INSTAAR), University of Colorado, Campus Box 450, Boulder, CO 80309-0450, USA
* *E-mail address*: guillaume_st-onge@inrs-ete.uquebec.ca (G. St-Onge), now at INRS-ETE, C.P. 7500, Ste-Foy, Québec, G1V 4C7, Canada

ABSTRACT

High-resolution grain size analyses from sediment cores were used to derive a sub-decadal paleodischarge proxy for the St. Lawrence Estuary, Eastern Canada. Based on the very strong influence of the spring freshet on both discharge and sediment load in the St. Lawrence River, the impossibility of generating a flood-induced turbidite, spectral analysis and the observed relationship between percent silt and spring discharge of the St. Lawrence River from 1914 to 1999 AD, we interpret percent silt to reflect changes in the spring freshet. The percent-silt record for the past 800 cal BP is characterised by high frequency decadal-scale fluctuations along with a few exceptional events. Decadal-scale variations are also observed in the reconstructed February sea-surface temperatures (SST) of the St. Lawrence Estuary and indicate an important variability in winter conditions over Eastern Canada during the last centuries. In addition, a synchronous change in the average percent silt and average reconstructed February SST was recorded around ~500 cal BP. The timing of the concomitant change along with the subsequent colder reconstructed February SST hint at the inception of the Little Ice Age. A relationship between the percent silt and a NAO index from 1865 to 2000 AD is also observed, suggesting that multidecadal-scale precipitation variations in the Great Lakes/St. Lawrence River watershed may have been influenced by the NAO during the last centuries. Finally, the percent-silt record indicates that the frequency of large spring freshets drastically increased since 1975 AD.

INTRODUCTION

Examples of extreme hydrological and climatic events such as floods and droughts were abundant during the last decade. In the Great Lakes/St. Lawrence watershed, a spectacular flood of the Saguenay River (Quebec) occurred in 1996 and three of the ten warmest and two of the ten driest springs of the last 55 years were recorded during the past five years. Increased concentrations of greenhouse gases in the next decades may lead to increased frequency and magnitude of such events (IPCC, 2001). Reliable climatic data including extreme events beyond instrumental records, which rarely exceed the last century in Canada, are essential to understand the natural variability of the climate and the impact of human activity on climate.

The St. Lawrence Estuary, lying between the St. Lawrence River and the Gulf of St. Lawrence in Eastern Canada (Fig. 1), offers unique archives for paleoclimatic reconstructions as recent sedimentation rates can exceed 0.5 cm/yr (e.g., Zhang, 2000, St-Onge et al, 2003). In order to derive a paleodischarge proxy for the last 800 cal BP, we have obtained grain size data at 1 cm intervals from the first 150 cm of a long Holocene piston core (MD99-2220, hereafter referred to as core 2220: latitude/longitude: 48°38.32N/68°37.93W, water depth 320 m, length 51.6 m) and from a 51-cm box core (BC-2220) sampled at the same site as core 2220 (Fig. 1). Grain size analyses were performed using a Coulter Counter TAII analyzer following the procedure of Cramp et al. (1997). February sea-surface temperatures were reconstructed at 2 cm intervals using transfer functions based on dinocyst assemblages according to the procedures described in de Vernal et al. (2001).

SETTING

The Great Lakes/St. Lawrence River system drains a very large watershed of 1 610 000 km^2. Near the mouth of the Saguenay Fjord, in the Estuary, the mean annual discharge is about 16 000 m^3/s, of which 54% originates from the Great Lakes (St. Lawrence Centre, 1996). Near the end of the Estuary, the minimum and maximum mean monthly discharges were respectively 13282±1377 and 23641±3812 m^3/s between 1950-1984 (Koutitonsky and Bugden, 1991). Despite its large watershed and strong discharge, the St. Lawrence River carries low concentrations of suspended particulate matter (SPM), as the result of the upstream presence of the Great Lakes (Rondeau et al, 2000). Historically, pluriannual flow fluctuations in the St. Lawrence River are related to changes in precipitation over the entire watershed (Morin and Leclerc, 1998). Freshwater mixes with saline water of the North Atlantic in the Estuary. Physiographically, the Estuary comprises the Laurentian Channel, a long U-shaped glaciated valley with depths between 200-540 m, with narrow shelves on either side. In recent sediments, fine grained, greenish-grey mud are observed on the deep central parts of the Laurentian Channel, whereas sandy mud are present on the sides and lower slopes as well as on the headward parts of the Laurentian Channel (Loring and Nota, 1973). Most of the sediment settling in the Estuary comes from the erosion of the bed and banks of the St. Lawrence River (d'Anglejan, 1990; Rondeau et al., 2000). Nonetheless, at the head of the Upper Estuary, about 19 % and 13 % of the particulate load originates from the south shore and the north shore tributaries of the St. Lawrence River, respectively (Rondeau et al., 2000). During the last millennium, glacio-isostatic uplift of the land

averaged a few millimeters per century, whereas twentieth century tide-gauge data show no consistent trends in sea-level (cf. Dionne, 2001 and references therein).

CHRONOLOGY

Using thirteen AMS ^{14}C dates on mollusc shells and paleomagnetic correlations with a nearby piston core, St-Onge et al. (2003) established a chronology for core 2220 over the last ~8500 cal BP, with sedimentation rates varying from 0.15 to 0.42 cm/yr. Comparisons of the relative paleointensity record of core 2220 with the flux of ^{10}Be from the GISP2 ice core (Finkel and Nishiizumi, 1997) and with a ^{14}C production rate record (Bond et al., 2001) indicate that core 2220 chronology is in good agreement with the GISP2 chronology (Meese et al., 1994) and the tree-ring chronology from Stuiver et al. (1998). To establish a chronology for BC-2220, we used the sedimentation rates derived from ^{210}Pb measurements[1]. For the top 20 cm, we applied a constant sedimentation rate of 0.74 cm/yr, whereas below 20 cm, we interpolated a constant sedimentation rate of 0.28 cm/yr (St-Onge et al., 2003).

RECENT VARIATIONS IN FRESH WATER DISCHARGE AND GRAIN SIZE

As mentioned earlier, SPM concentrations in the St. Lawrence River are low due to the upstream presence of the Great Lakes. These low concentrations prevent the formation of hyperpycnal flows and the consequent deposition of flood-induced turbidites (Mulder and Syvitski, 1995). The St. Lawrence River is also characterised by a very long sediment flux duration, with 50% of the sediment load carried in 17% of time (Maybeck et al., in press),

[1] GSA Data Repository item XXX. Document Secretary, GSA, P.O. Box 9140, Boulder, CO 80301-9140, USA.

indicating that the sediment flux of the St. Lawrence River is not affected by very short flux events. In contrast, smaller mountainous rivers such as the Eel (USA), Walla Walla (USA) or the Piray (Bolivia) carry 50% of the sediment load in less than 0.4% of the time (Maybeck et al., in press). Nevertheless, at the head of the Upper Estuary, a linear log-log relationship is observed between SPM concentrations and discharge, illustrating that higher discharge strongly increases the SPM concentration (Maybeck et al., in press). The highest discharge and thus highest SPM in the St. Lawrence River occurs during the spring freshet, accounting for an important part of the annual sediment load. Indeed, Frenette et al. (1989) estimated that 60-70% of the annual sediment load is carried at the head of the Estuary following the spring freshet. In addition, Silverberg (1985) estimated the downward flux of SPM in the Lower St. Lawrence Estuary to be about 4.5 times higher during the spring than during the fall. Moreover, the mean diameter of the SPM in the Lower Estuary rises from < 1.5 μm to about 6 μm following the spring freshet (Lucotte et al., 1991), indicating that the coarser particles are mostly transported into the Lower Estuary following the spring freshet because of greater discharge. The nature and grain size distribution of the bottom sediments in the Estuary reflect the SPM in the above water column (Kranck, 1979; Pocklington and Tan, 1987), suggesting sediment grain size could be used to develop a paleodischarge proxy. Such proxies were previously successfully used to derived paleocurrent speed (e.g., Bianchi and McCave et al., 1999) or spring freshet discharge (e.g., Smith and Schafer, 1987).

In order to develop a Late Holocene paleodischarge proxy for the St. Lawrence River, we first compared the grain size record of BC-2220 with the RIVSUM fresh water

discharge index from 1914 to 1999. The RIVSUM index is defined as the sum of fresh water discharges of the St. Lawrence River at Cornwall, the Ottawa River at Carillon and the Saguenay River at the Isle Maligne dam (Gilbert et al., 1996). Spectral analysis reveals that the percent silt and the mean RIVSUM discharge for the months of March-April-May, when the maximum discharge is generally first observed at the head of the St. Lawrence Estuary due to the spring freshet (Hélie, 2003), are coherent over several frequencies, including periods of 6 and 8 years and a broader set of frequencies centered around ~25 years (Fig. 2a). These periods are observed in both the RIVSUM and percent silt power spectra (2b-c) and are very close to the periods of 6-8, 20-22 and 28 years identified in a St. Lawrence River runoff timeseries for 1860-1998 (Pekárová et al., 2003) and to cycles of 6-8 and 22 years identified in Great Lakes water level series (Hillaire-Marcel et al., 1981), suggesting a relationship between spring freshet and percent silt. Furthermore, a significant period centered at 13.3 years is also observed in the power spectrum of the percent-silt record (Fig. 2c) and is close to the period of 14 years identified by Pekárová et al. (2003) in the long St. Lawrence River runoff timeseries.

A link between the spring freshet and the percent silt is illustrated in Fig. 3 where, despite the scarcity of percent-silt data-points between 1960 and 1970, a relationship between percent silt and the mean RIVSUM discharge for the months of March-April-May is observed, suggesting that silt particles are mostly transported and deposited distally into the Lower Estuary following the spring freshet because of higher discharge. This is notably seen at the decadal timescale, where, for example, a concomitant increasing trend in percent silt and the mean RIVSUM discharge for the months of March-April-May from 1925-1950

and a synchronous decreasing trend in both parameters from 1975-1995 are observed. These results are consistent with the work of Zhang (2000) who, based on a positive relationship between grain size and ^{137}Cs activity, suggested that during periods of high erosion rates (such as during the spring freshet) larger particles are transported and deposited into the Lower Estuary. Discrepancies between the RIVSUM discharge and percent-silt timeseries could be due to the different temporal resolution and to small offsets associated with the ^{210}Pb chronology of BC-2220.

We have also examined the possibility that the variations seen in the percent-silt record could be related to changes in relative sea-level or the amplitude of tides. Spectral analysis using two different methods (maximum entropy and Blackman-Tukey) of the tide gauge data from Pointe-au-Père (1897-1983) and Rimouski (1984-2003) reveals significant periods at 6.3, 8.6, 13.5 and 58.8 years[2], matching approximately the periods of 6, 8 and 14 years identified by Pekárová et al. (2003) in the long St. Lawrence River runoff record, suggesting a link between discharge and water levels. Furthermore, the 18.6-year lunar nodal cycle is not recognised in the data. The linear correlation (r=0.46) between the smoothed mean RIVSUM discharge and the smoothed mean annual water levels at Pointe-au-Père/Rimouski for the 1914-1999 period indicates that on pluriannual to decadal timescales, the water levels in the Lower St. Lawrence Estuary are primarily controlled by the discharge from the entire Great Lakes/St. Lawrence River watershed, rather than by changes in relative sea-level or tidal amplitude.

---

[2] GSA Data Repository item XXX. Document Secretary, GSA, P.O. Box 9140, Boulder, CO 80301-9140, USA.

Other factors possibly influencing the percent-silt record include mass movements along the side wall slopes of the Laurentian Channel and resuspension of sediments. For example, mass wasting deposits were recently discovered in the Lower St. Lawrence Estuary at the mouth of north shore rivers using high-resolution multibeam sonar and seismic data (Duchesne et al., 2003; Locat, personal communication), but the deposits were observed downstream and at shallower depths than the sampling location of cores BC-2220 and 2220. In fact, cores BC-2220 and 2220 were retrieved upstream of all the major north shore rivers (Betsiamites, aux Outardes, Manicouagan), minimizing fluvial or mass wasting inputs from these rivers. Furthermore, detailed visual description, computed axial tomography (CAT-scan)[3] or ^{210}Pb analysis[1] of BC-2220 reveal no signs of mass wasting deposits nor of any sedimentary structures, indicating that the sediments were deposited under « normal » sedimentary conditions.

Using a compilation of direct current measurements, El-Sabh (1979) showed that the bottom water layer (< 250 m) of the Lower St. Lawrence Estuary, near Rimouski, flowed landward with a weak and uniform velocity of 2 cm/s. Similarly, based on direct observations from a submersible, Syvitski et al. (1983) revealed that the bottom current velocity was too low to resuspend the bottom sediments of the Laurentian Channel and that the surface water layer (outflow from the St. Lawrence River) was the source of most SPM observed below. In addition, based on *in situ* tests, they concluded that « the sediment-water interface is quite definite in the Laurentian Channel » and that considerable energy is needed to resuspend the surface layer. Such energy could come from short-lived storm-

[3] GSA Data Repository item XXX. Document Secretary, GSA, P.O. Box 9140, Boulder, CO 80301-9140, USA.

generated waves, but the influence of such events on the bottom sediments is confined to regions of shallow depths (< 30 m; Drapeau and Morin, 1981; Syvitski et al., 1983), whereas the influence of such waves on the sedimentation in the deep central part of the Laurentian Channel is currently unknown. Despite this lack of knowledge, a mass balance budget could give insights into the different sources of sediment settling in the Laurentian Channel. For example, based on the mean annual suspended load calculated by Rondeau et al. (2001) at the head of the Upper Estuary from 1989-1993 (6.9 x 10^6 t/yr), possible erosion of exposed glaciomarine clays in the Upper Estuary (0.5 x 10^6 t/yr; d'Anglejan, 1990) and the annual sediment input into the Laurentian Channel as determined from ^{210}Pb-derived mass accumulation rates from sediment cores (8.8 x 10^6 t/yr; Smith and Schafer, 1999), we can estimate that about 84% of the annual sediment input into the Laurentian Channel comes from the St. Lawrence River. Consequently, all other possible sources of sediment could account for about 16% of the annual sediment input, which is well within observed natural fluctuations of the annual sediment load from the St. Lawrence River. Indeed, Frenette (1989) showed that the annual sediment load at the head of the Upper Estuary could vary between 4 and 12 x 10^6 t/yr, depending on the intensity of the spring freshet, again highlighting the influence of the spring freshet on the sediment load into the Estuary. Moreover, part of the 16% difference could be attributed to the fact that the annual sediment input estimated by Smith and Schafer (1999) into the Laurentian Channel was integrated over the entire Lower Estuary, thus including possible inputs from the major north shore rivers (Saguenay, Betsiamites, aux Outardes, Manicouagan), which were not included in the mass budget of Rondeau (2001). Therefore, even though we cannot entirely

discard the possibility that other factors than the spring freshet discharge can influence the percent-silt record, the presented data and arguments suggest that the spring freshet is the dominant factor at the sampling location of the studied cores, in the deep central part of Laurentian Channel (water depth: 320 m).

A PALEODISCHARGE RECORD FOR THE LAST 800 YEARS

Based on the arguments presented above, the very strong influence of the spring freshet on both discharge and sediment load in the St. Lawrence River, the impossibility of generating a flood-induced turbidite, the spectral analysis results and the observed relationship between the RIVSUM spring discharge and the percent silt during the 20th century, we interpret percent silt to reflect changes in the spring freshet. The percent-silt record for the past 800 cal BP is illustrated in Fig. 4 and is characterised by high frequency decadal-scale fluctuations along with a few exceptional events, as defined here by a standard deviation 2σ above (large spring freshet) or below (low spring freshet) the average percent silt. Decadal-scale variations are also observed in the reconstructed February sea-surface temperatures (SST) of the St. Lawrence Estuary and indicate an important variability in winter conditions over Eastern Canada during the last centuries. Furthermore, the change in the average percent silt around ~535 cal BP is synchronous with a change in the average reconstructed February SST (Fig. 4) and suggests it could be associated with a major climatic shift that occurred over Eastern Canada. The timing of the concomitant change along with the subsequent colder reconstructed February SST hint at the inception

of the Little Ice Age, which is consistent with the rapid cooling of Northern Hemisphere temperatures following the 14th century (Mann et al., 1999).

Spectral analysis using two different methods (maximum entropy and Blackman-Tukey) of the percent-silt record reveals three significant cycles centered around 21, 30 and 47 years (Fig. 5). Again, these cycles are very close to the periods of 20-22 and 28 years previously identified in the St. Lawrence River runoff (Pekárová et al., 2003) and to those of 22 and 33 years identified in the Great Lakes water level series (Hillaire-Marcel et al., 1981), further supporting percent silt as a paleodischarge proxy. Morin and Leclerc (1998) also identified cyclic 20-35 year variations in the St. Lawrence discharge and related them to precipitation changes in the entire watershed. Moreover, the 20-22-year and 28-year cycles are also observed in runoff series of several large rivers from the Northern Hemisphere (Pekárová et al., 2003), hinting at an atmospheric teleconnection. For example, Shorthouse and Arnell (1997) showed that Northern European river discharge is positively correlated to the North Atlantic Oscillation (NAO) while Southern European river discharge is negatively correlated to the NAO, a pattern consistent with the precipitation changes related to the NAO (Hurrell et al., 2003).

The NAO is now recognised as the most prominent and recurrent pattern of winter atmospheric variability over the middle and high latitudes of the Northern Hemisphere (Hurrell et al., 2003). The NAO varies with periods ranging between 7 and 25 years (Cook, 2003 and references therein), but also at lower frequencies with periods of 29-32 years (Schöne et al., 2004), 54-68 years (Lutherbacher et al., 1999) and 80 to 90 years (Appenzeller, 1998). These periods are close to the ones found in the percent-silt record

(Fig. 5) and suggest a link between the NAO and the hydrologic balance in the Great Lakes/St. Lawrence River watershed during the last 800 cal BP. Such a link is illustrated in Fig. 6, where a long-term relationship between the percent-silt record from the BC-2220 core and a NAO index for the 1865 to 2000 period is observed. This relationship is consistent with the work of Brown and Goodison (1996) which revealed that winter snow cover is correlated to the NAO in Southern Quebec and Ontario, where above normal winter snow cover occurs during a negative NAO-like behavior (i.e. weakened Icelandic Low and weak circulation over the Atlantic). Similarly, Hartley (1998) and Hartley and Keables (1998) revealed a negative correlation between winter snowfall and the NAO in New England and over much of the south and central Appalachian region, where elevated winter snowfall coincides with a negative NAO and colder sea-surface temperatures along the northeastern coast of the United States. It thus seems possible that the NAO also affected winter snowfall at the multidecadal timescale in the Great Lakes/St. Lawrence River system watershed during the last 800 cal BP, leading to changes in the St. Lawrence River spring freshet discharge and consequently to the transport and deposition of silt particles distally in the St. Lawrence Estuary.

RECENT CHANGE IN THE FREQUENCY OF EXCEPTIONAL EVENTS

During the last 25 years, one and almost two percent-silt data-points are above the 2σ standard deviation (std) compared to zero data points below the 2σ std (Fig. 3). These two data points fall within 2 years of the two highest peak spring freshet discharge recorded at the head of the Estuary from 1975 to 2000 (Bouchard and Morin, 2000) and supports

both the ^{210}Pb chronology of BC-2220 and the relationship between spring freshet and percent silt. In contrast, prior to 1975, the number of percent-silt data-points above the 2σ std is only two compared to nine data points below the 2σ std, suggesting that the frequency of large spring freshets drastically increased since 1975 (Figs. 3-4). Whether or not this observation is the result of increasing atmospheric concentration of greenhouse gases needs to be better addressed, but our data seem to suggest that this trend was unique during the last 800 cal BP. Finally, compared to other paleoclimatic proxies, which mostly reflect average climatic conditions or only one aspect of an extreme, the percent-silt proxy presented here can capture both low and high exceptional spring freshets.

ACKNOWLEDGMENTS

We are in debt to the captain, officers, crew and scientific participants of Legs 1 and 2 of the IMAGES-V cruise. This study was supported by the IMAGES and CSHD programs, the CCAF and the CFCAS. G.S. was supported by postgraduate scholarships from NSERC, FCAR, Natural Resources Canada and by Fisheries and Oceans Canada. Special thanks to Denis Gilbert for providing the RIVSUM data.

REFERENCES CITED

Appenzeller, C., Stocker, T.F., and Anklin, M., 1998, North Atlantic Oscillation dynamics recorded in Greenland ice cores: Science, v. 282, p. 446-449.

Bianchi, G.G., and McCave, N., Holocene periodicity in North Atlantic climate and deep-ocean flow south of Iceland: Nature, v. 397, p. 515-517.

Bond, G., Kromer, B., Beer, J., Muscheler, R., Evans, M.N, Showers, W., Hoffmann, S., Lotti-Bond, R., Hajdas, I., and Bonani, G., 2001, Persistent solar influence on North Atlantic climate during the Holocene: Science, v. 294, p. 2130-2136.

Bouchard, A., and Morin, J., 2000, Reconstitution des débits du fleuve Saint-Laurent entre 1932 et 1998: Environment Canada, Technical Paper RT-101, 71 p.

Brown, R.D., and Goodison, B.E., 1996, Interannual variability in reconstructed Canadian snow cover, 1915-1992: Journal of Climate, v. 9, p. 1299-1318.

Cramp, A., Lee, S.V., Herniman, J., Hiscott, R.N., Manley, P.L., Piper, D.J.W., Deptuck, M., Johnston, S.K., and Black, K.S., 1997, Interlaboratory comparison of sediment grain-sizing techniques: data from the Amazon fan upper levee complex sediments: Proceedings of the Ocean Drilling Program, Scientific Results, v. 155, p. 217-228.

Cook., E.R., 2003, Multi-proxy reconstruction of the North Atlantic Oscillation (NAO) index: a critical review and a new well-verified winter NAO index reconstruction back to AD 1400, *in* Hurrel, J.W., et al., eds., The North Atlantic Oscillation Climatic Significance and Environemental Impact: Washington, DC, American Geophysical Union, Geophysical Monograph, v. 134, p. 63-79.

d'Anglejan, B., 1990, Recent sediments and sediment transport processes in the St. Lawrence Estuary, *in* El-Sabh, M.I., and Silverberg, N., eds., Oceanography of a Large-Scale Estuarine System-The St. Lawrence: New York, Springer-Verlag, p. 109-129.

de Vernal, A., Henry, M., Matthiessen, M., Mudie, P.J., Rochon, A., Boessenkool, K.P., Eynaud, F., Grøsfeld, K., Guiot, J., Hamel, D., Harland, R., Head, M.J., Kunz-Pirrung,

M., Levac, E., Loucheur, V., Peyron, O., Pospelova, V., Radi, T., Turon, J.-L., and Voronina, E., 2001, Dinoflagellate cyst assemblages as tracers of sea-surface conditions in the northern North Atlantic, Arctic and sub-Arctic seas: the new 'n=677' data base and its application for quantitative palaeoceanographic reconstruction: Journal of Quaternary Science, v. 16, p. 681-698.

Dionne, J.-C., 2001, Relative sea-level changes in the St. Lawrence Estuary from deglaciation to present day, *in* Weddle, T.K., and Retelle, M.J., eds., Deglacial History and Relative Sea-level Changes, Northern New England and Adjacent Canada: Boulder, Geological Society of America, Geological Society of America Special Paper, v. 351, p. 271-284.

Drapeau, G., and Morin, R., 1981, Contribution des vagues au transport des sédiments littoraux dans la région de trois-pistoles, estuaire du Saint-Laurent: Géographie physique et Quaternaire, v. XXXV, p. 245-251.

Duchesne, M., Long. M., Long, B.F., Urgeles, R., and Locat, J., 2003, New evidence of slope instability in the Outardes Bay delta area, Quebec, Canada: Geo-Marine letters, v. 22, p. 233-242.

El-Sabh, M., 1979, The lower St. Lawrence Estuary as a physical oceanographic system: Le Naturaliste canadien, v. 106, p. 55-73.

Finkel, R.C., and Nishiizumi, K., 1997, Beryllium 10 concentrations in the Greenland Ice Sheet Project 2 ice core from 3 to 40 ka: Journal of Geophysical Research, v. 102, p. 26699-26706.

Frenette, M., Barbeau, C., and Verrette, J.L., 1989, Aspects quantitatifs, dynamiques et qualitatifs des sédiments du Saint-Laurent: Hydrotech Consultants Inc., for Environment Canada and the Government of Quebec, pp. 185.

Gilbert, D., Pettigrew, B., Swain, D., and Couture, M., 1996, State of the Gulf of St. Lawrence: oceanographic conditions in 1994: Canadian Data Report of Hydrography and Ocean Sciences, v. 143, 85 p.

Hartley, S., 1988, Winter Atlantic climate and snowfall in the south and central appalachians: Physical Geography, v. 20, p. 1-13.

Hartley, S., and Keables. M., 1998, Synoptic associations of winter climate and snowfall variability in New England, USA, 1950-1992: International Journal of Climatology, v. 18, p. 281-298.

Hélie, J.-F., 2003, Geochemistry and fluxes of organic and inorganic carbon in aquatic systems of Eastern Canada: examples of the St. Lawrence River and the Robert-Bourassa reservoir-Isotopic approach [Ph.D. thesis]: Montréal, UQÀM, 213 p.

Hillaire-Marcel, C., Occhietti, S., Marchand, L., and Rajewicz, R., 1981, Analysis of recent climatic changes in Quebec: some preliminary data: Syllogeus, v. 33, p.28-47.

Hurrel, J.W., Kushnir, Y., Ottersen, G., and Visbeck, M., 2003, An overview of the North Atlantic Oscillation, *in* Hurrel, J.W., et al., eds., The North Atlantic Oscillation Climatic Significance and Environemental Impact: Washington, DC, American Geophysical Union, Geophysical Monograph, v. 134, pp. 1-35.

IPCC, 2001, Summary for Policymakers. A report of working group I of the International Panel on Climate Change: Cambridge, Cambridge University Press, 20 p.

Koutitonsky, V.G., and Bugden, G.L., 1991, The physical oceanography of the Gulf of St. Lawrence: a review with emphasis on the synoptic variability of the motion, *in* Therriault, J.-C., ed., The Gulf of St. Lawrence: Small Ocean or Big Estuary ?: Canadian Special Publication of Fisheries and Aquatic Sciences, v. 113, pp. 57-90.

Kranck, K., 1979, Dynamics and distribution of suspended particulate matter in the St. Lawrence Estuary: Naturaliste canadien, v. 106, p. 163-173.

Loring, D.H., and Nota, D.J.G., 1973, Morphology and Sediments of the Gulf of St. Lawrence: Bulletin of the Fisheries Research Board of Canada, v. 182, 147 p.

Lucotte, M., Hillaire-Marcel, C., and Louchouarn, P., 1991, First-order organic carbon budget in the St. Lawrence Lower Estuary from ^{13}C data: Estuarine, Coastal and Shelf Science, v. 32, p. 297-312.

Lutherbacher, J., Schmutz, C., Gyalistras, D., Xoplaki, E., and Wanner, H., 1999, Reconstruction of monthly NAO and EU indices back to AD 1675: Geophysical Research Letters, v. 26, p. 2745-2748.

Mann, M.E., Bradley, R.S., and Hughes, M.K., 1999, Northern Hemisphere temperatures during the past millennium: inferences, uncertainties, and limitations: Geophysical Research Letters, v. 26, p. 759-762.

Maybeck, M., Laroche, L., Dürr, H.H., and Syvitski, J.P.M., in press, Global variability of daily total suspended solids and their fluxes in rivers: Global and Planetary Change.

Meese, D.A., Alley, R.B., Fiacco, R.J., Germani, M.S., Gow, A.J., Grootes, P.M., Illing, M., Mayewski, P.A., Morrison, M.C., Ram, M., Taylor, K.C., Yang, Q., and Zielinski,

G.A., 1994, Preliminary depth-age scale of the GISP2 ice core: Hanover, Special CRREL Report 94-1.

Morin, J., and Leclerc, M., 1998, From pristine to present state: hydrology evolution of Lake Saint-François, St. Lawrence River: Canadian Journal of Civil Engineering, v. 25, p. 864-879.

Mulder, T., and Syvitski, J.P.M., 1995, Turbidity currents generated at river mouths during exceptional discharges to the world oceans: The Journal of Geology, v. 103, p.285-299.

Paillard, D., Labeyrie, L., and Yiou, P., 1996, Macintosh program performs time-series analysis: Eos, Transactions, American Geophysical Union, v. 77, p. 379.

Pekárová, P., Miklánek, P., and Pekár, J., 2003, Spatial and temporal runoff oscillation analysis of the main rivers of the world during the 19^{th}-20^{th} centuries: Journal of Hydrology, v. 274, p. 62-79.

Pocklington, R., and Tan, F.C., 1987, Seasonal and annual variations in the organic matter contributed by the St. Lawrence River to the Gulf of St. Lawrence: Geochimica and Cosmochimica Acta, v. 51, p. 2579-2586.

Rondeau, B., Cossa, D., Gagnon, P., and Bilodeau, L., 2000, Budget and sources of suspended sediment transported in the St. Lawrence River, Canada: Hydrological Processes, v. 14, p. 21-36.

Shaw, J., Gareau, P., and Courtney, R.C., 2002, Palaegeography of Atlantic Canada 13-0 kyr: Quaternary Science Reviews, v. 21, p. 1861-1878.

Shöne, B.N., Oschmann, W., Rössier, J., Freyre Castro, A.D., Houk, S.D., Krönke, I., Dreyer, W., Janssen, R., Rumohr, H., and Dunca, E., 2004, North Atlantic dynamics recorded in shells of a long-lived bivalve mollusk: Geology, v.31, p. 1037-1040.

Shorthouse, C.A., and Arnell, N.W., 1997, Spatial and temporal variability in European river flows and the North Atlantic Oscillation: IAHS Publication Number 246, p. 77-85.

Silverberg, N., Edenborn, H.M., and Belzile, N., 1985, Sediment response to seasonal variations in organic matter input, *in* Siglo, A.C., and Hattori, A., eds., Marine and Estuarine Geochemistry: Chelsea, Lewis Publishing Inc., p. 69-80.

Smith, J.N., and Schafer, C.T., 1999, Sedimentation, bioturbation, and Hg uptake in the sediments of the estuary and Gulf of St. Lawrence: Limnology and Oceanography, v. 44, p. 207-219.

Smith, J.N., and Schafer, C.T., 1987, A 20th-century record of climatologically modulated sediment accumulation rates in a Canadian fjord: Quaternary Research, v. 27, p. 232-247.

St. Lawrence Centre, 1996, State of the Environment Report on the St. Lawrence River: Montréal, Éditions MultiMondes, The St. Lawrence Ecosystem, v. 1, 664 p.

St-Onge, G., Stoner, J.S., and Hillaire-Marcel, C., 2003, Holocene paleomagnetic records from the St. Lawrence Estuary : centennial- to -millennial-scale geomagnetic modulation of cosmogenic isotopes: Earth and Planetary Science Letters, v. 209, p. 113-130.

Stuiver, M., Reimer, P. J., Bard, E., Beck, J. W., Burr, G.S., Hughen, K. A., Kromer, B., McCormac, G., van Der Plicht, J., and Spurk, M., 1998, INTCAL98 radiocarbon age calibration, 24,000-0 cal BP: Radiocarbon, v. 40, p. 1041-1083.

Syvitski, J.P.M., Silverberg, N., Ouellet, G., and Asprey, K.W., 1983, First observations of benthos and seston from a submersible in the Lower St. Lawrence Estuary: Géographie physique et Quaternaire, v. XXXVIII, p. 227-240.

Zhang, D., 2000, Fluxes of short-lived radioisotopes in the marginal marine basins of Eastern Canada [Ph.D. thesis]: Montréal, UQÀM, 193 p.

FIGURE CAPTIONS

Fig. 1. The St. Lawrence Estuary along with the sampling site (star) of core 2220 and BC-2220. St. Law. Estuary=St. Lawrence Estuary, QC=Québec City, SF=Saguenay Fjord, PAP=Pointe-au-Père, RIM=Rimouski, LC=Laurentian Channel. Modified from Shaw et al. (2003).

Fig. 2. Spectral analysis of the RIVSUM and BC-2220 percent-silt timeseries. A) Coherence between the percent silt and the mean RIVSUM discharge for the months of March-April-May for the period 1915-1999. Spectral analysis of B) the mean RIVSUM discharge for the months of March-April-May for the period 1915-1999 and C) BC-2220 percent-silt record. The coherence was calculated with a Blackman-Tukey cross-spectral analysis with a Bartlett window using Analyseries (Paillard et al., 1996). The solid line represents the 95 % confidence limit. The power spectra were calculated with the maximum entropy method (solid line) and the Blackman-Tukey method with a Bartlett window (dashed line) using Analyseries (Paillard et al., 1996). The most significant periods common in the three analyses are highlighted in grey.

Fig. 3. Comparison of the mean RIVSUM discharge for the months of March-April-May and the percent silt from BC-2220 from 1914 to 1999. The heavy line represents a 5-point smooth. Also illustrated is the average percent silt (horizontal solid line) along with the 2σ standard deviation (horizontal dashed line).

Fig.4. Comparison of the percent-silt record (2-63 μm) with dinocyst-based reconstructed February sea-surface temperatures from core 2220. Also illustrated is the average percent silt and reconstructed temperatures (horizontal solid line) along with the 2σ standard deviation (horizontal dashed line).

Fig. 5. Spectral analysis of core 2220 percent-silt record. The power spectra were calculated with the maximum entropy method (solid line) and the Blackman-Tukey method with a Bartlett window (dashed line) using Analyseries (Paillard et al., 1996). The three most significant periods common in the two methods are highlighted in grey.

Fig. 6. Comparison of the percent silt (2-63 μm) from BC-2220 with the annual NAO index from 1865-2000 (data from www.cgd.ucar.edu/~jhurrell/nao.stat.ann.html). A 5-point smooth and a 13-point smooth, both representing a ~13-year smooth, were applied to the percent silt and annual NAO index data, respectively. The dashed line is the smoothed record without the data point at 1905.

GSA Data Repository

Fig. 1. Sedimentation rates (SR) derived from ^{210}Pb measurements in BC-2220. Using the regional ^{210}Pb supported value of Zhang (2000), we calculated a mean sedimentation rate of 0.74 cm/yr from 0-20 cm and 0.28 cm/yr below 20 cm within the box core. The ^{210}Pb measurements were made after chemical treatment, purification and deposition on a silver disk following routine procedures at GEOTOP (see Zhang, 2000 for details) by alpha counting of the daughter ^{210}Po. From St-Onge et al. (2003).

References cited

St-Onge, G., Stoner, J.S., and Hillaire-Marcel, C., 2003, Holocene paleomagnetic records from the St. Lawrence Estuary : centennial- to -millennial-scale geomagnetic modulation of cosmogenic isotopes: Earth and Planetary Science Letters, v. 209, p. 113-130.

Zhang, D., 2000, Fluxes of short-lived radioisotopes in the marginal marine basins of Eastern Canada [Ph.D. thesis]: Montréal, UQÀM, 193 p.

Fig. 2. Spectral analysis of the Pointe-au-Père/Rimouski tide gauge data from 1867-2003. The power spectra were calculated with the maximum entropy method (solid line) and the Blackman-Tukey method with a Bartlett window (dashed line) using Analyseries (Paillard et al., 1996). The four most significant periods common in the two methods are highlighted in grey.

References cited

Paillard, D., Labeyrie, L., and Yiou, P., 1996, Macintosh program performs time-series analysis: Eos, Transactions, American Geophysical Union, v. 77, p. 379.

Fig. 3. Computed axial tomography (CAT-scan) of a replicate core of BC-2220. The image was obtained with a General Electric™ model B7590K Hi-speed Advantage 2.X CAT-scan at the Centre Hospitalier Régional de Rimouski.

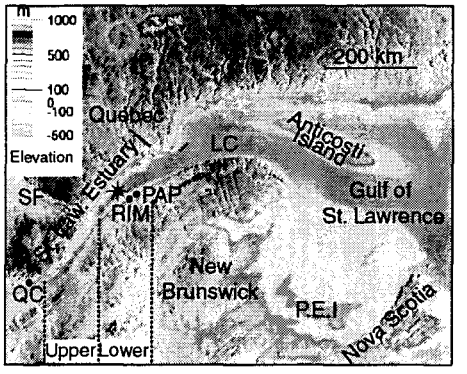
m
1000
500
100
0
-100
-500
Elevation
200 km
Quebec
LC
Anticosti Island
Estuary
SF
PAP
RIM
Gulf of St. Lawrence
New Brunswick
QC
P.E.I
Nova Scotia
Upper
Lower

Fig. 1

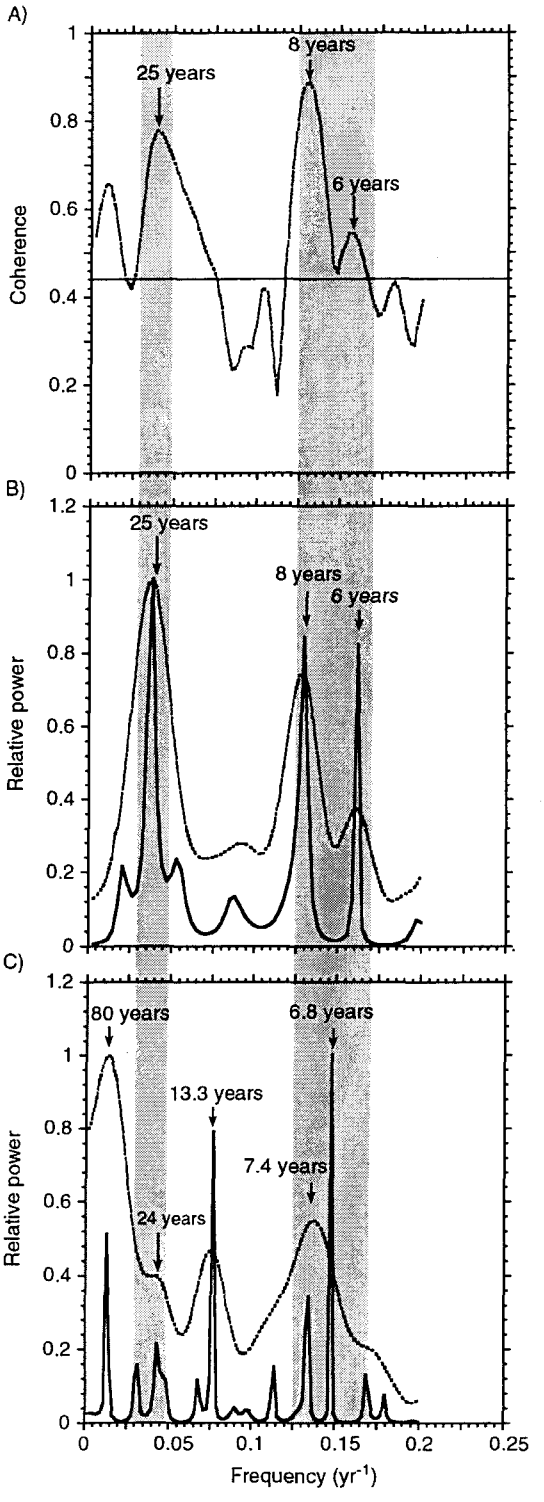
A)
25 years
8 years
6 years
Coherence
B)
25 years
8 years
6 years
Relative power
C)
80 years
6.8 years
13.3 years
7.4 years
24 years
Relative power
Frequency (yr-1)

Fig. 2

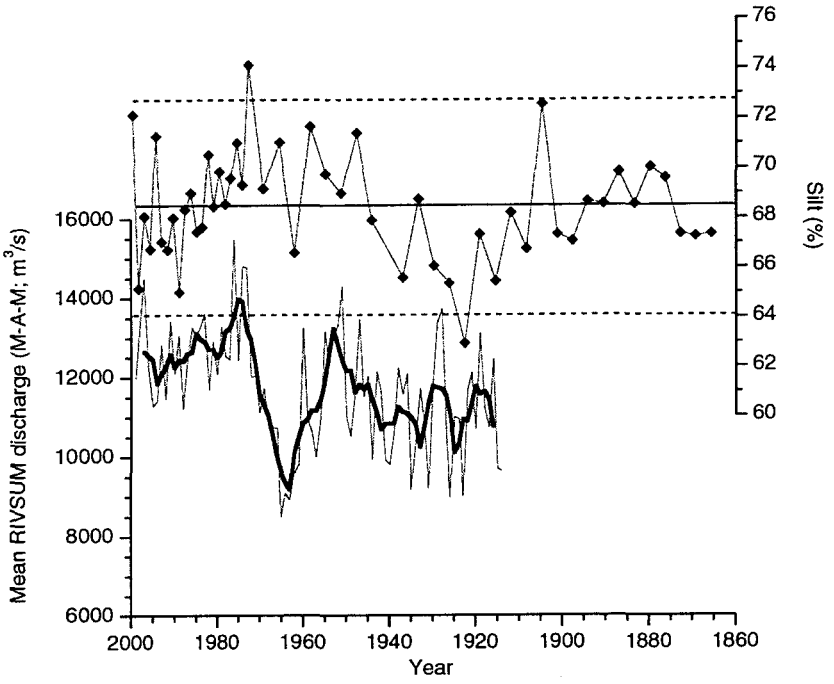
Mean RIVSUM discharge (M-A-M; m3/s)
16000
14000
12000
10000
8000
6000
2000
1980
1960
1940
1920
1900
1880
1860
Year
Silt (%)
76
74
72
70
68
66
64
62
60

Fig. 3

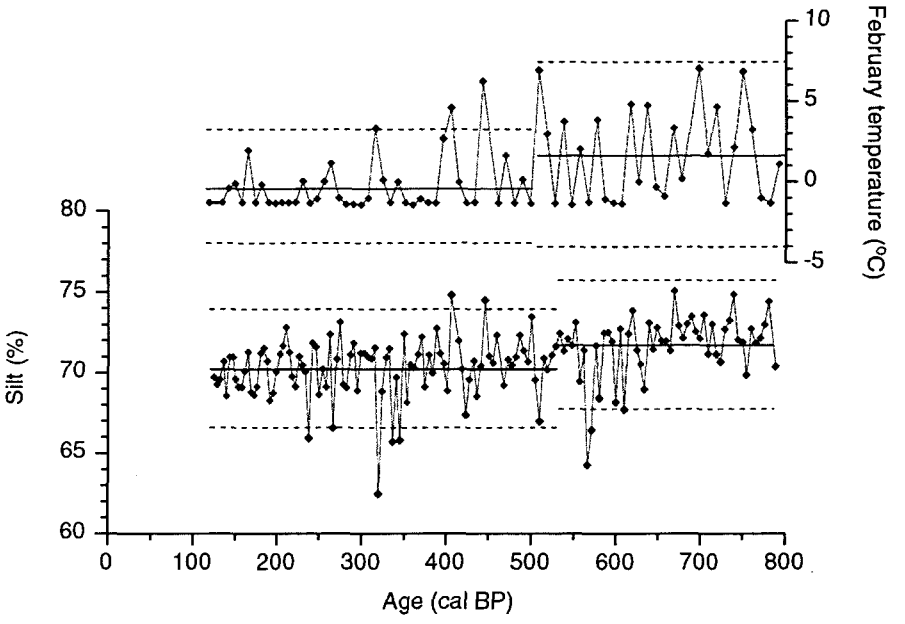
Silt (%)
80
75
70
65
60
0
100
200
300
400
500
600
700
800
Age (cal BP)
10
5
0
-5
February temperature (°C)

Fig. 4

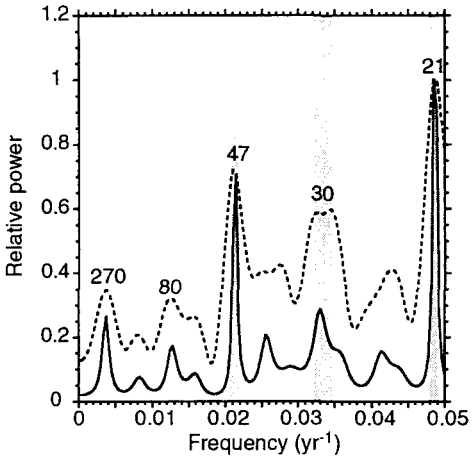
1.2
1
0.8
0.6
0.4
0.2
0
Relative power
270
80
47
30
21
0
0.01
0.02
0.03
0.04
0.05
Frequency (yr-1)

Fig. 5

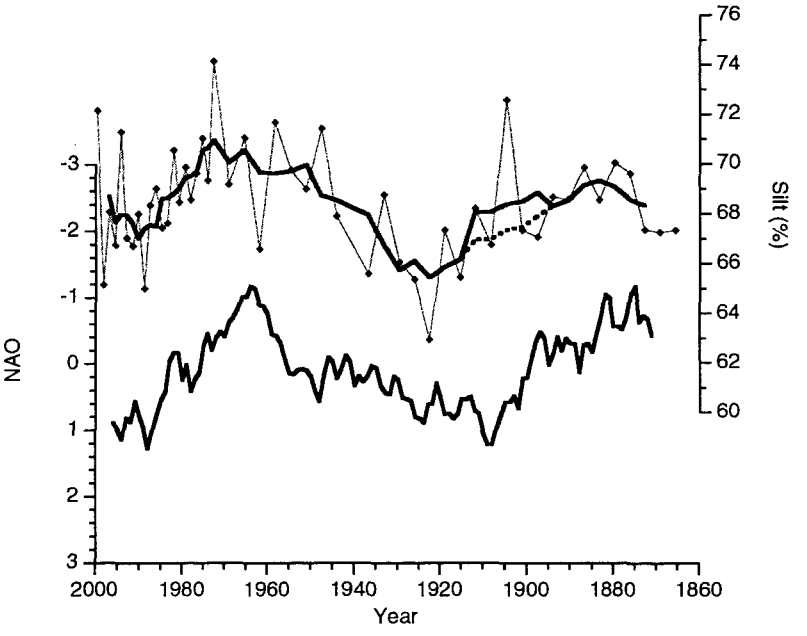
NAO
Silt (%)
Year
-3
-2
-1
0
1
2
3
76
74
72
70
68
66
64
62
60
2000
1980
1960
1940
1920
1900
1880
1860

Fig. 6

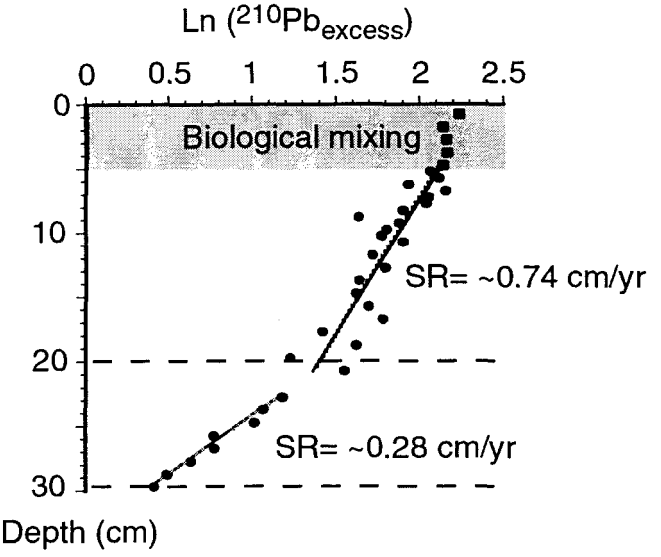

GSA Data Repository 1

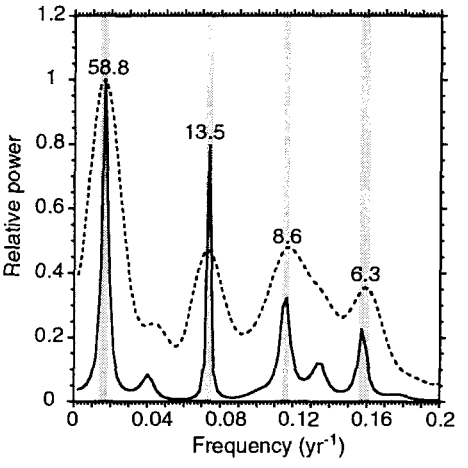

GSA Data Repository 2

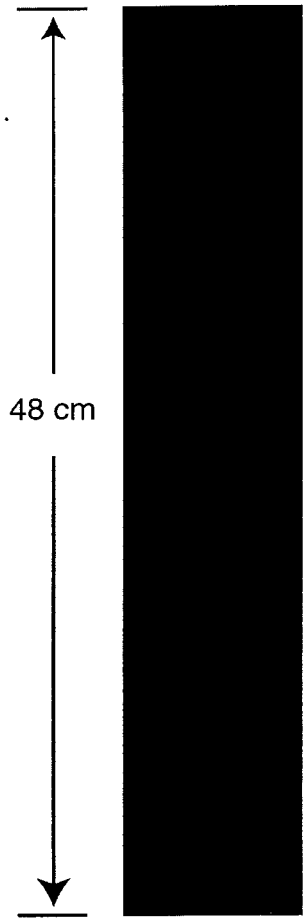

GSA Data Repository 3

CHAPITRE V

DISCUSSION ET CONCLUSIONS GÉNÉRALES

L'analyse des propriétés magnétiques de séquences sédimentaires prélevées dans l'estuaire du St-Laurent dans le cadre de la campagne océanographique IMAGES-V a permis de reconstruire les variations d'orientation et d'intensité du champ magnétique terrestre au cours des 8500 dernières années avec une résolution temporelle jusqu'ici inégalée. La comparaison des variations d'inclinaison et de déclinaison de la carotte MD99-2220 avec celles d'enregistrements lacustres nord-américans montre que les variations d'orientation sont similaires de l'Orégon (USA) à l'estuaire du St-Laurent et que les décalages temporels entre les enregistrements sont problement liés aux différentes chronologies plutôt qu'à la dérive de la composante non-dipolaire du champ magnétique. Ceci est confirmé par Stoner *et al.* (en préparation) qui, en comparant des enregistrements holocènes archéomagnétiques et paléomagnétiques, incluant celui de la carotte MD99-2220 synchronisée sur la dendrochronologie de Stuiver *et al.* (1998), montrent que les variations de déclinaison sont cohérentes de l'Orégon (USA) jusqu'en Europe, au cours de la majeure partie de l'Holocène. Toutefois, à partir de 2000 ans, le champ magnétique terrestre est beaucoup plus complexe, avec notamment la présence de deux lobes de flux dans l'Hémisphère Nord tels qu'on les observe aujourd'hui.

La comparaison des fluctuations de la paléointensité relative (PIR) enregistrées dans les sédiments de la carotte MD99-2220 avec celles d'enregistrements lacustres d'Amérique du Nord et même d'Europe montre que les fluctuations séculaires à millénaires de l'intensité du champ magnétique terrestre peuvent être corrélées. De plus, la corrélation entre les variations de la PIR de la carotte MD99-2220 et le flux de ^{10}Be estimé à partir de la carotte de glace GISP2, au Groenland (Finkel et Nishiizumi, 1997), ainsi que le taux de production du ^{14}C calculé à partir des concentrations de ^{14}C dans les cernes de croissance d'arbres (Bond *et al.*, 2001), indique que les oscillations séculaires à millénaires de la PIR sont produites par la composante dipolaire du champ magnétique terrestre. L'hypothèse généralement admise que les variations de l'intensité du champ magnétique terrestre n'affecte que le taux de production d'isotopes cosmogéniques avec des périodes supérieures à 10^3 ans devra ainsi être réévaluée. Le calcul des variations du taux de production du ^{14}C, à partir de la courbe de PIR de la carotte MD99-2220, est présentement en cours avec la collaboration de Raimund Muscheler (Université de Lund, Suède). Il devrait permettre de distinguer l'influence réelle des variations solaires et de la circulation thermohaline sur le taux de production du ^{14}C au cours de l'Holocène. Par ailleurs, la corrélation entre les variations de la PIR de la carotte MD99-2220 et le flux de ^{10}Be ainsi que le taux de production du ^{14}C illustre également l'intérêt des courbes de PIR pour la synchronisation d'enregistrements sédimentaires holocènes avec la chronologie de la carotte de glace GISP2 (Meese *et al.*, 1994) ou de la dendrochronologie de Stuiver *et al.* (1998).

Les propriétés magnétiques des carottes de l'estuaire du St-Laurent, ainsi que des datations au ^{14}C, ont permis l'établissement d'une chronostratigraphie holocène de référence pour les séquences sédimentaires de l'est du Canada. Ils indiquent que cette chronostratigraphie présente un décalage maximal de 200 ans par rapport à la chronologie de la carotte de glace GISP2 (Meese *et al.*, 1994) ou de la dendrochronologie de Stuiver *et al.* (1998). Cette nouvelle chronostratigraphie holocène pourra ainsi servir à de futures études paléoclimatiques dans l'est du Canada. Par exemple, en raison de la dissolution des fossiles carbonatés dans les sédiments du fjord du Saguenay, les courbes d'inclinaison, déclinaison et de la PIR ont été utilisées pour dater les sédiments du fjord du Saguenay.

Or, grâce à cette nouvelle chronologie, l'analyse à haute résolution des propriétés magnétiques, sédimentologiques et physiques de la carotte MD99-2222 a mis en évidence plusieurs couches accidentelles déposées au cours des derniers 7200 ans dans le fjord du Saguenay. Ces couches sont facilement identifiables par leur couleur gris pâle et par leur base sableuse et diffèrent fortement des sédiments très foncés et « bioturbés » mis en place sous des conditions plus stables. Des analyses aux rayons-X et granulométriques réalisées à maille serrée dans chacune des couches accidentelles a permis de déterminer leur mécanisme de dépôt. L'ensemble des données ainsi que la situation géologique et sédimentologique du fjord du Saguenay laissent croire que la grande majorité de ces couches auraient été déposées à la suite de séismes de magnitude élevée. Ainsi, la fréquence de séismes majeurs dans le fjord du Saguenay aurait grandement diminué depuis ~4000 ans, ce qui est en en accord avec le modèle numérique de Wu (1998) qui montre que

la réactivation des failles, en raison de l'allègement glacio-isostatique post-glaciare, aurait eu lieu principalement entre ~7000 et 4000 ans.

Finalement, l'analyse à maille serrée de la granulométrie de la carotte MD99-2220 et d'une carotte boîte, prélevée au même site dans l'estuaire du St-Laurent, a permis de développer un traceur du débit printannier du fleuve St-Laurent. L'importance de la crue printannière autant en ce qui a trait au débit et à la charge sédimentaire du fleuve St-Laurent, l'impossibilité de générer des courants hyperpycnaux dans le fleuve, les résultats de l'analyse spectrale ainsi que la relation entre le pourcentage de silt (2-63 μm) et un indice du débit du fleuve St-Laurent pour la période de 1914 à 1999 (Gilbert *et al.*, 1996) démontrent qu'un débit printannier élevé accroît le transport et le dépôt de silts dans l'estuaire du St-Laurent. Ainsi, des fluctuations décennales et quelques événements exceptionnels ont-ils été décelés dans le pourcentage de silt au cours des derniers 800 ans. Des variations décennales des températures hivernales de l'eau de surface de l'estuaire du St-Laurent ont aussi été observées et indiquent une variabilité importante des conditions hivernales dans l'est du Canada au cours des derniers siècles. De plus, un changement concomitant des moyennes du pourcentage de silt et des températures de surface a été enregistré vers ~500 années cal. BP. La date de ce changement ainsi que la baisse subséquente des températures de surface marquent probablement le début du Petit Âge Glaciaire. Le pourcentage de silt est également corrélé à un indice de l'oscillation nord-atlantique de 1865 à 2000, ce qui laisse croire que les précipitations dans le bassin versant des Grands-Lacs/fleuve St-Laurent auraient pu être influencées par l'oscillation nord-atlantique au cours des derniers siècles. Par ailleurs, le pourcentage de silt met en évidence

une augmentation importante de la fréquence des fortes crues printannières, depuis 1975. Même si la cause de cette augmentation reste hypothétique, nos données montrent qu'elle serait unique à l'échelle des 800 dernières années. Le pourcentage de silt est donc un traceur avatageux puisqu'il permet de retracer les deux aspects d'une crue exceptionnelle (fort et faible débit) comparativement à la plupart des traceurs paléoclimatiques qui reflètent soit des moyennes saisonnières ou bien seulement l'un des deux aspects de l'événement extrême.

Références

Bond, G., Kromer, B., Beer, J., Muscheler, R., Evans, M.N., Showers, W., Hoffmann, S., Lotti-Bond, R., Hajdas, I., et Bonani, G. 2001. Persistent solar influence on North Atlantic climate during the Holocene. Science, **294** : 2130-2136.

Finkel, R.C., et Nishiizumi, K. 1997. Beryllium 10 concentrations in the Greenland Ice Sheet Project 2 ice core from 3 to 40 ka. Journal of Geophysical Research, **102** : 26699-26706.

Gilbert, D., Pettigrew, B., Swain, D., et Couture, M. 1996. State of the Gulf of St. Lawrence: oceanographic conditions in 1994: Canadian Data Report of hydrography and Ocean Sciences, **143**.

Meese, D.A., Alley, R.B., Fiacco, R.J., Germani, M.S., Gow, A.J., Grootes, P.M., Illing, M., Mayewski, P.A., Morrison, M.C., Ram, M., Taylor, K.C., Yang, Q., et Zielinski,

G.A. 1994. Preliminary depth-age scale of the GISP2 ice core. Special CRREL Report, **94-1**.

Stoner, J.S., St-Onge, G., Andrews, J.T., Hardadottir, J., Kristjansdottir, G.B., et Koc, N. En préparation. Two distinct modes of Holocene geomagnetic field behavior derived from a new high-resolution Icelandic sediment record. Science.

Stuiver, M., Reimer, P.J., Bard, E., Beck, J.W., Burr, G.S., Hughen, K.A., Kromer, B., McCormac, G., van der Plicht, J., et Spurk, M. 1998. INTCAL98 radiocarbon age calibration, 24,000-0 cal BP. Radiocarbon, **40** : 1041-1083.

Wu, P., 1998. Intraplate earthquakes and post-glacial rebound in eastern Canada and Northern Europe. *in* Dynamics of the Ice Age Earth, a modern perspective, P. Wu (Éd.), Trans Tech Publications, Zurich, 603-628.